

~~SECRET~~

Copy 22
RM SL53K12a

C. 2

~~NACA~~

*Abstracts & Review Notes
Effective Date of Revision: Aug 14, 1957*

*Sept. 26, 1957
Luy JBE*

RESEARCH MEMORANDUM

for the

U. S. Air Force

STABILITY AND CONTROL CHARACTERISTICS AT

HIGH SUBSONIC SPEEDS OF A 1/30-SCALE

MODEL OF THE MX-1554A DESIGN

By Vernard E. Lockwood, Arvo A. Luoma, and Martin Solomon

Langley Aeronautical Laboratory
Langley Field, Va.

*12-29-65
KML
1-28-66
NASA CR-01-43*

1.1. 7958

CLASSIFIED DOCUMENT

This material contains information affecting the National Defense of the United States within the meaning of the espionage laws, Title 18, U.S.C., Secs. 793 and 794, the transmission or revelation of which in any manner to unauthorized person is prohibited by law.

NATIONAL ADVISORY COMMITTEE
FOR AERONAUTICS
WASHINGTON

~~SECRET~~

NACA RM SL53K12a

NATIONAL ADVISORY COMMITTEE FOR AERONAUTICS

RESEARCH MEMORANDUM

for the

U. S. Air Force

STABILITY AND CONTROL CHARACTERISTICS AT
HIGH SUBSONIC SPEEDS OF A 1/30-SCALE
MODEL OF THE MX-1554A DESIGN

By Vernard E. Lockwood, Arvo A. Luoma, and Martin Solomon

SUMMARY

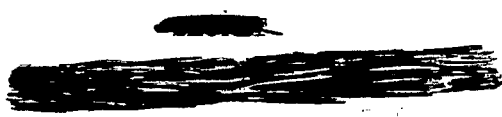
An investigation has been made in the subsonic speed range to determine the stability and control characteristics of a 1/30-scale model of the proposed MX-1554A design. (The design is an interceptor airplane employing a triangular wing and triangular stabilizing and control surfaces.) The tests were performed on a sting-supported model in the Langley high-speed 7- by 10-foot tunnel over a Mach number range from 0.40 to 0.95. The results of a low-speed investigation of a 1/10-scale model of this design are reported in NACA RM SL53A05.

The present paper contains the results of a relatively complete investigation of the stability and control characteristics of the model in a high-speed flight configuration. Some data are also presented on the effect of speed brakes, tanks, and fences on the longitudinal characteristics. The results include some corrections which can be made to the longitudinal-force coefficient for internal flow as determined from some unpublished data on the same model configuration in the Langley 8-foot transonic tunnel.

INTRODUCTION

An investigation has been made at the request of the U. S. Air Force on a 1/30-scale model of the MX-1554A airplane design to determine the stability and control characteristics in the high subsonic speed range. This investigation was conducted in the Langley high-speed 7- by 10-foot

*NASA CRN #42
RML
1-25-66
12-29-65*



tunnel over a Mach number range from 0.40 to 0.95. The results of a low-speed investigation of the preliminary design are reported in reference 1.

The present paper contains the results of a stability and control investigation of the model in the high-speed configuration. This paper also contains the results of the effect of fences, tanks, and speed brakes on longitudinal characteristics. The results of surveys of the internal flow within the duct while the model was in the Langley 8-foot transonic tunnel are incorporated in the paper. In order to expedite the publication of these data no analysis has been made.

SYMBOLS

All data are referred to the stability axes as indicated in figure 1. The moment center was located on the model reference line at 36 percent of the wing mean aerodynamic chord as is shown in figure 2. The coefficients and symbols used in this report are defined as follows:

C_L	lift coefficient, $Lift/qS$
C_X	longitudinal-force coefficient, X/qS
ΔC_X	incremental longitudinal-force coefficient
C_Y	lateral-force coefficient, Y/qS
C_l	rolling-moment coefficient, L/qSb
C_m	pitching-moment coefficient, $M'/qS\bar{c}$
C_n	yawing-moment coefficient, N/qSb
X	longitudinal force along X-axis, lb
Y	lateral force along Y-axis, lb
Z	force along Z-axis (lift equals $-Z$), lb
L	rolling moment about X-axis, ft-lb
M'	pitching moment about Y-axis, ft-lb
M	Mach number
N	yawing moment about Z-axis, ft-lb

- q free-stream dynamic pressure, $\rho V^2/2$, lb/sq ft
- S wing area, sq ft
- \bar{c} wing mean aerodynamic chord, ft
- b wing span, ft
- V free-stream velocity, ft/sec
- ρ mass density of air, slug/cu ft
- α angle of attack of fuselage reference line, deg
- i_t angle of incidence of stabilizer with respect to fuselage reference line, deg
- δ control-surface deflection in a plane perpendicular to hinge line, deg
- β angle of sideslip, deg

Lateral-stability parameters:

$$C_{l_\beta} = \frac{\partial C_l}{\partial \beta}$$

$$C_{n_\beta} = \frac{\partial C_n}{\partial \beta}$$

$$C_{Y_\beta} = \frac{\partial C_Y}{\partial \beta}$$

Subscripts:

- a aileron
- r rudder
- t tail (horizontal)
- L left

APPARATUS AND METHODS

The model used in the present investigation was a sting-supported 1/30-scale model of the MX-1554A design with the forces and moments being determined with a six-component strain-gage balance. The wing and stabilizing surfaces have notched delta plan forms. The physical characteristics of the model are presented in figure 2. The model was of steel construction throughout.

Two wings were supplied for the investigation; one was of solid construction and the other with controls was equipped with flaps and ailerons. During this investigation, however, the flaps were never deflected. Most of the investigation was performed on the control wing which had a fence on the top surface between the aileron and the wing. Two fences, the details of which are given in figure 3, were tested on this wing.

The model was equipped with internal ducting leading from the air scoop or inlet which is situated on the bottom surface of the fuselage. The inlet could be closed when desired by placing a faired plug in the mouth of the duct as shown in figure 4. The internal flow was "dumped" around the sting within the fuselage at a location behind the strain-gage balance and approximately five inches from the end of the fuselage.

Some internal-flow measurements were made by means of a rake attached to the sting. The tubes of the rake were distributed about the sting (1/16 of an inch behind the fuselage exit) so that the average flow through the duct could be determined. Additional pressure orifices were located in the sting to determine pressures at different locations in the duct.

The model was also equipped with wing tanks and speed brakes which were furnished by the manufacturer.

TESTS

The tests were conducted in the Langley high-speed 7- by 10-foot tunnel on a sting-supported strain-gage balance system which allows pivoting of the model about the tunnel center line. (The pivot point for this model was on the model reference line at 36 percent wing mean aerodynamic chord.) With the bent-sting arrangement shown in figure 5, an angle-of-attack range of -3° to 23° was possible. For the investigation of the characteristics in sideslip, the model was rotated 90° .

The Reynolds number variation with Mach number for these tests is shown in figure 6. The Reynolds number is based on a wing mean aerodynamic chord of 0.498 foot. The average temperature at a particular Mach number was used in computing the Reynolds number of these tests.

Most of the tests were made with the duct inlet open and, except where noted in the figures, this configuration exists.

CORRECTIONS

No blockage or jet boundary corrections have been applied to the data as calculations have shown these to be negligible for this size of model. Corrections were applied, however, to the angle of attack and sideslip angle as a result of balance and sting deflections.

The magnitude of the longitudinal-force coefficient of the configurations with internal flow as presented herein appears to be considerably greater than would be expected for a model of this design. These data have not been corrected for the internal drag of the model and for the pressure drags resulting from the deviation of the pressures in the strain-gage-balance chamber and at the end of the fuselage from the free-stream value. The corrected longitudinal-force coefficient is obtained from the equation

$$C_{X_{\text{corrected}}} = C_{X_{\text{measured}}} + \Delta C_X$$

where the term ΔC_X is in turn obtained from the equation

$$\Delta C_X = C_{D_i} + C_{D_c} + C_{D_b}$$

The new symbols introduced herein are defined as follows:

C_{D_i} internal drag coefficient, $\frac{m}{qS}(V - V_d \cos \alpha) - P_d \frac{A_d}{S} \cos \alpha$

where

m mass flow in model duct

V_d velocity of internal flow at end of fuselage

P_d pressure coefficient of internal flow at end of fuselage

A_d area of duct at end of fuselage

C_{D_c} strain-gage-balance chamber drag coefficient, $-P_c \frac{A_s}{S} \cos \alpha$

where

A_s cross-sectional area of sting within fuselage

P_c pressure coefficient within balance chamber

C_{D_b} base drag coefficient, $-P_d \frac{A_r}{S} \cos \alpha$

where

A_r area at end of fuselage enclosed by inner and outer walls of fuselage

The correction term ΔC_x as obtained from tests of the same model in the Langley 8-foot transonic tunnel is shown plotted against angle of attack at a Mach number of 0.96 in figure 7(a) for the complete model and for the complete model less the horizontal tail and plotted against Mach number at an angle of attack of 0° in figure 7(b). (The results of some unpublished data indicate that the variation of ΔC_x with α at other subsonic Mach numbers is similar to that shown for $M = 0.96$.) The internal drag coefficient C_{D_i} at an angle of attack of 0° (data not presented) was approximately 0.008 throughout the Mach number range; an increase in angle of attack increased the internal drag coefficient C_{D_i} up to a value of approximately 0.010 at the highest angles of attack. The balance chamber drag coefficient C_{D_c} was approximately 0.008 at a Mach number of 0.40 and decreased with Mach number to a value of approximately 0.004 at a Mach number of 0.98. The base drag coefficient C_{D_b} was negative and was less than 0.001 in magnitude at all conditions.

When there is no flow through the model (that is, the inlet is closed), the correction to the longitudinal-force coefficient becomes the usual base-pressure correction. For the complete model at $\alpha = 0^\circ$, this base-pressure correction is negligible up to $M = 0.92$. At $M = 0.94$, the value of C_x should be increased by -0.0003 and at $M = 0.96$, C_x should be increased by -0.0007.

PRESENTATION OF RESULTS

The results of the investigation of a 1/30-scale model of the MX-1554A design are presented in the following figures:

Description	Figures
Aerodynamic characteristics in pitch:	
Effect of Mach number	8
Effect of fences	9
Effect of negative angle of attack	10
Stability and control:	
Fuselage and tail	11
Complete model (no fence)	12
Complete model (fence A)	13
Effect of inlet closing	14 and 15
Effect of speed brakes	16 and 17
Effect of tanks	18
Lateral control	19
Characteristics in sideslip:	
Stability parameters	20
Effect of model configuration	21
Directional control	22

The flagged symbols in figures 8 and 14 are check tests made approximately three months later than the original investigation.

Langley Aeronautical Laboratory,
National Advisory Committee for Aeronautics,
Langley Field, Va., October 29, 1953.

Vernard E. Lockwood

Vernard E. Lockwood
Aeronautical Research Scientist

Arvo A. Luoma

Arvo A. Luoma
Aeronautical Research Scientist

Martin Solomon

Martin Solomon
Aeronautical Research Scientist

Approved:

Thomas A. Harris

Thomas A. Harris
Chief of Stability Research Division

Eugene C. Draley

Eugene C. Draley
Chief of Full-Scale Research Division

cg

REFERENCE

1. Lockwood, Vernard E., and Solomon, Martin: Stability and Control Characteristics at Low Speed of a $\frac{1}{10}$ - Scale Model of MX-1554A Design. NACA RM SL53A05, U. S. Air Force, 1953.

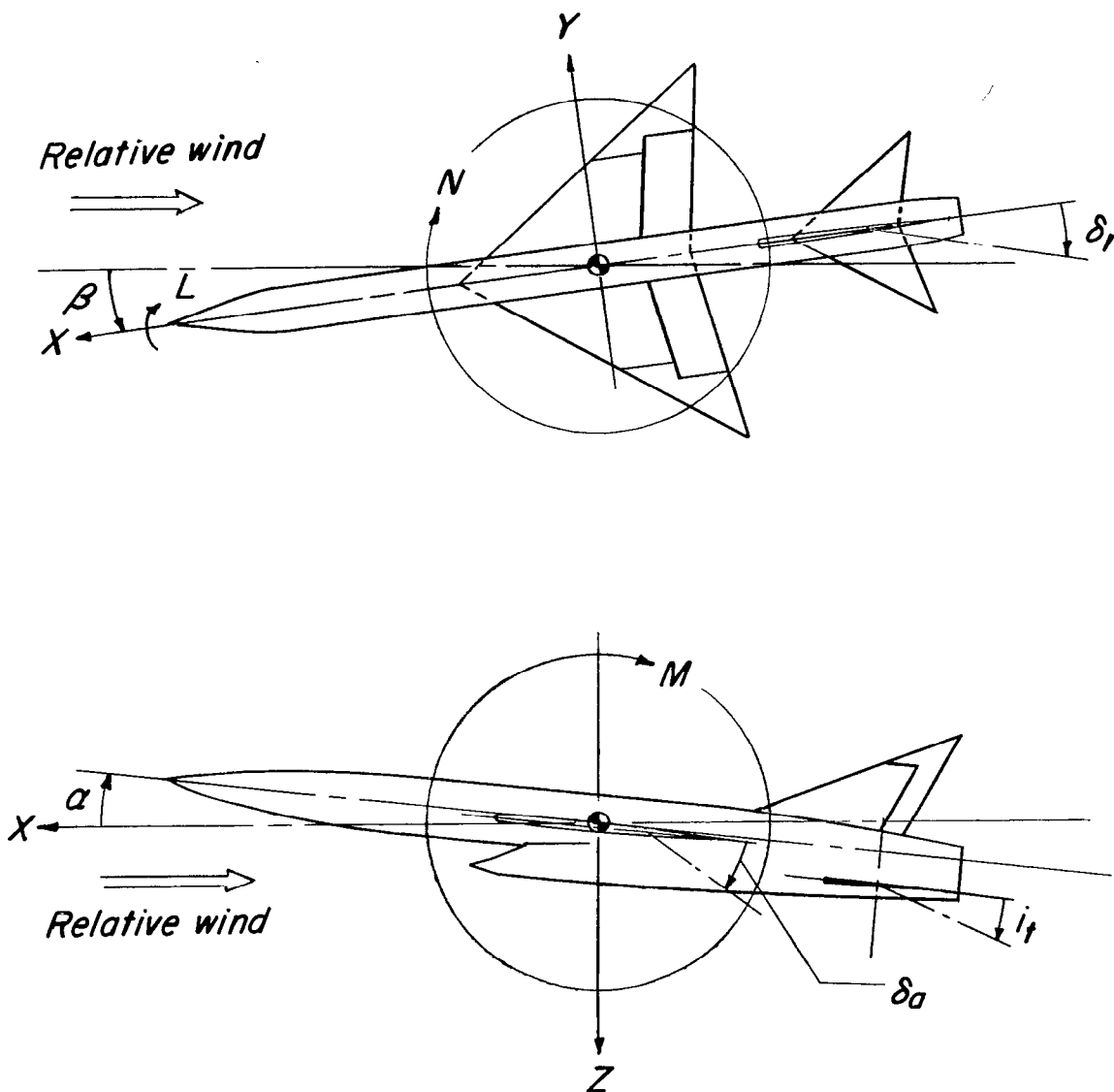


Figure 1.- System of axes and control surface deflections. Positive directions of forces, moments, and angles are indicated by arrows.

Physical characteristics

Wing

Aspect ratio 3.2
 Area (total) 0.446 sq ft
 Airfoil section NACA 65A003
 Mean aerodynamic chord 0.498 ft

Horizontal tail

Aspect ratio 3.4
 Area (total) 0.101 sq ft
 Airfoil section NACA 65A003

Vertical tail

Area (exposed) .079 sq ft
 Airfoil section NACA 65A003

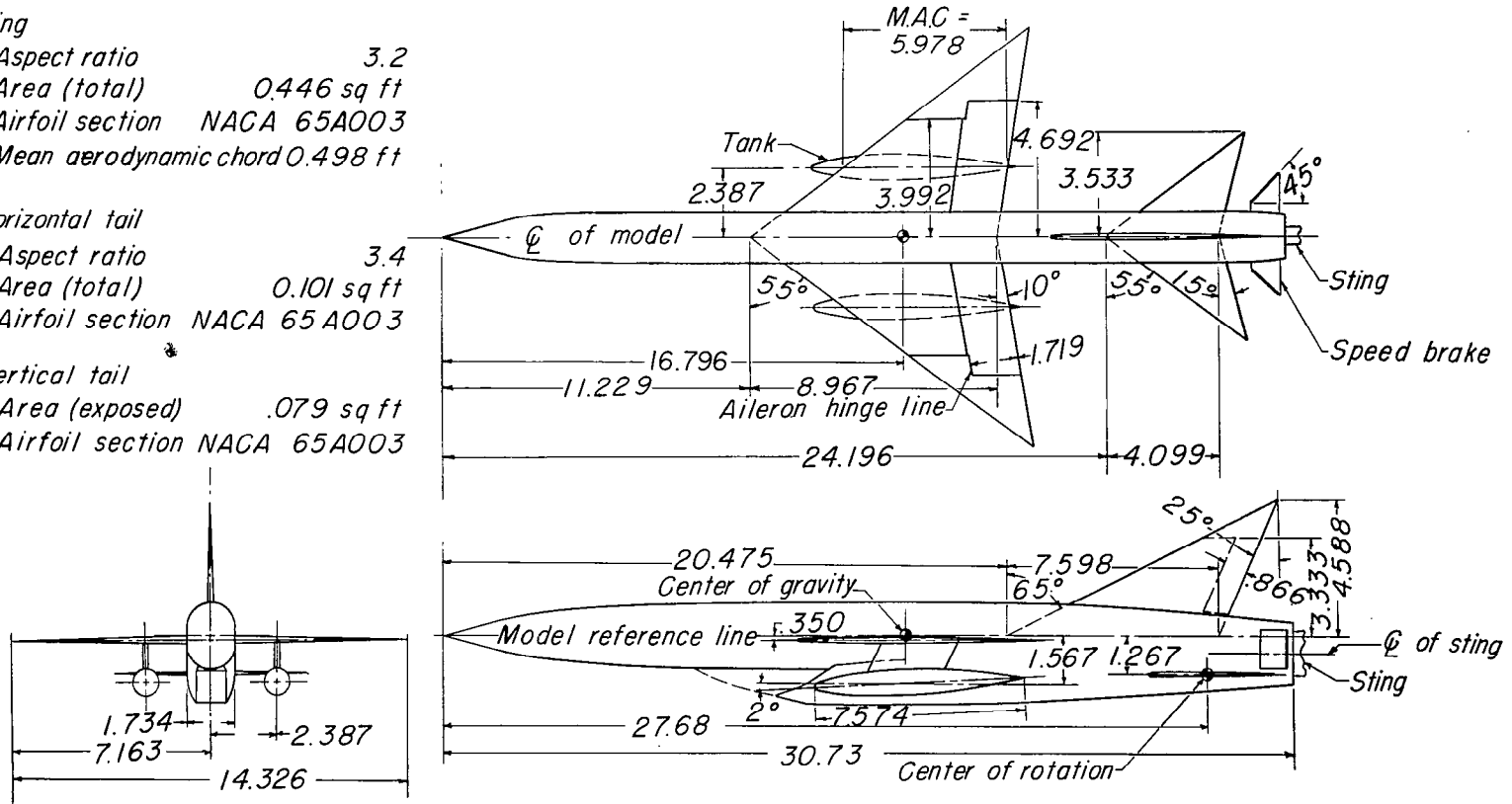


Figure 2.- Three-view drawing of model tested. All dimensions are in inches.

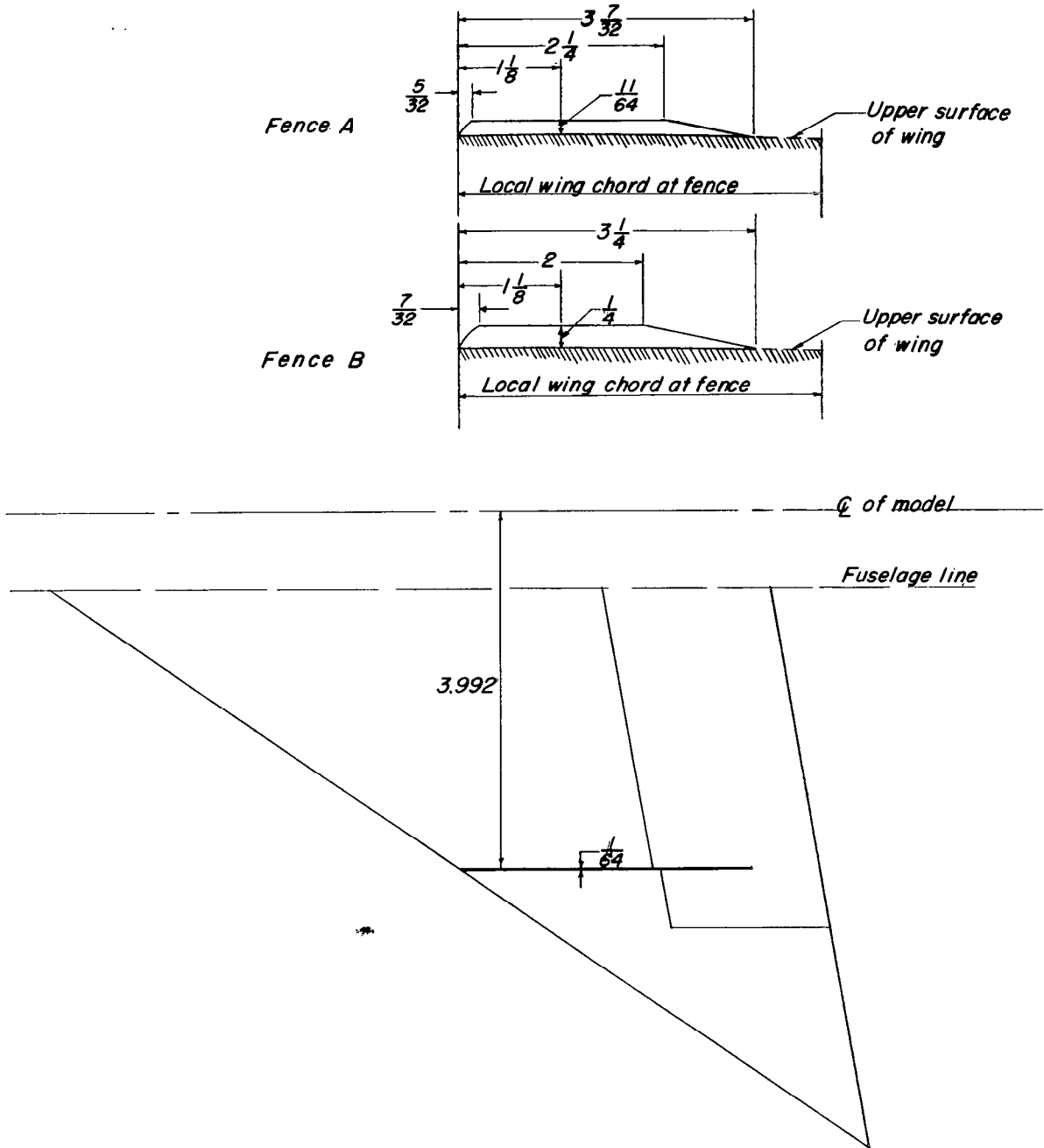


Figure 3.- Details of the two flow fences used. All dimensions are in inches.

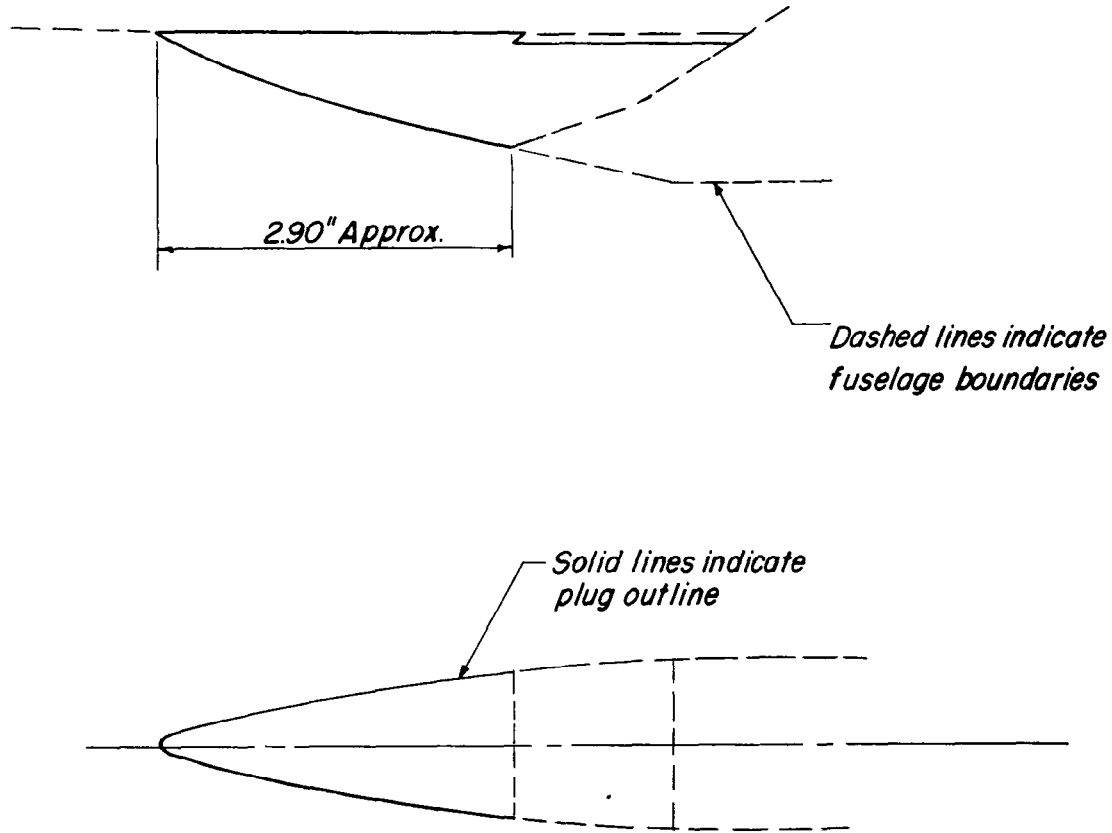
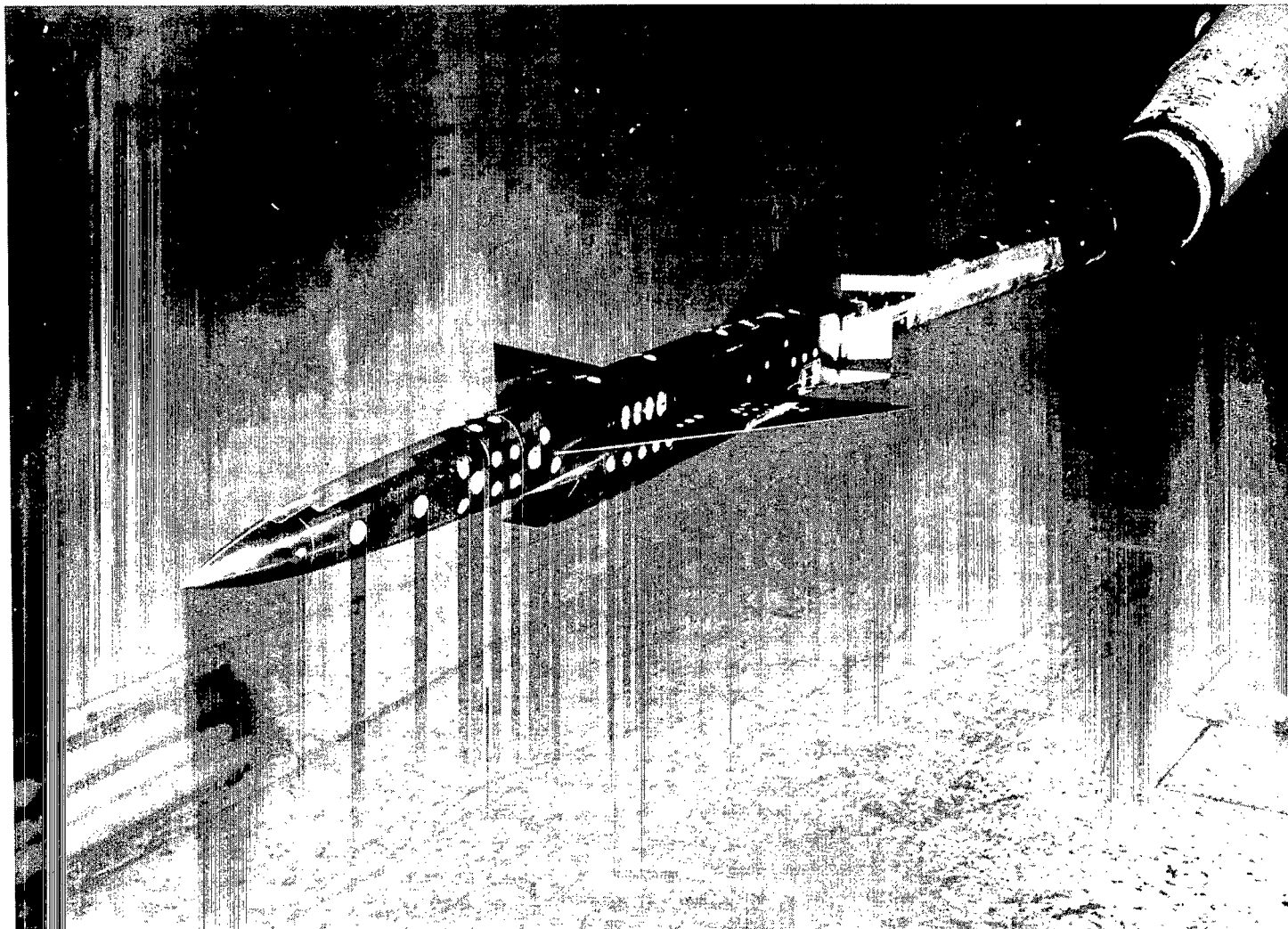
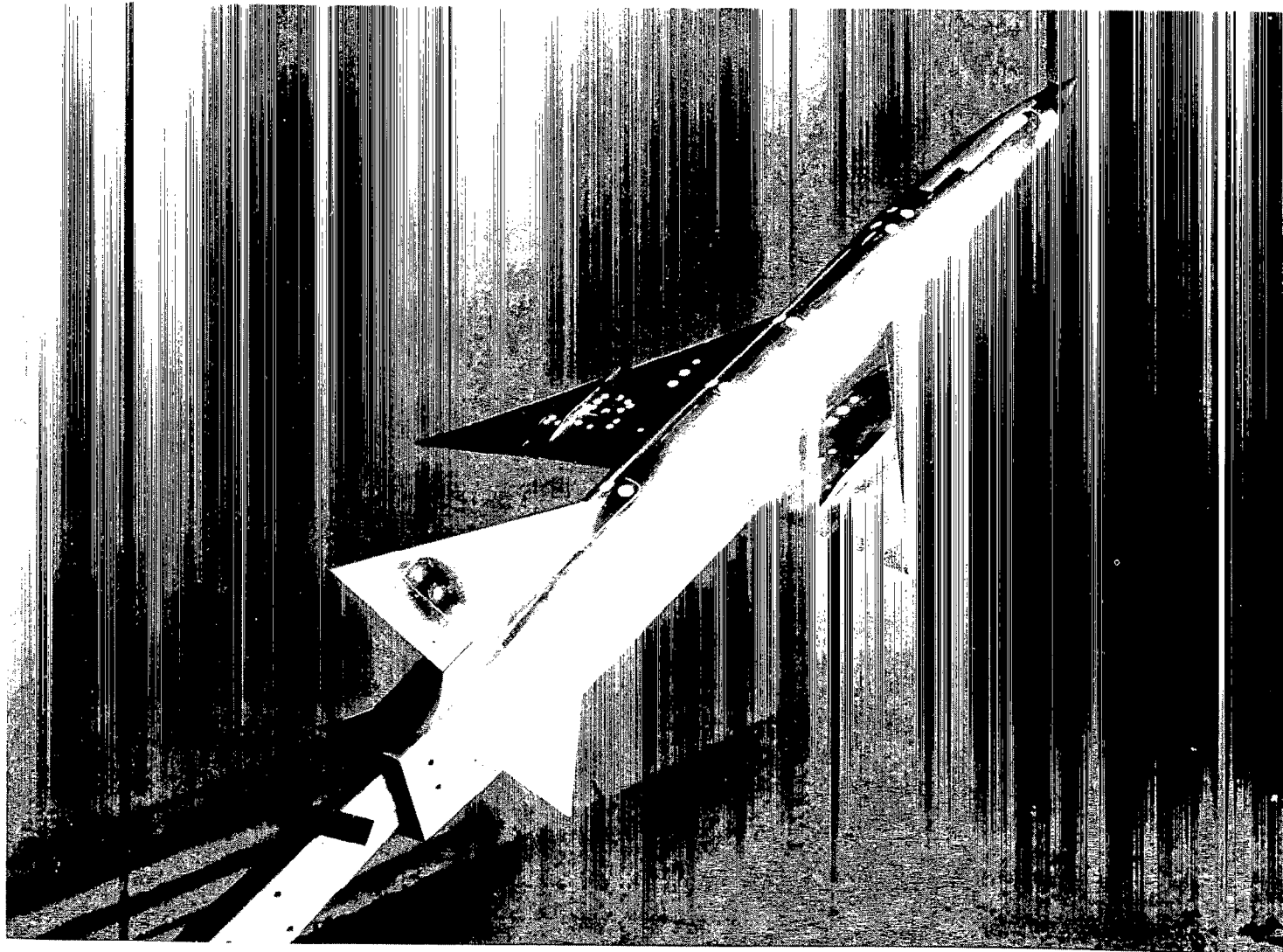


Figure 4.- Detail of plug for internal ducting, showing profile and bottom view of the exposed part.



L-79965.1

Figure 5.- 1/30-scale model of MX-1554A design mounted for testing in Langley 7- by 10-foot high-speed tunnel.



L-79966.1

Figure 5.- Concluded.

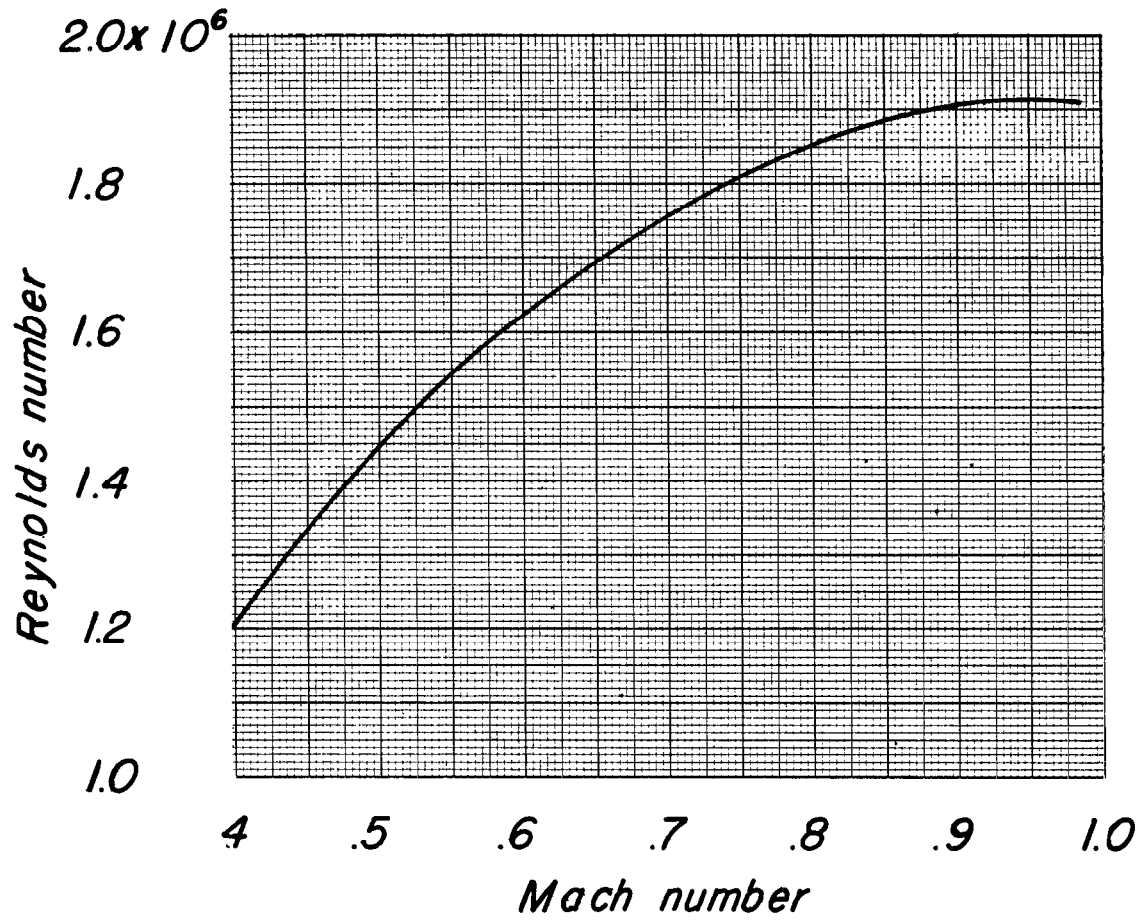
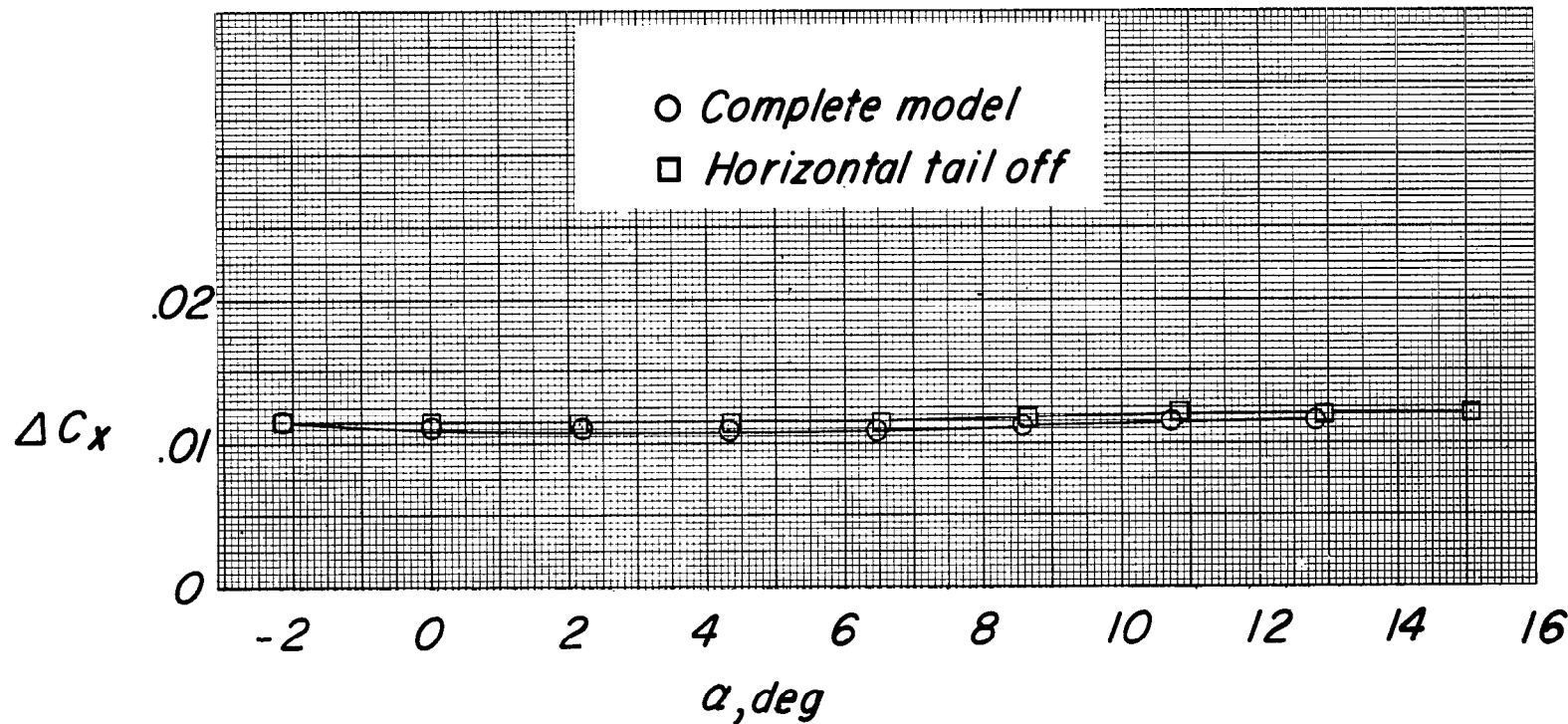
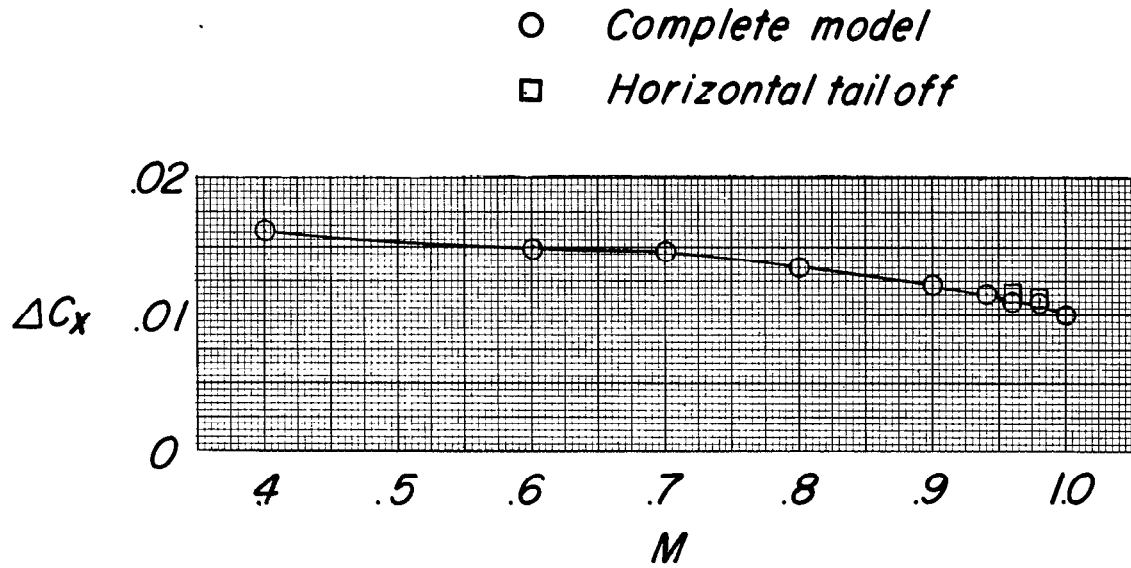


Figure 6.- Average variation of Reynolds number with Mach number for the model. (Reynolds number based on a mean aerodynamic chord of 0.498 foot.)



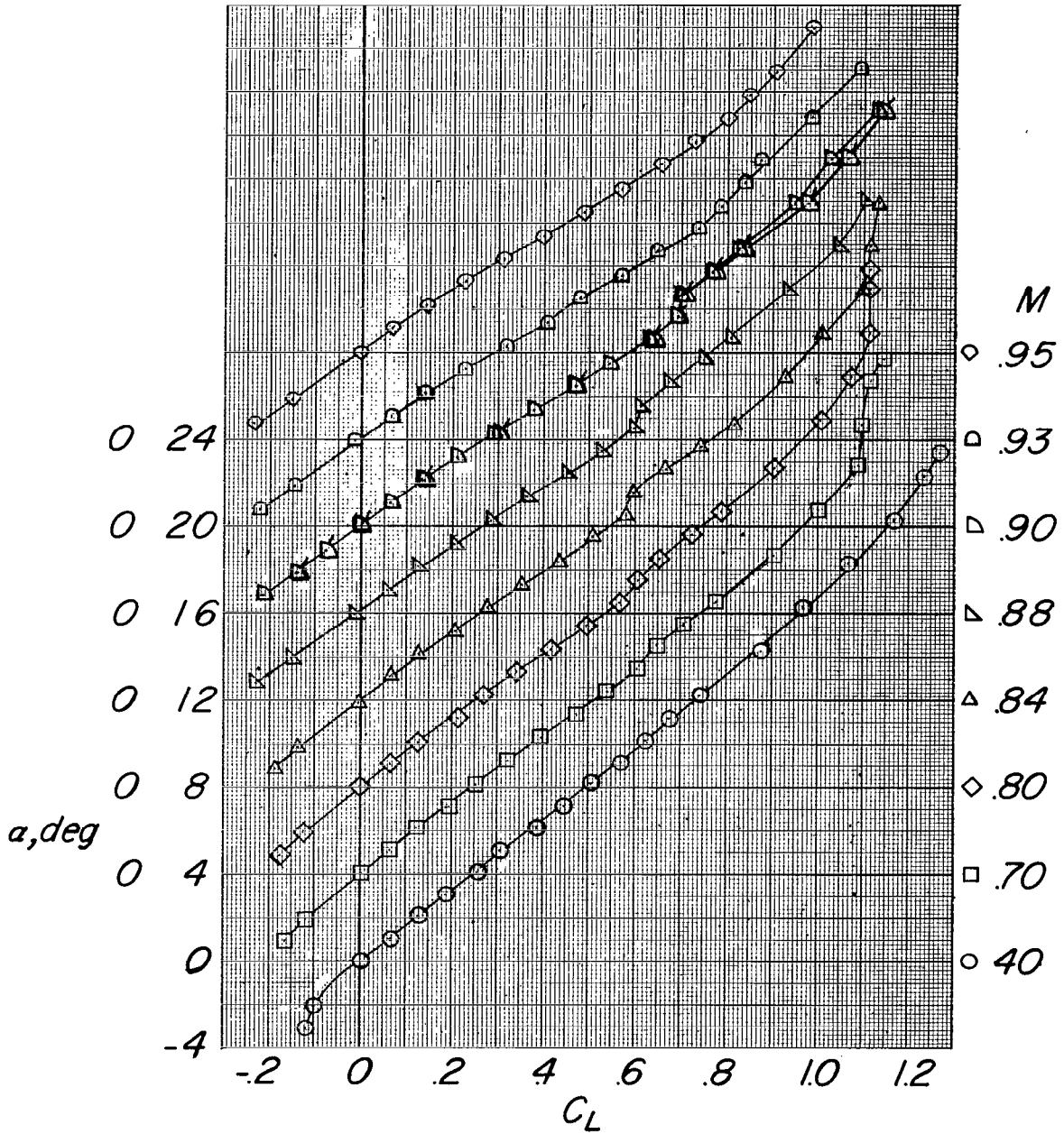
(a) ΔC_x against α ; $M = 0.96$.

Figure 7.- Variation of incremental longitudinal-force coefficients ΔC_x with angle of attack and Mach number. (From internal flow measurements of the model in the Langley 8-foot transonic tunnel.)



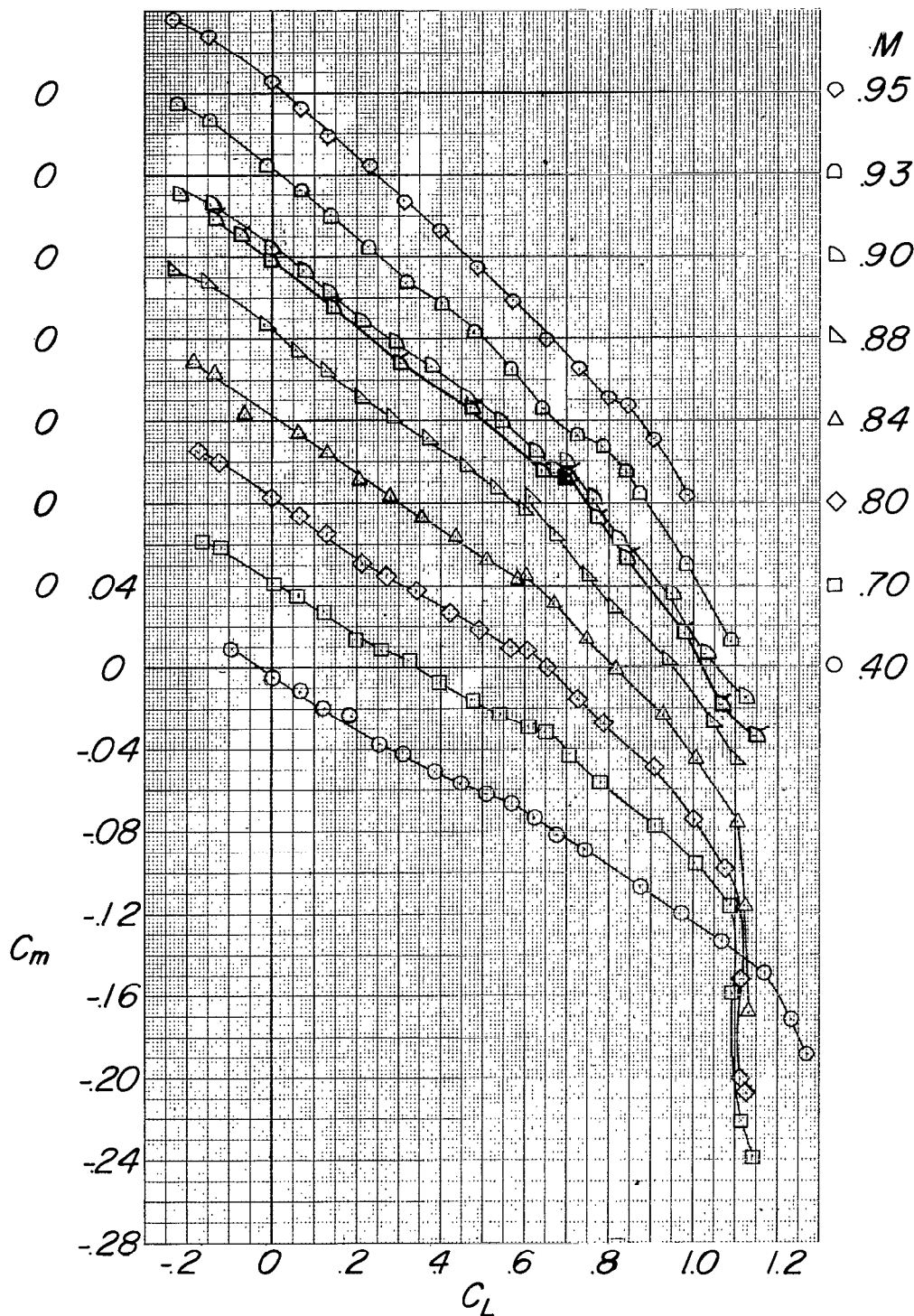
(b) ΔC_x against M ; $\alpha = 0^\circ$.

Figure 7.- Concluded.



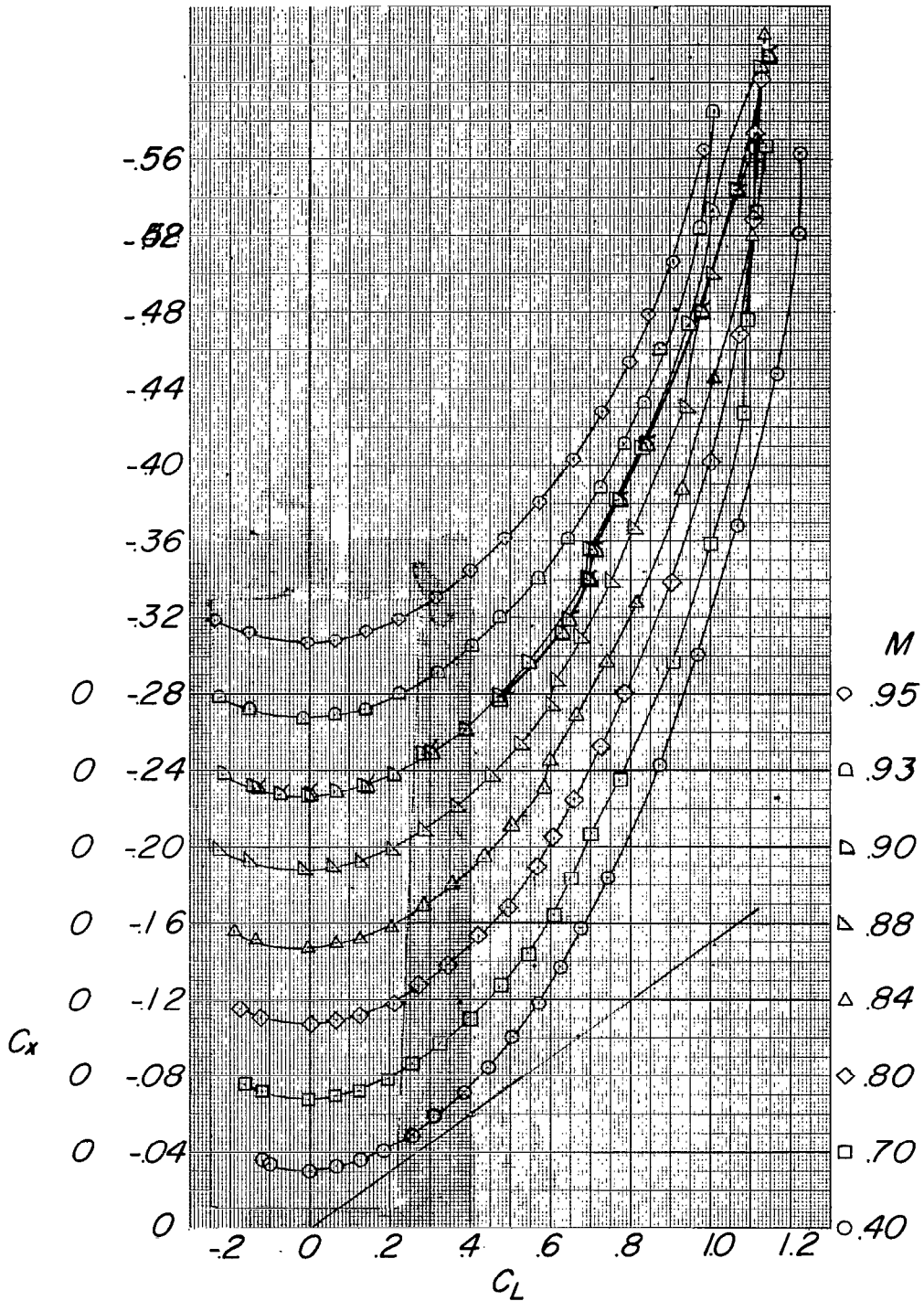
(a) α against C_L .

Figure 8.- The effect of Mach number on the aerodynamic characteristics in pitch. No fence; $i_t = 0^\circ$.



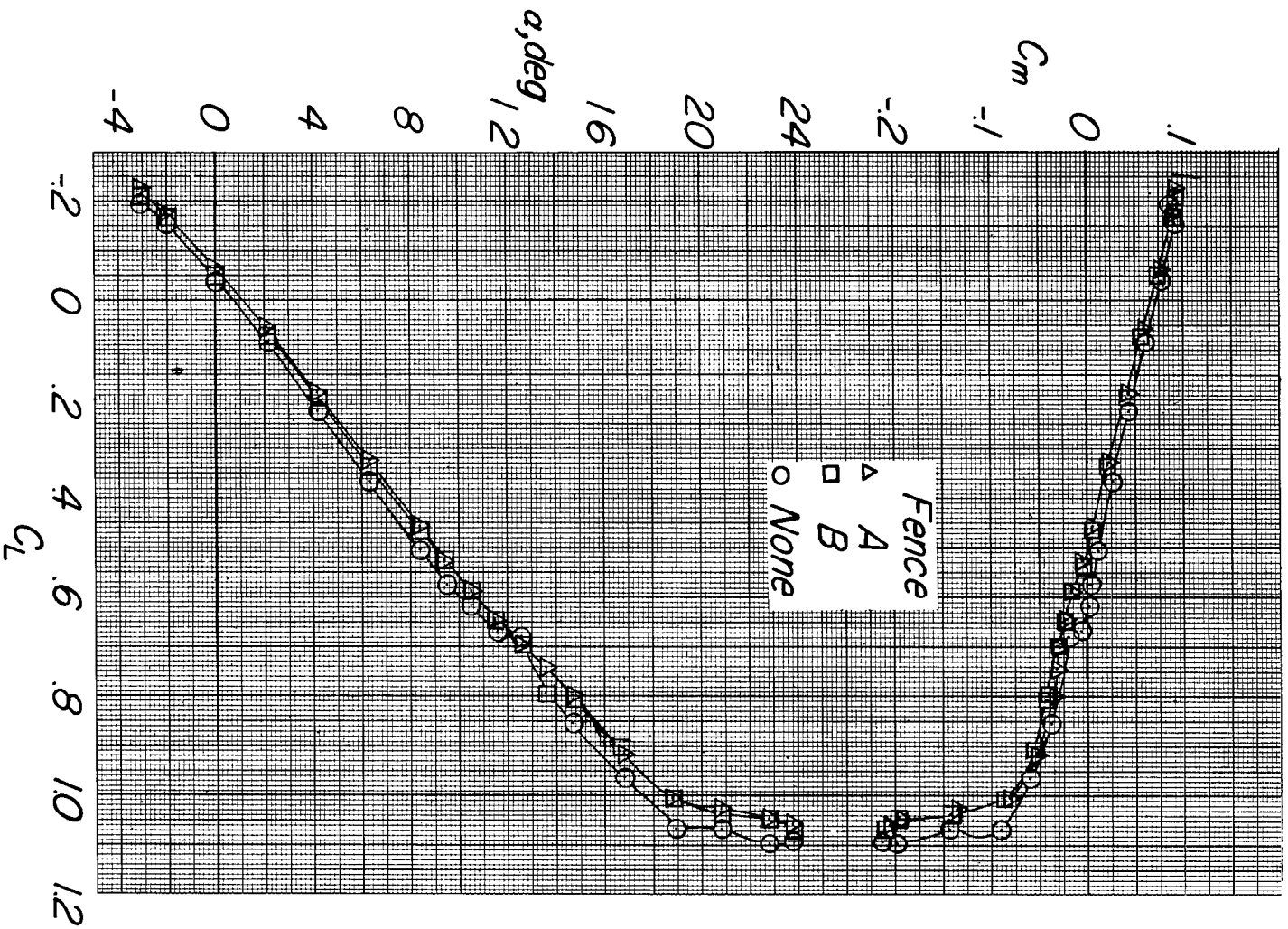
(b) C_m against C_L .

Figure 8.- Continued.



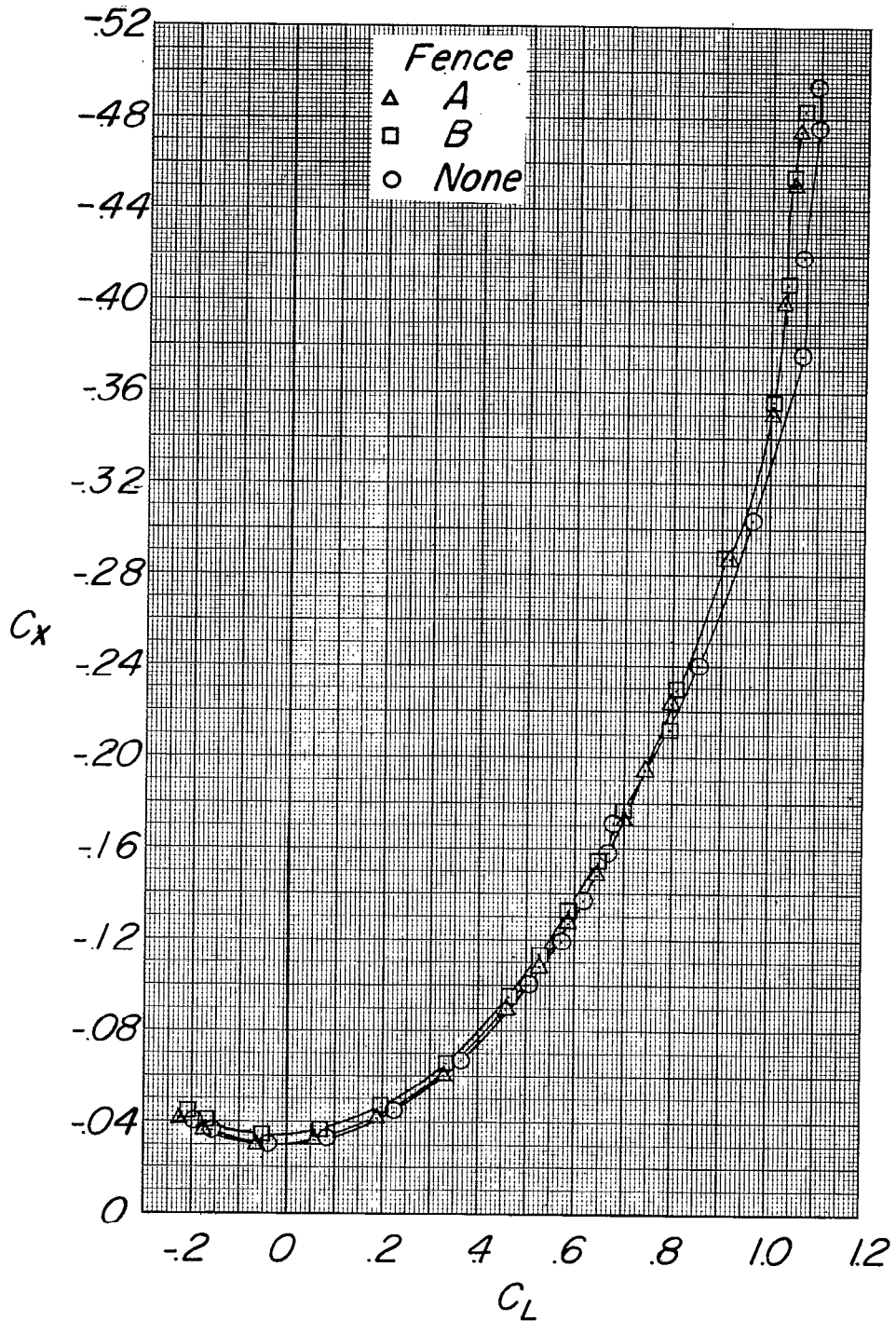
(c) C_x against C_L .

Figure 8.- Concluded.



(a) $M = 0.70$.

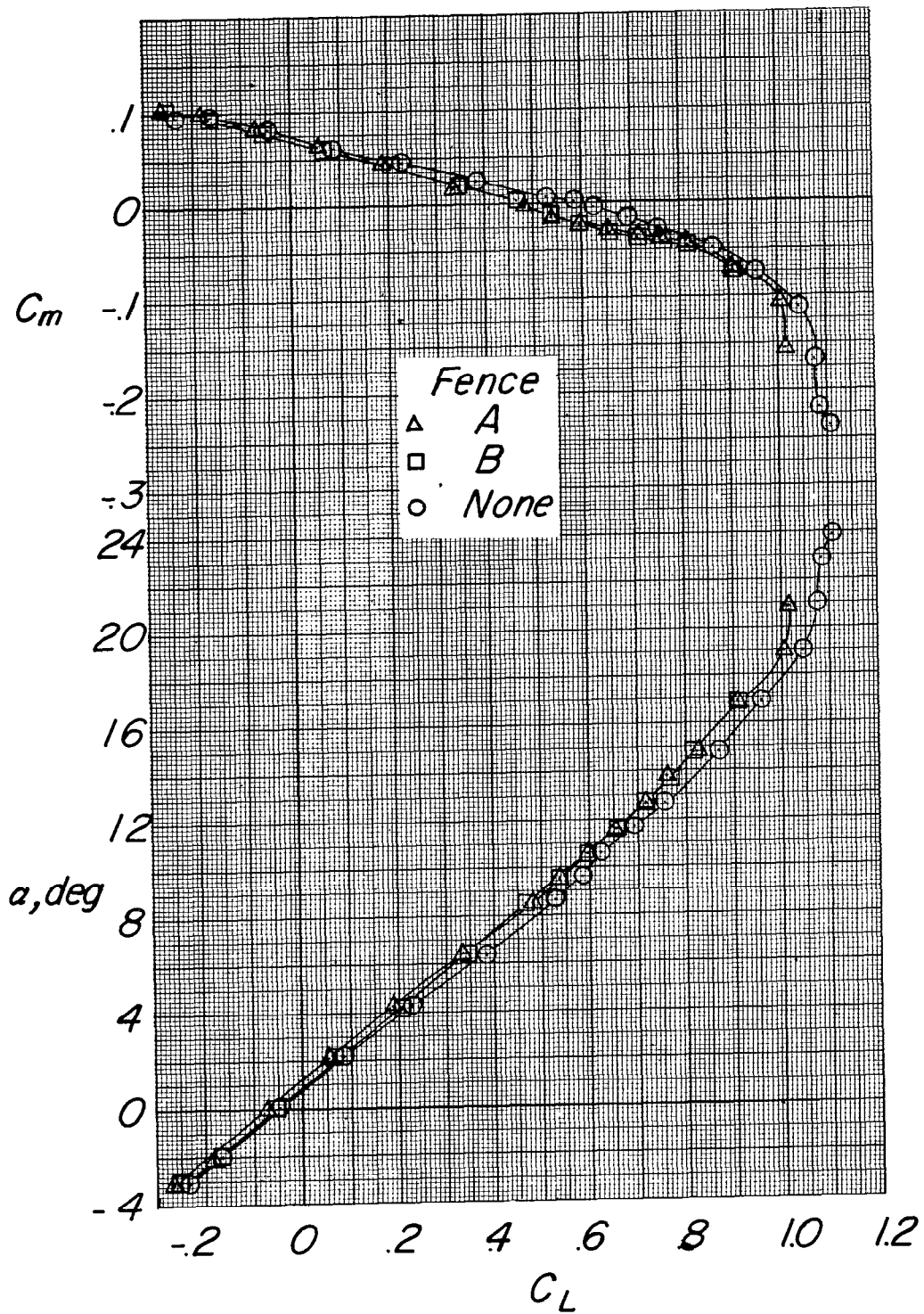
Figure 9.- The effect of fences on the aerodynamic characteristics in pitch. $i_t = -5^\circ$.



(a) Concluded.

Figure 9.- Continued.

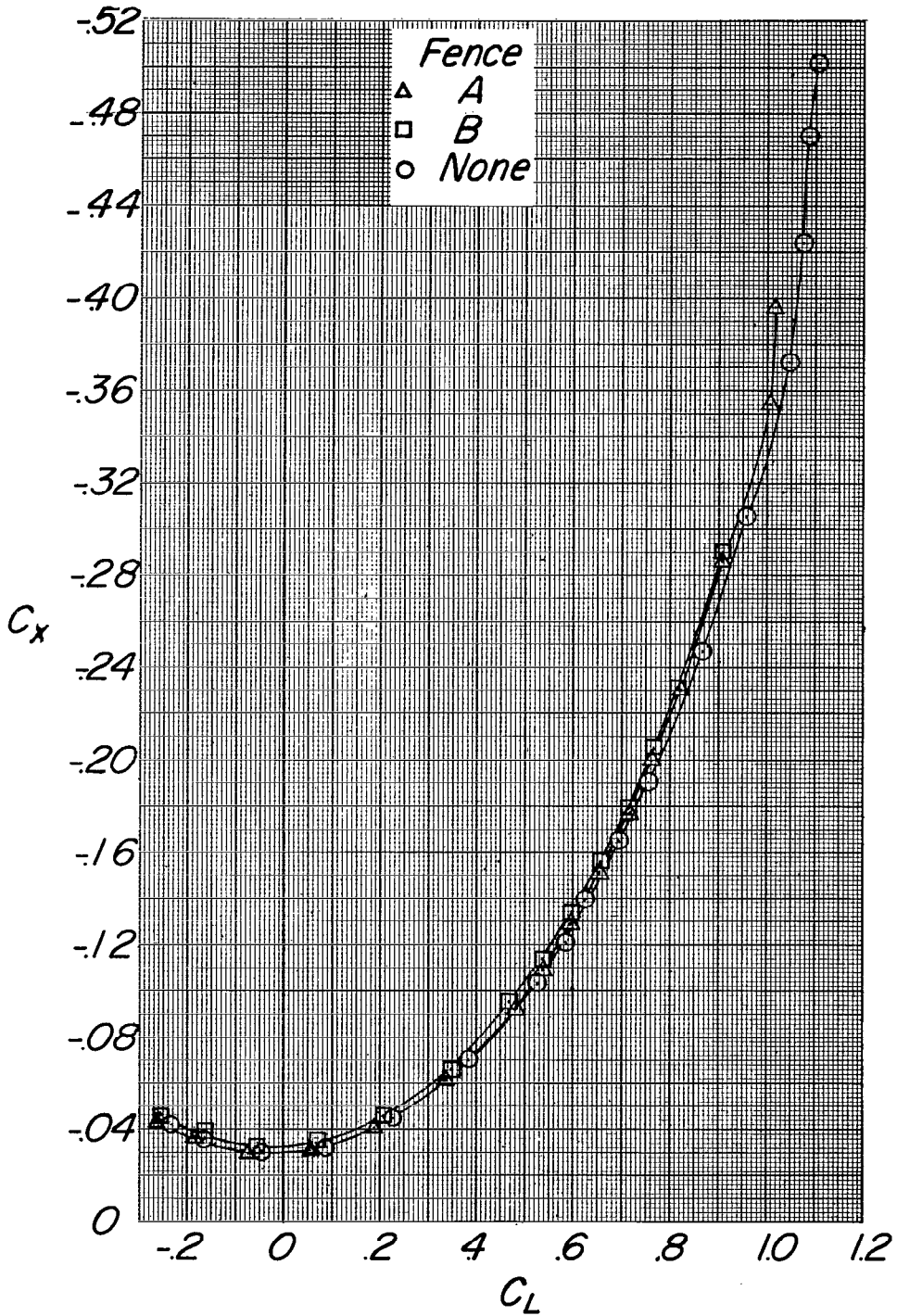
~~SECRET~~



(b) $M = 0.80$.

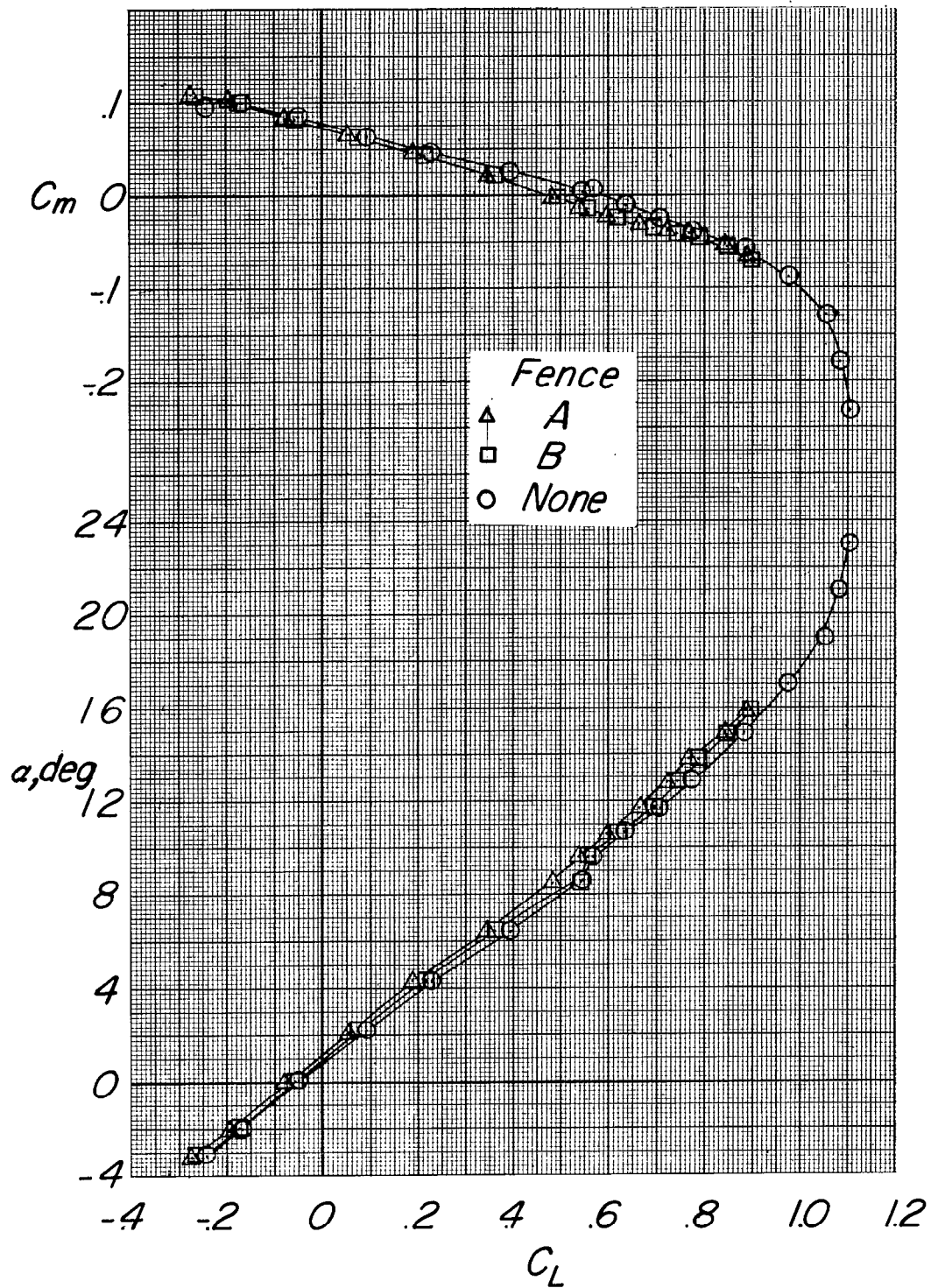
Figure 9.- Continued.

~~SECRET~~



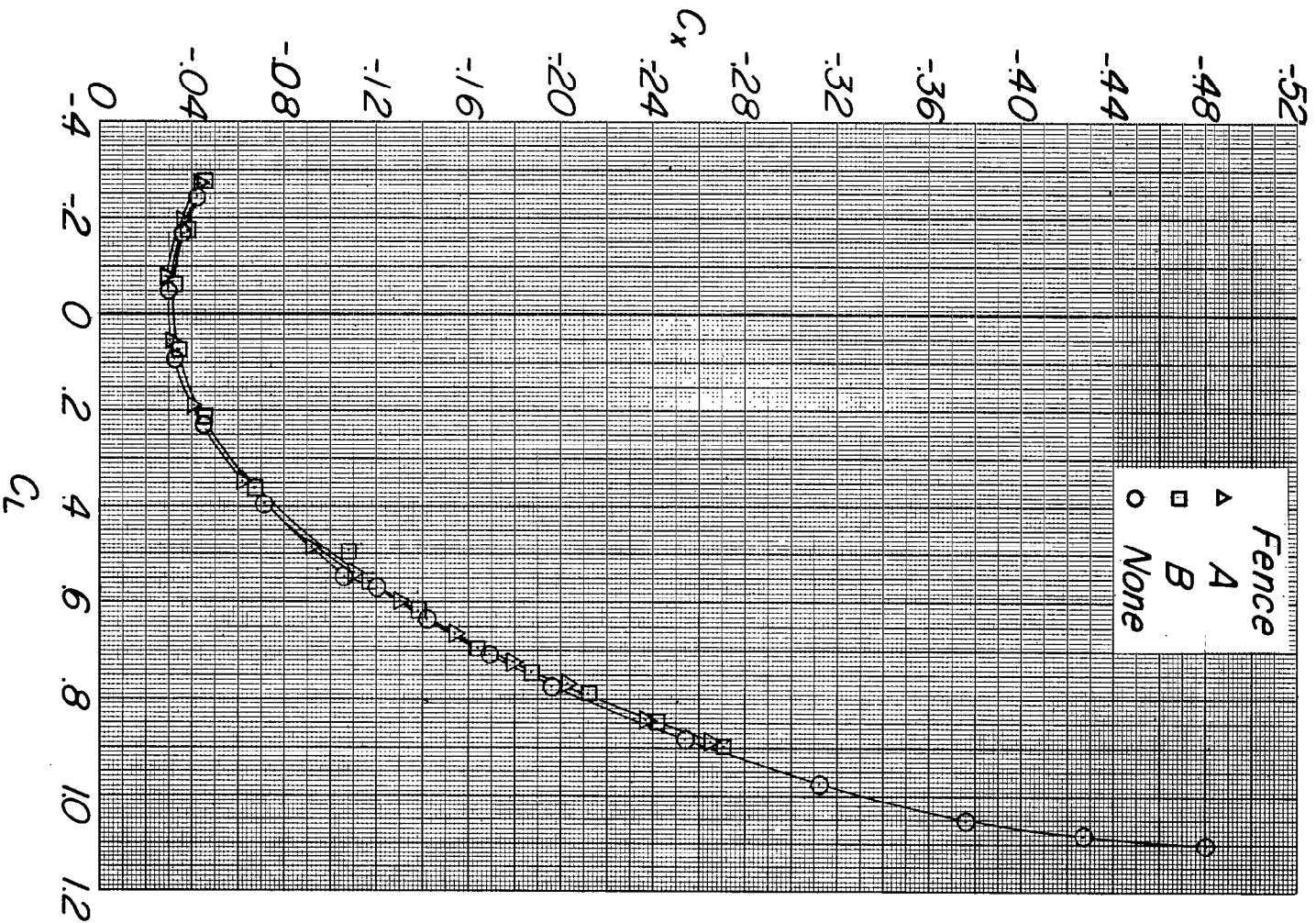
(b) Concluded.

Figure 9.- Continued.



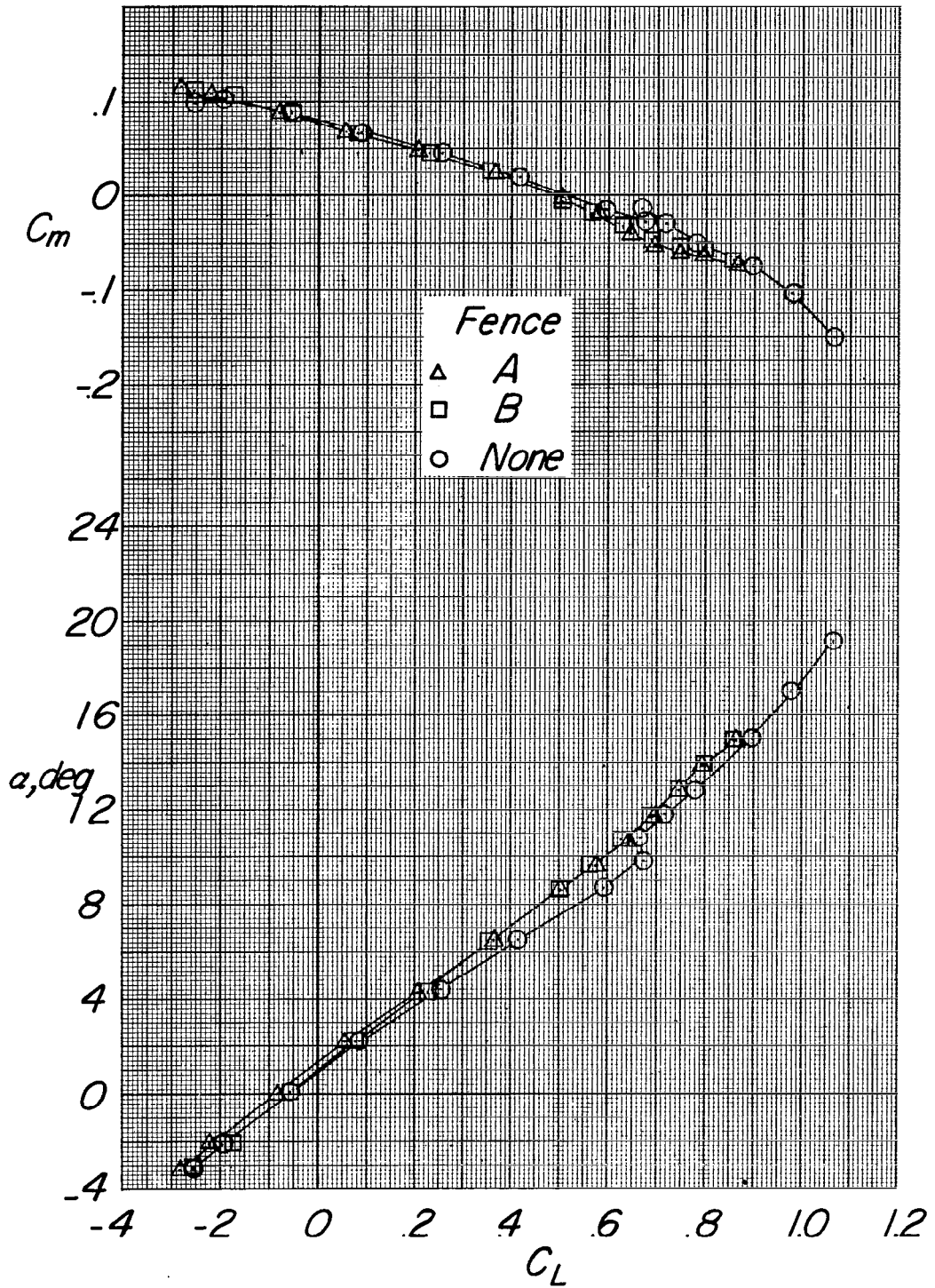
(c) $M = 0.84$.

Figure 9.- Continued.



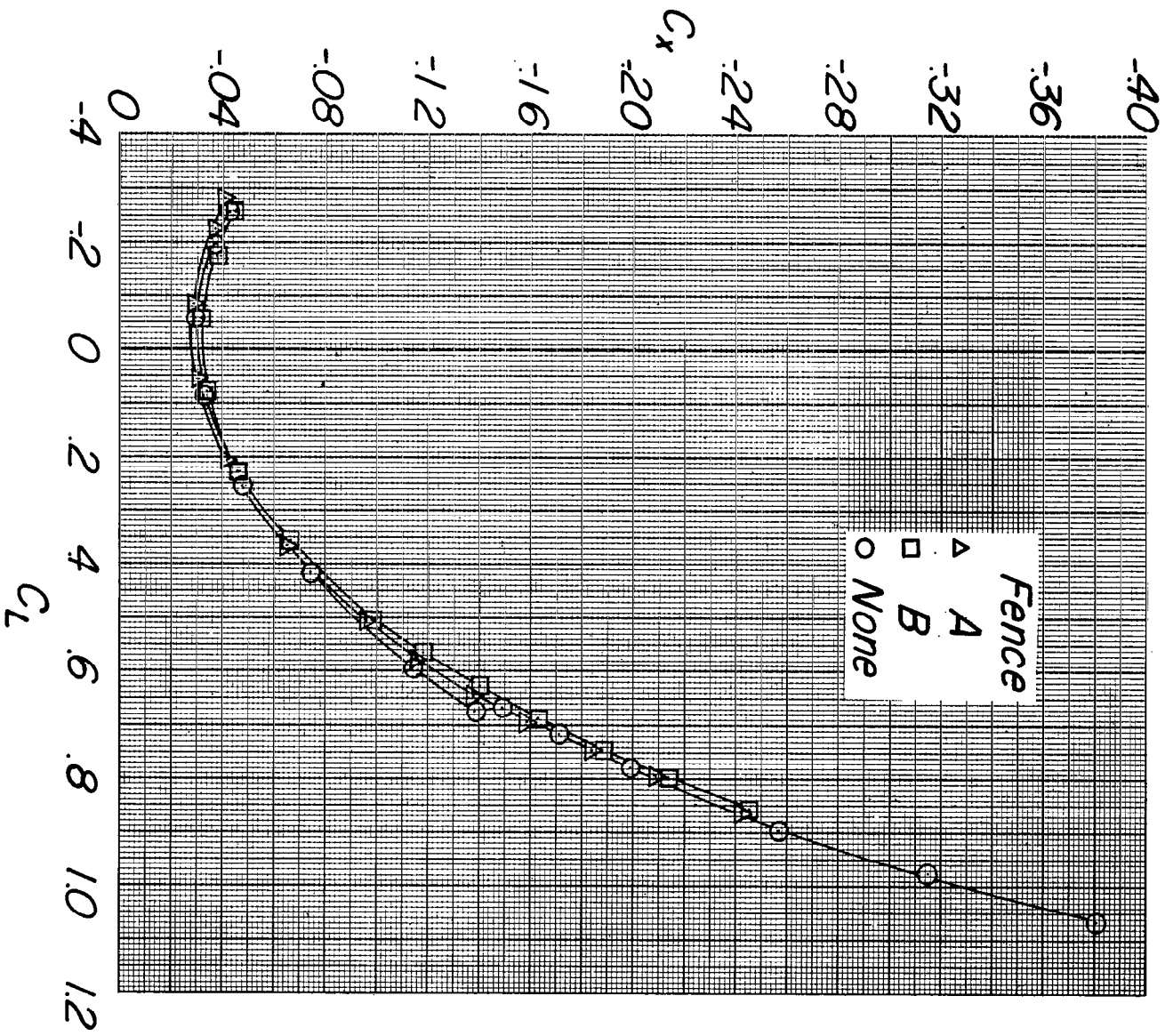
(c) Concluded.

Figure 9.- Continued.



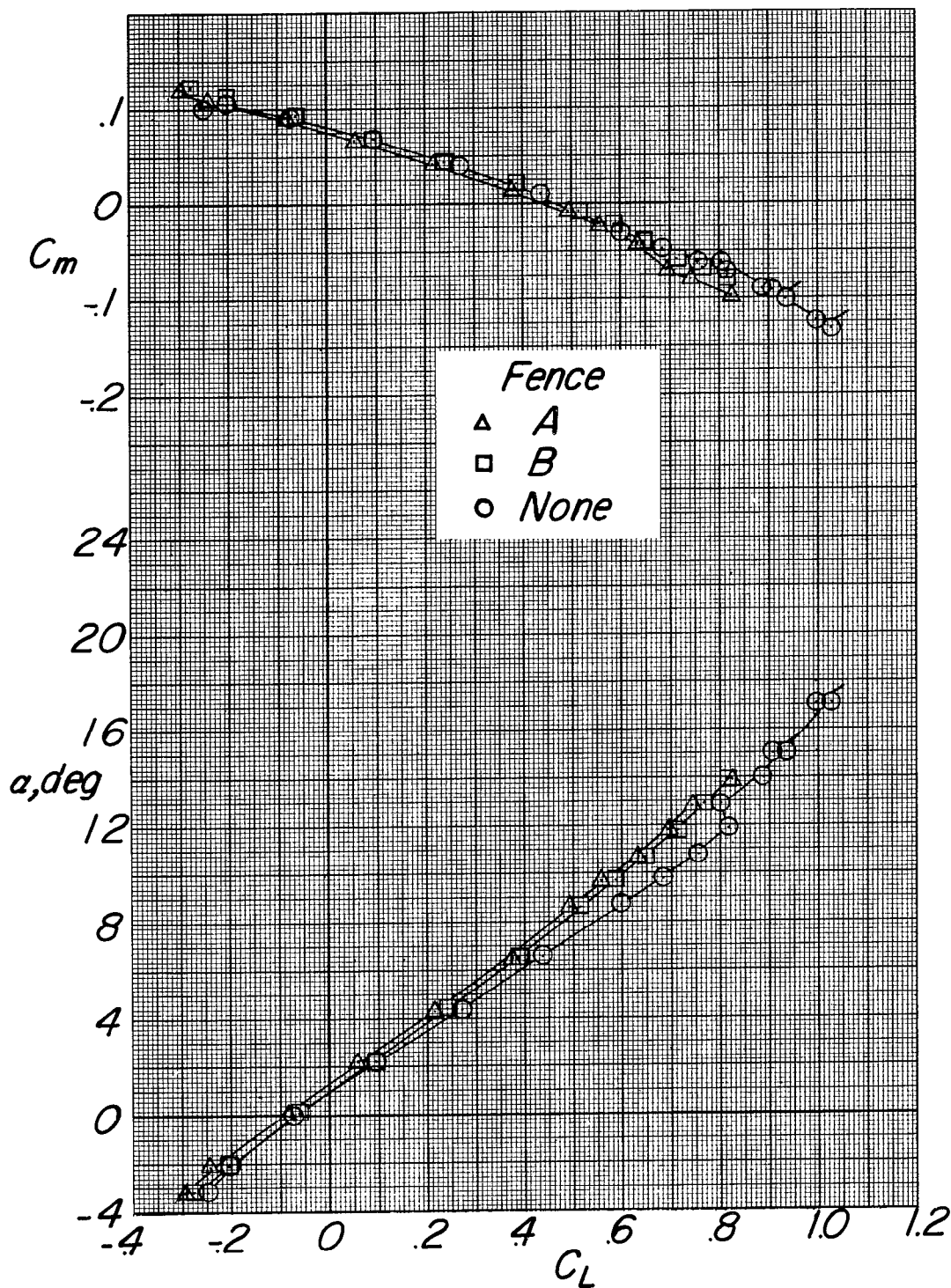
(d) $M = 0.90$.

Figure 9.- Continued.



(d) Concluded.

Figure 9.- Continued.

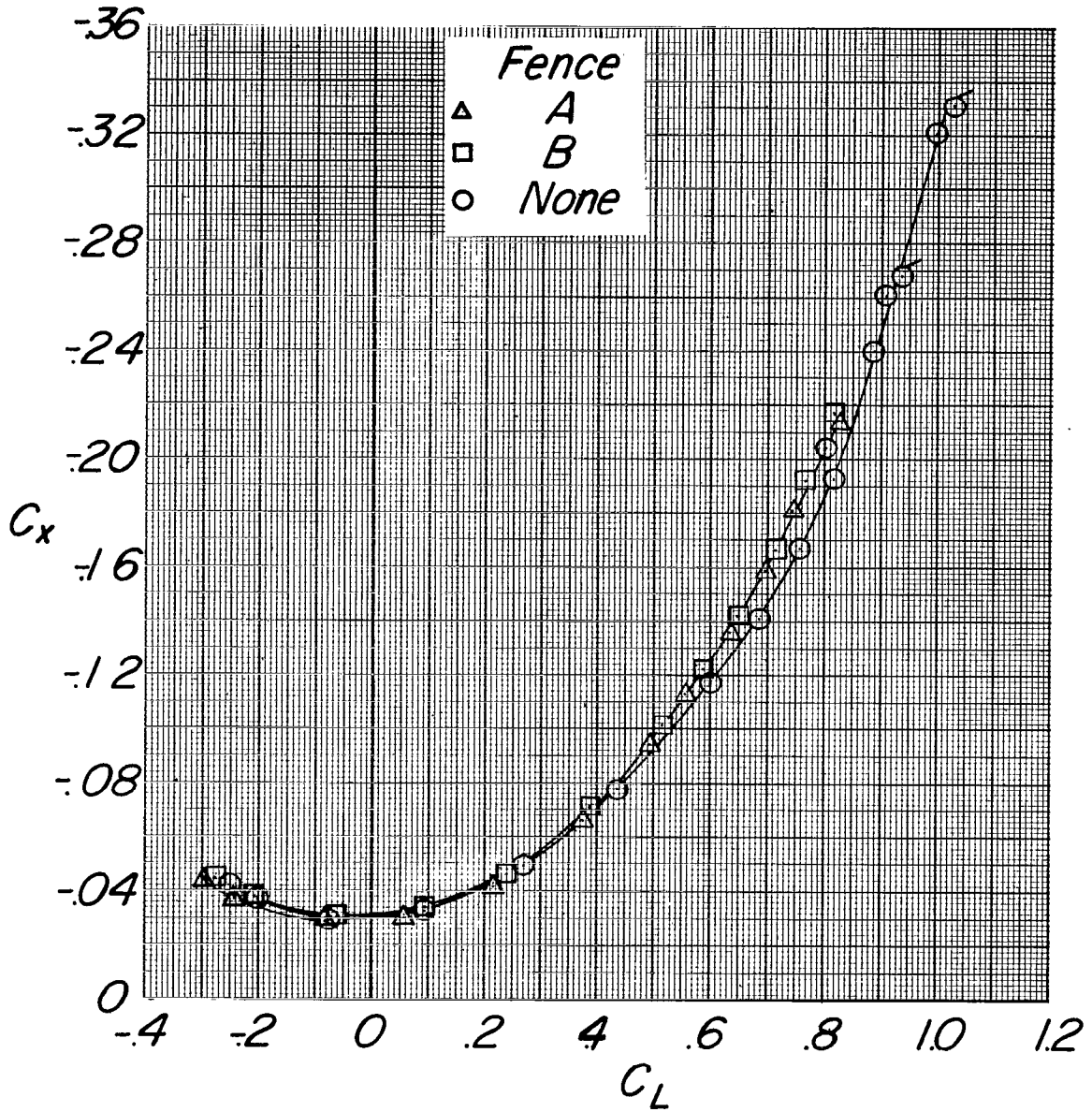


(e) $M = 0.95$.

Figure 9.- Continued.



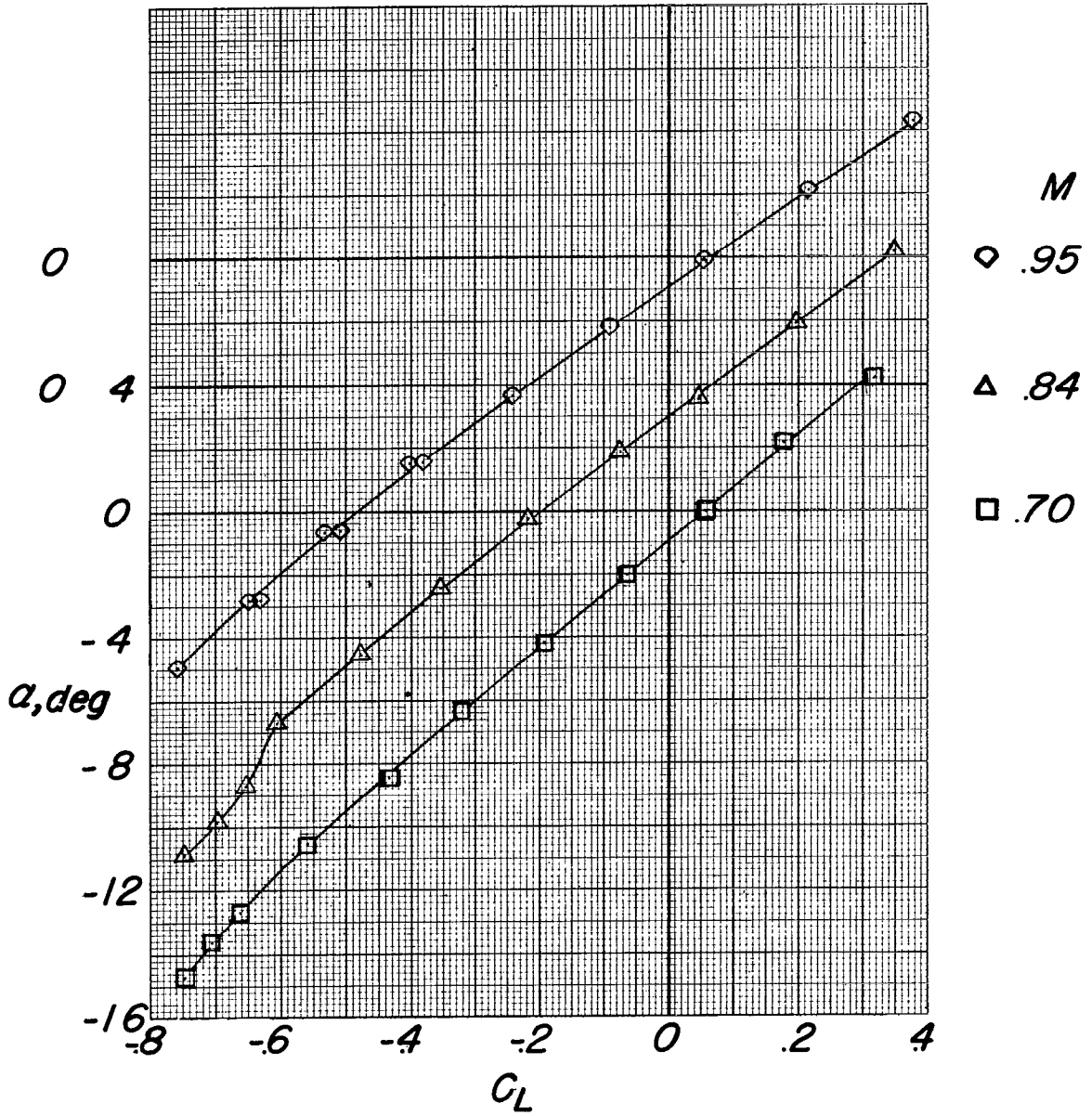
~~SECRET~~



(e) Concluded.

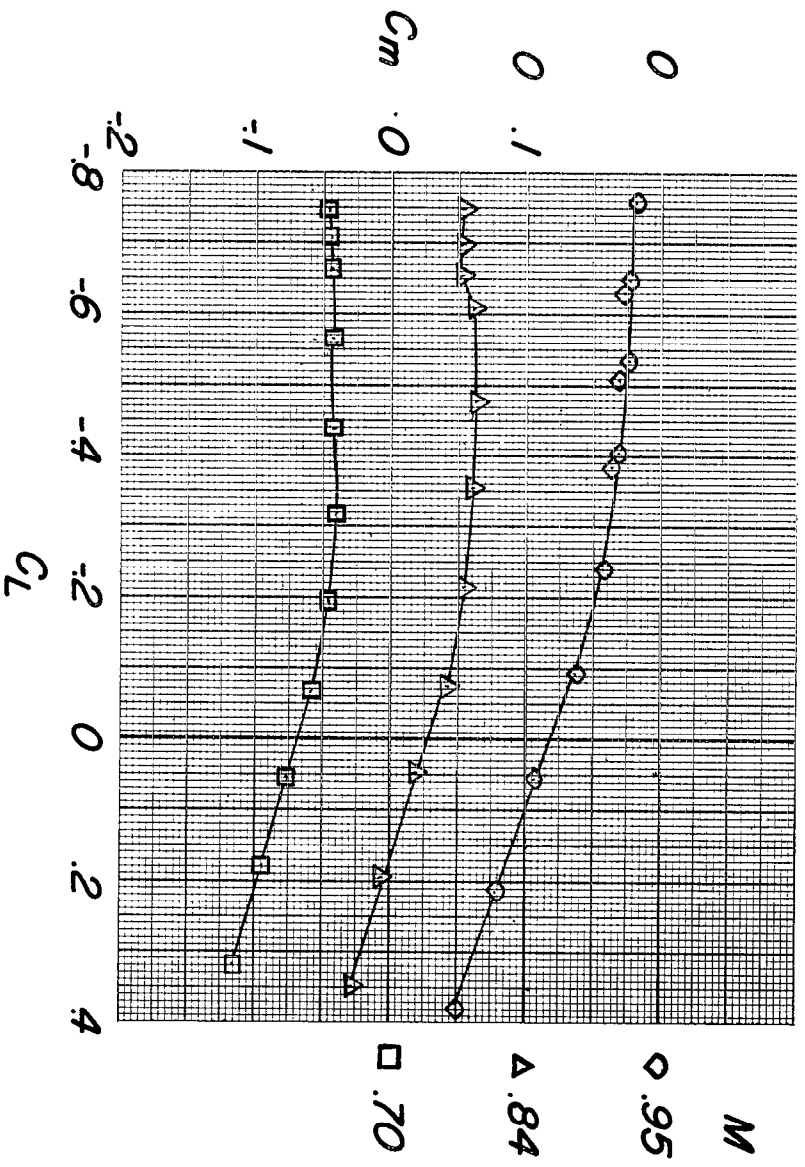
Figure 9.- Concluded.

~~SECRET~~



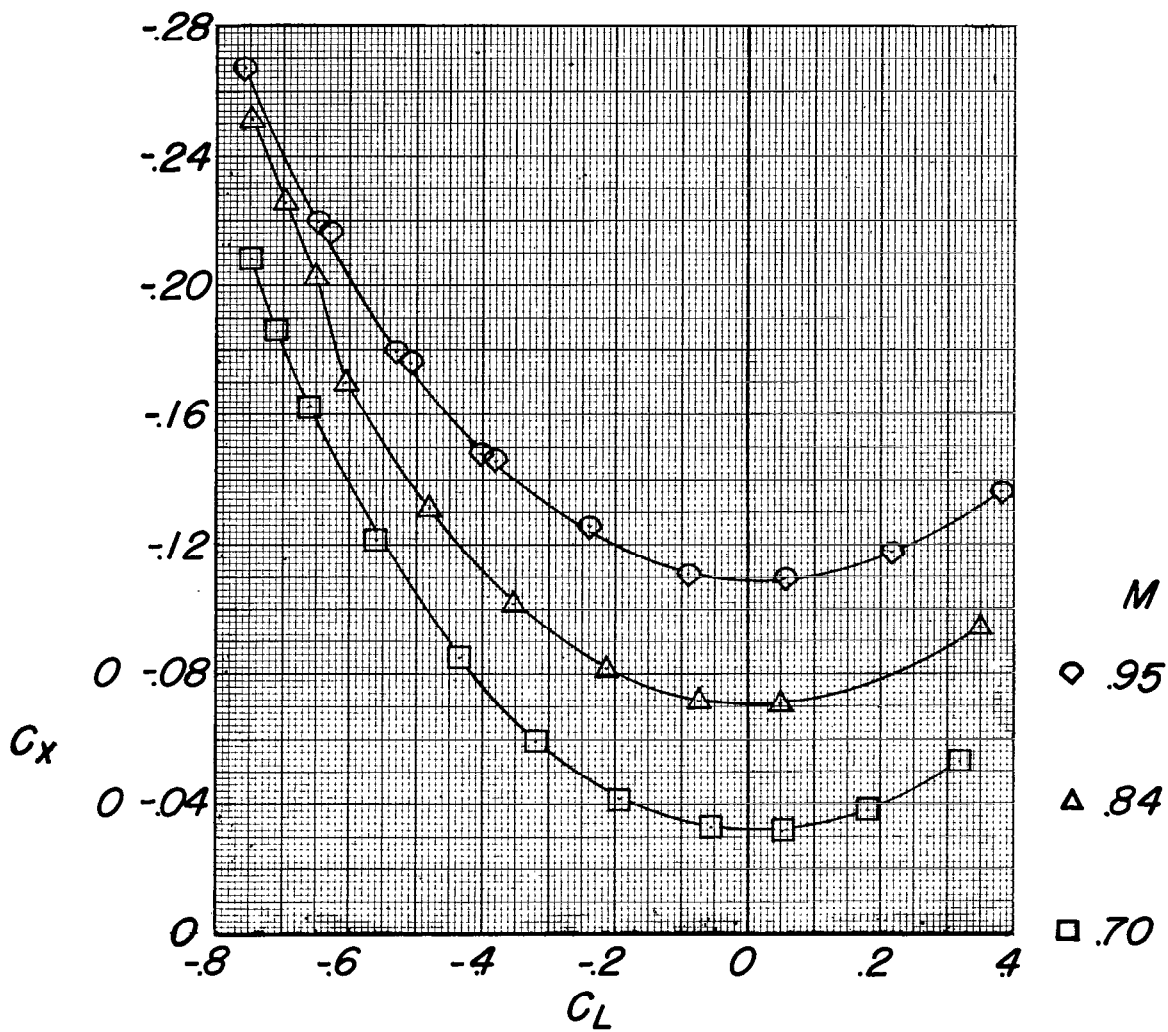
(a) α against C_L .

Figure 10.- The effect of Mach number on the aerodynamic characteristics in pitch at negative angles of attack. Fence A; $i_t = 5^\circ$.



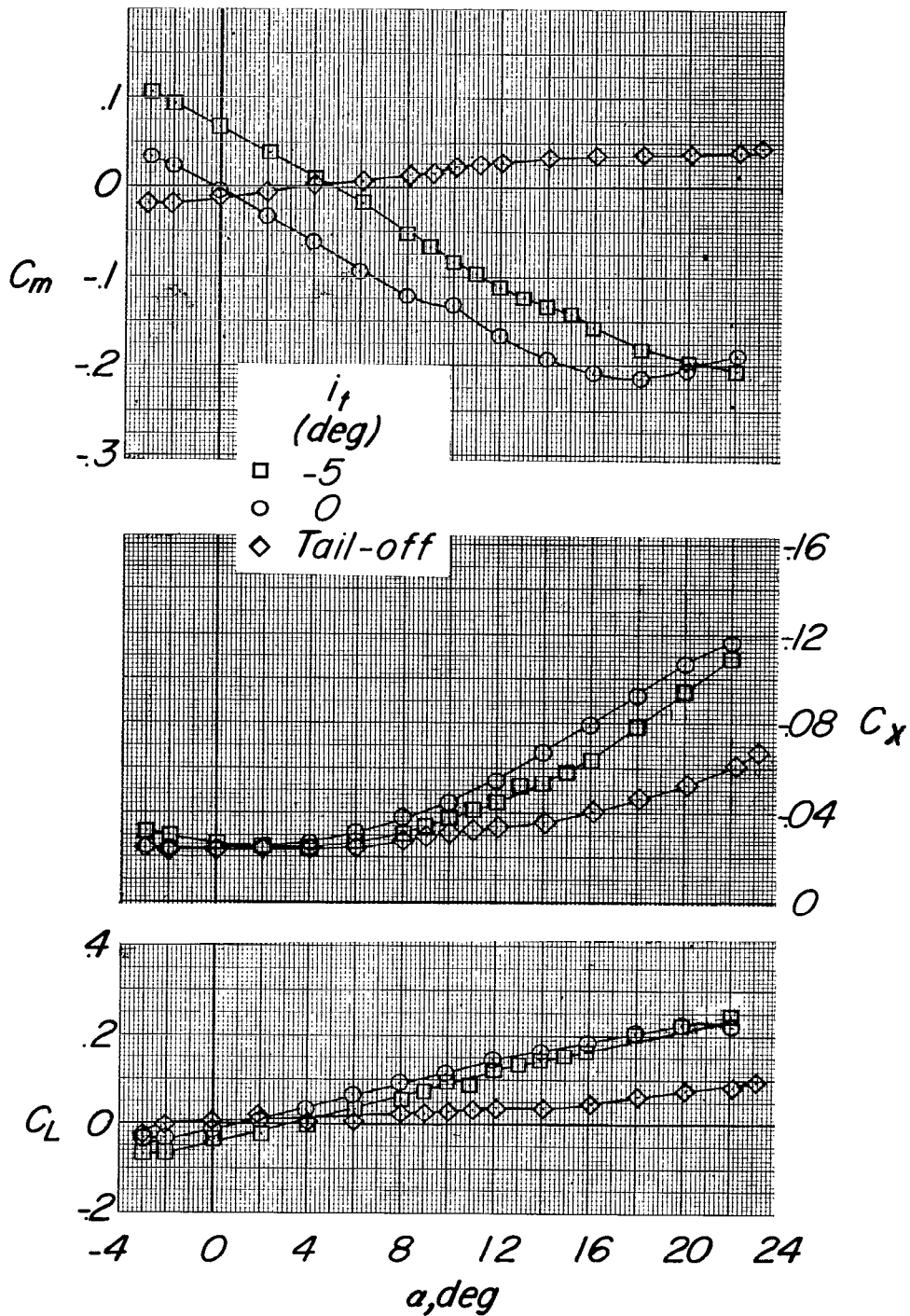
(b) C_m against C_L .

Figure 10.- Continued.



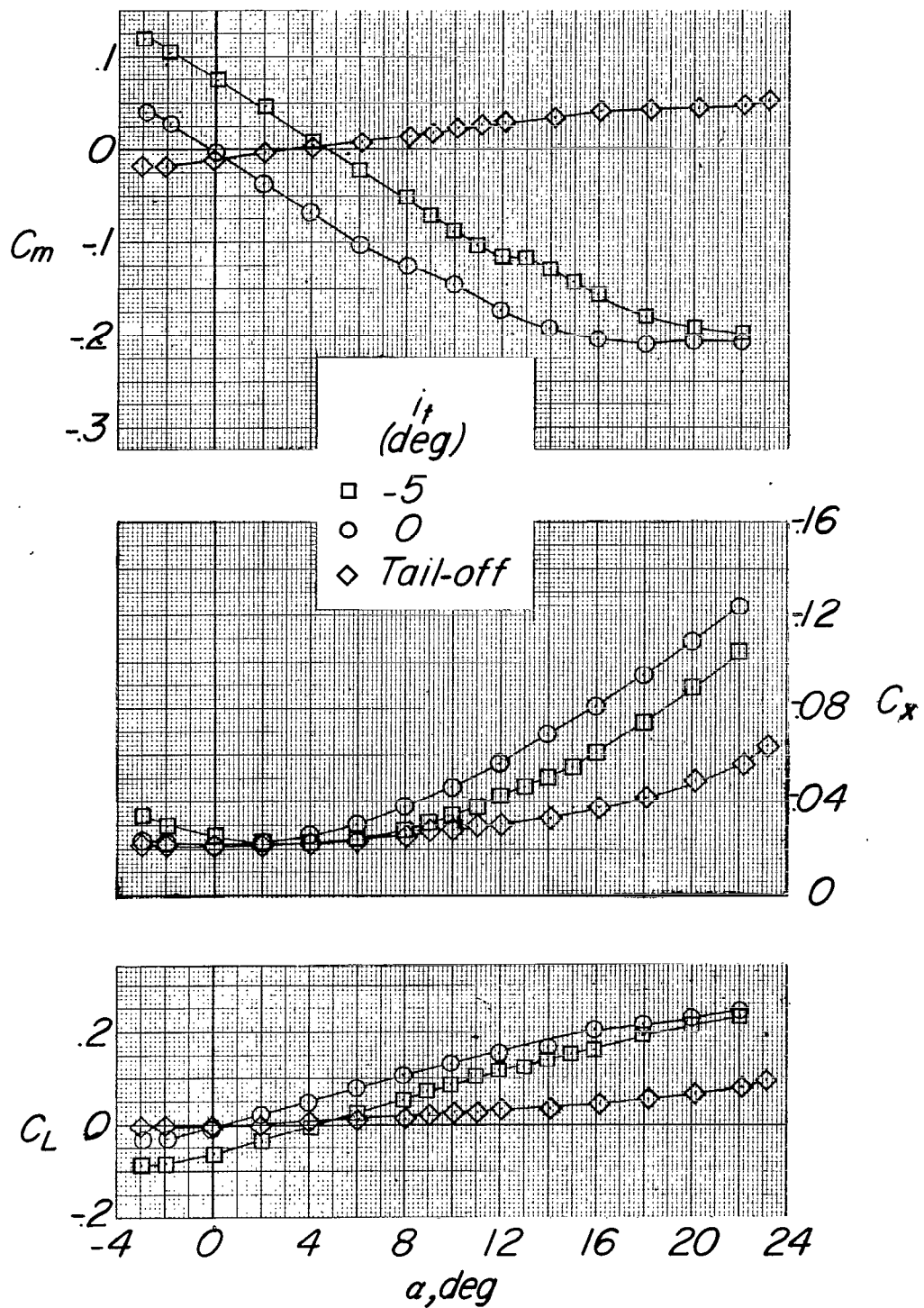
(c) C_x against C_L .

Figure 10.- Concluded.



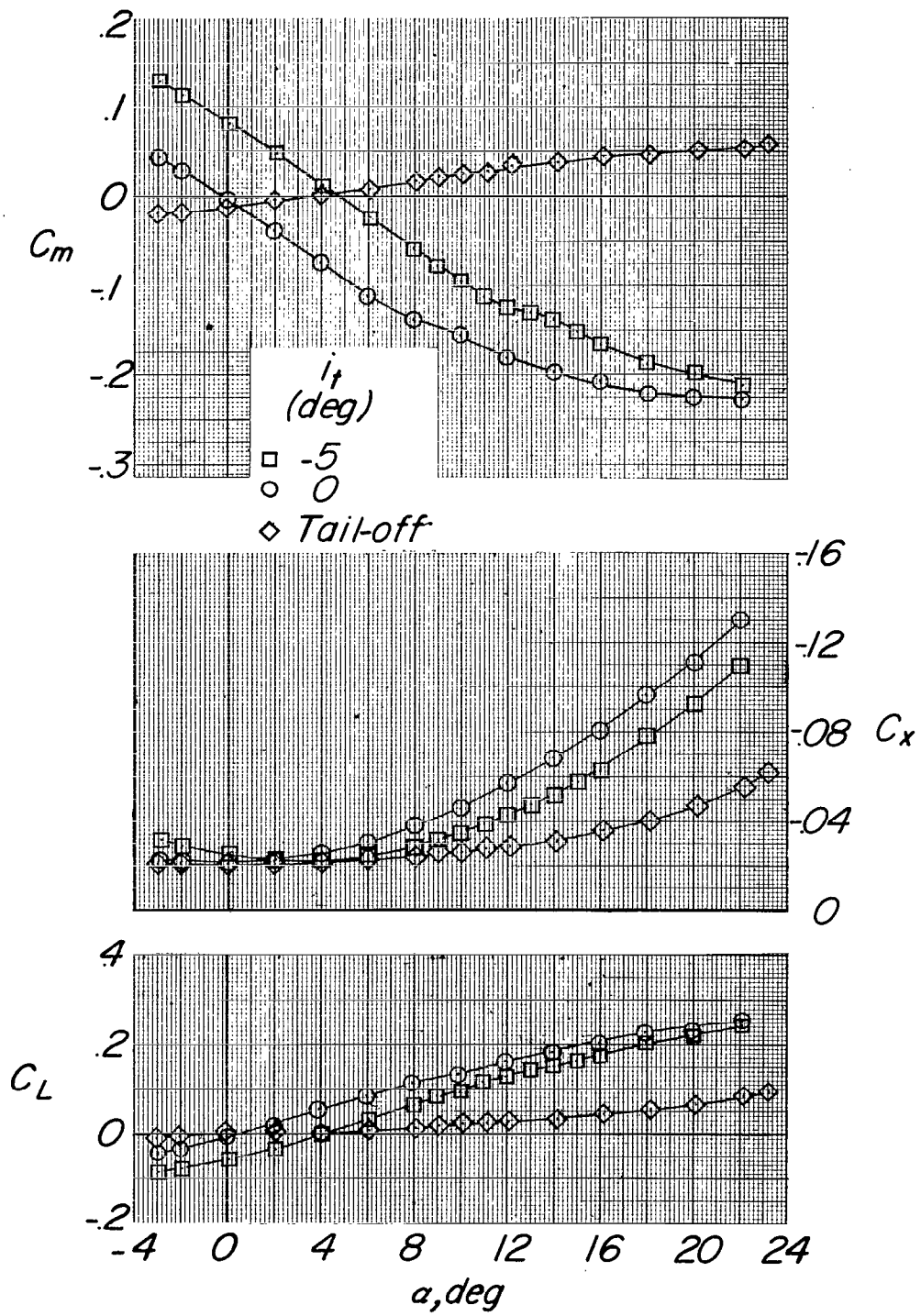
(a) $M = 0.70$.

Figure 11.- The effect of stabilizer incidence on the aerodynamic characteristics in pitch. Fuselage, horizontal- and vertical-tail combination.



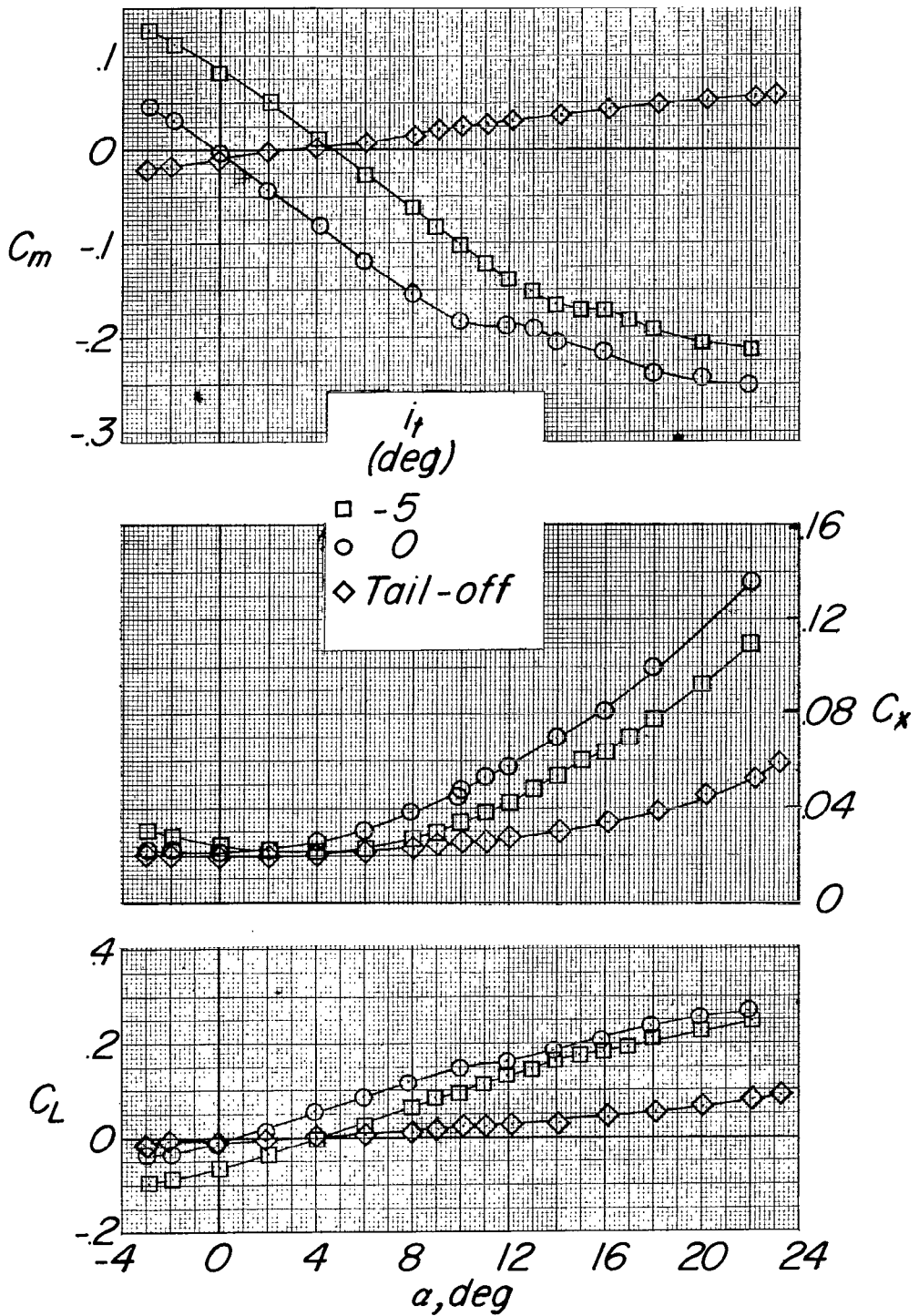
(b) $M = 0.84$.

Figure 11.- Continued.



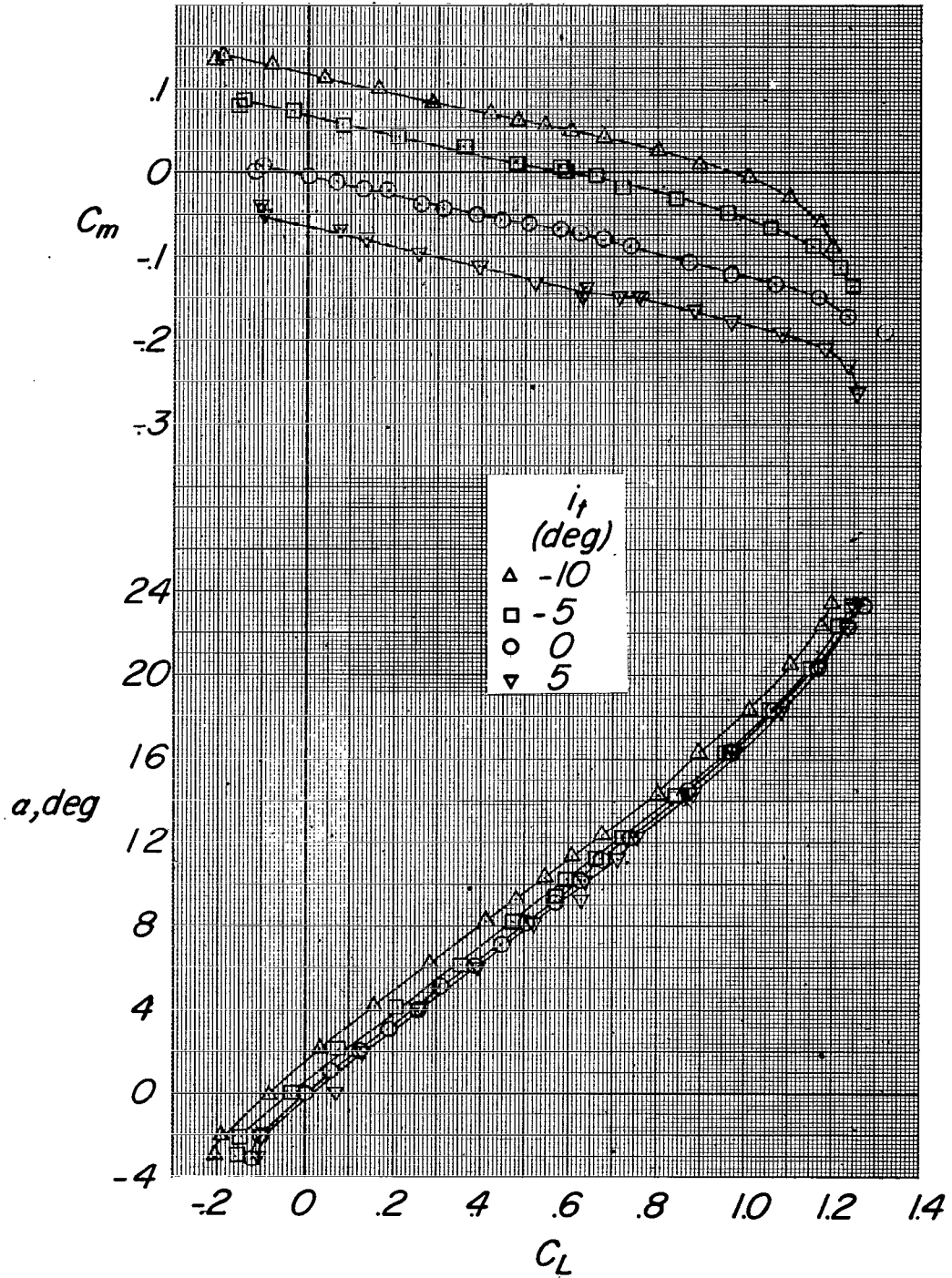
(c) $M = 0.90$.

Figure 11.- Continued.



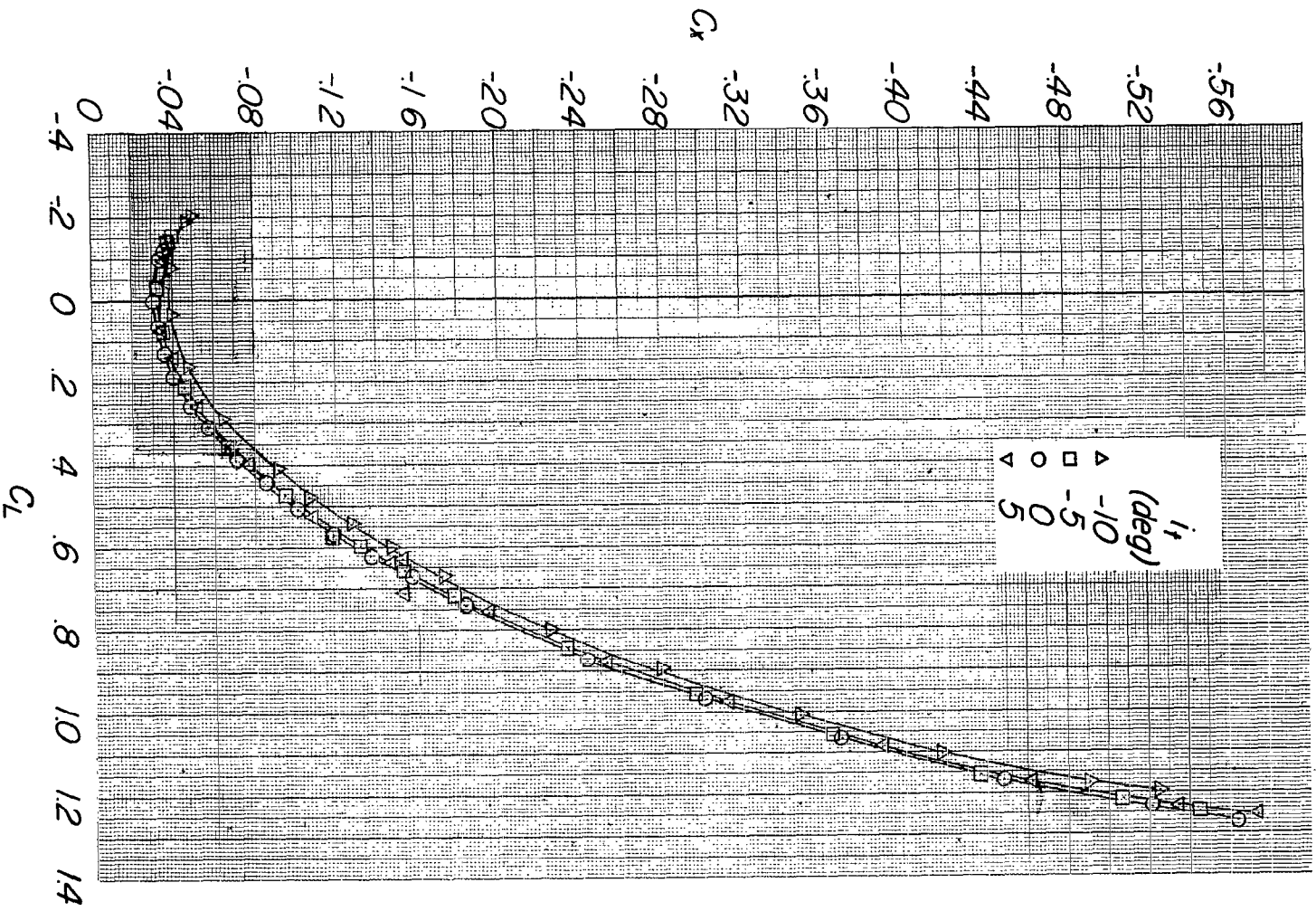
(d) $M = 0.95$.

Figure 11.- Concluded.



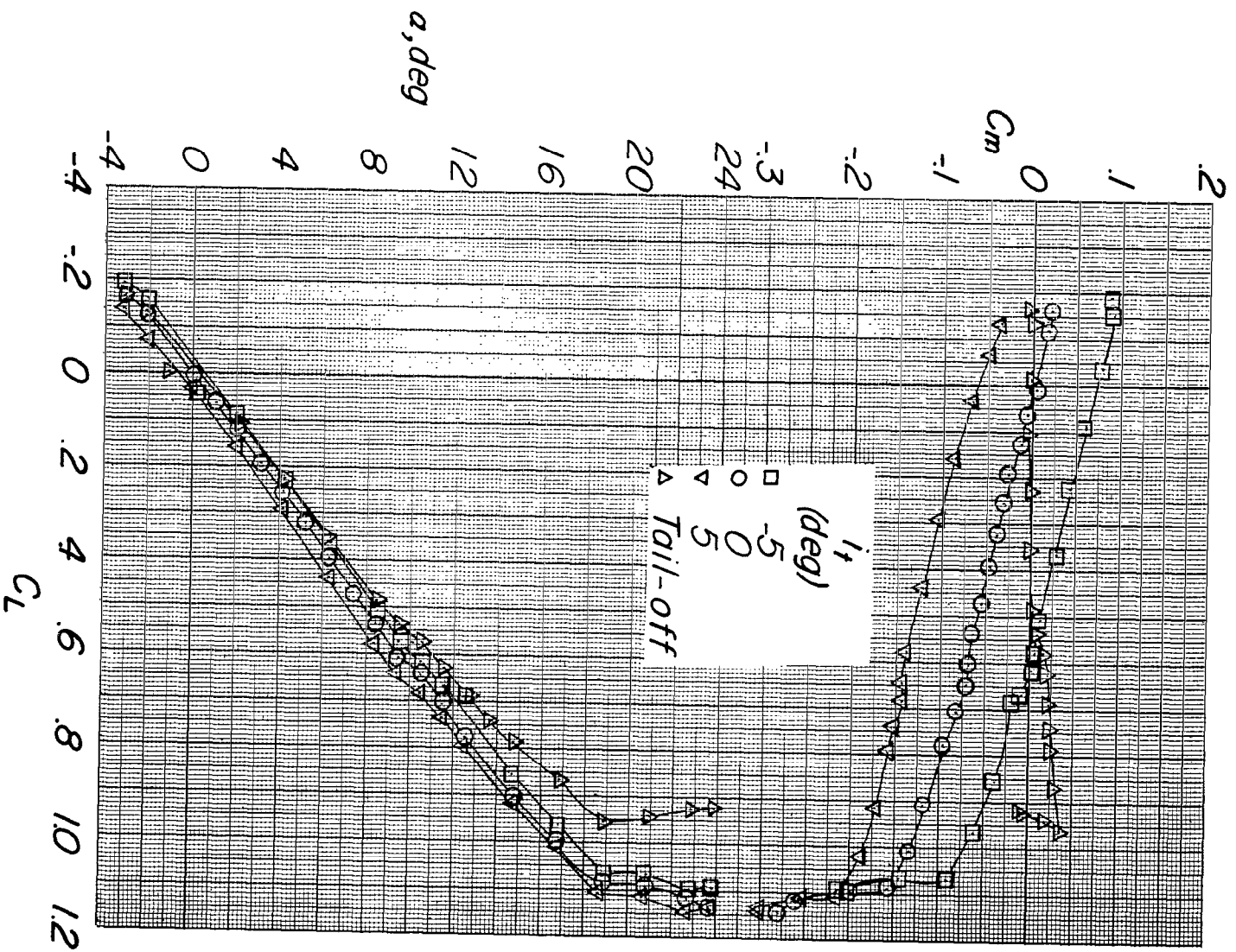
(a) $M = 0.40$.

Figure 12.- The effect of stabilizer incidence on the aerodynamic characteristics in pitch. No fence.



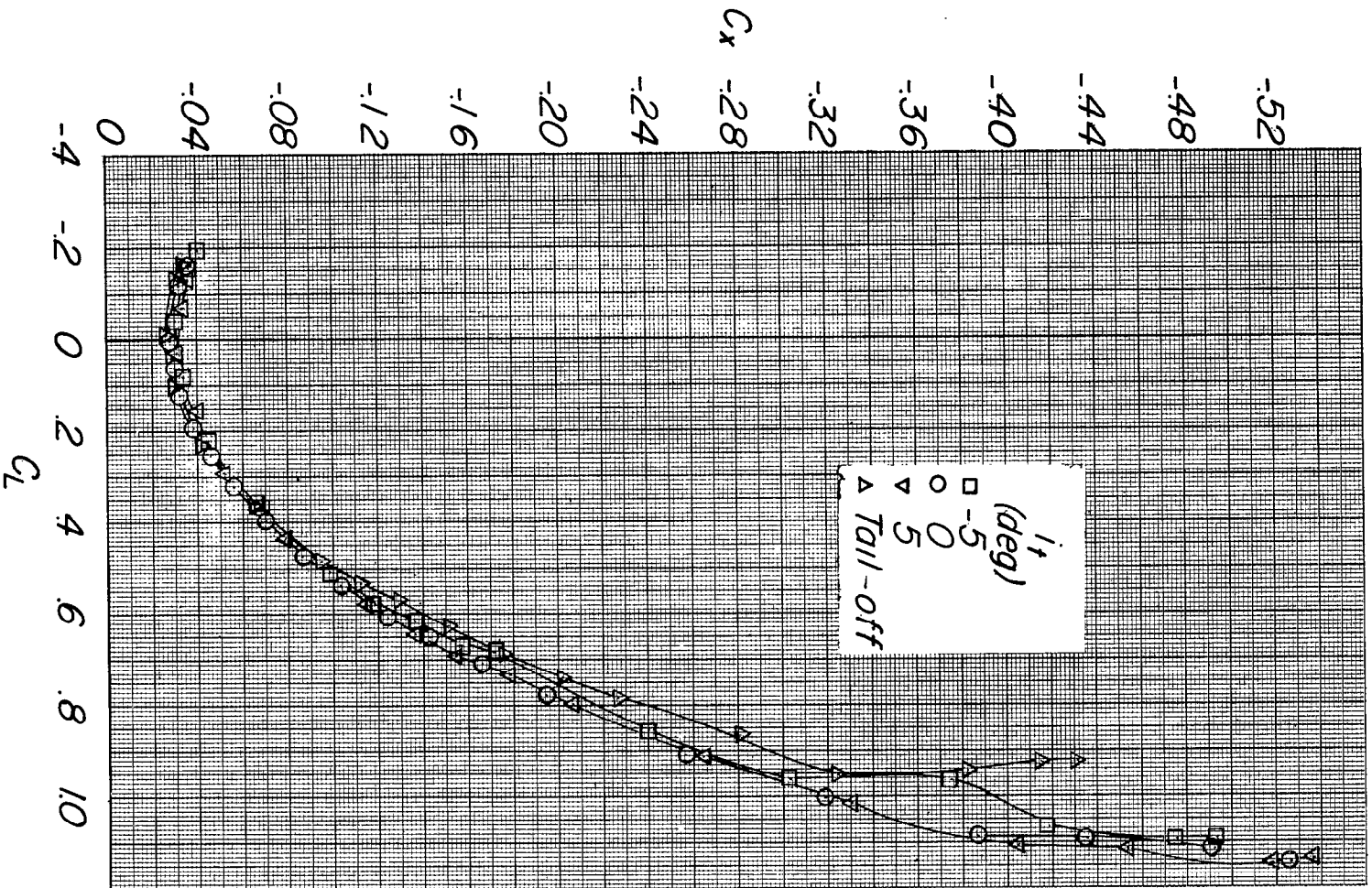
(a) Concluded.

Figure 12.- Continued.



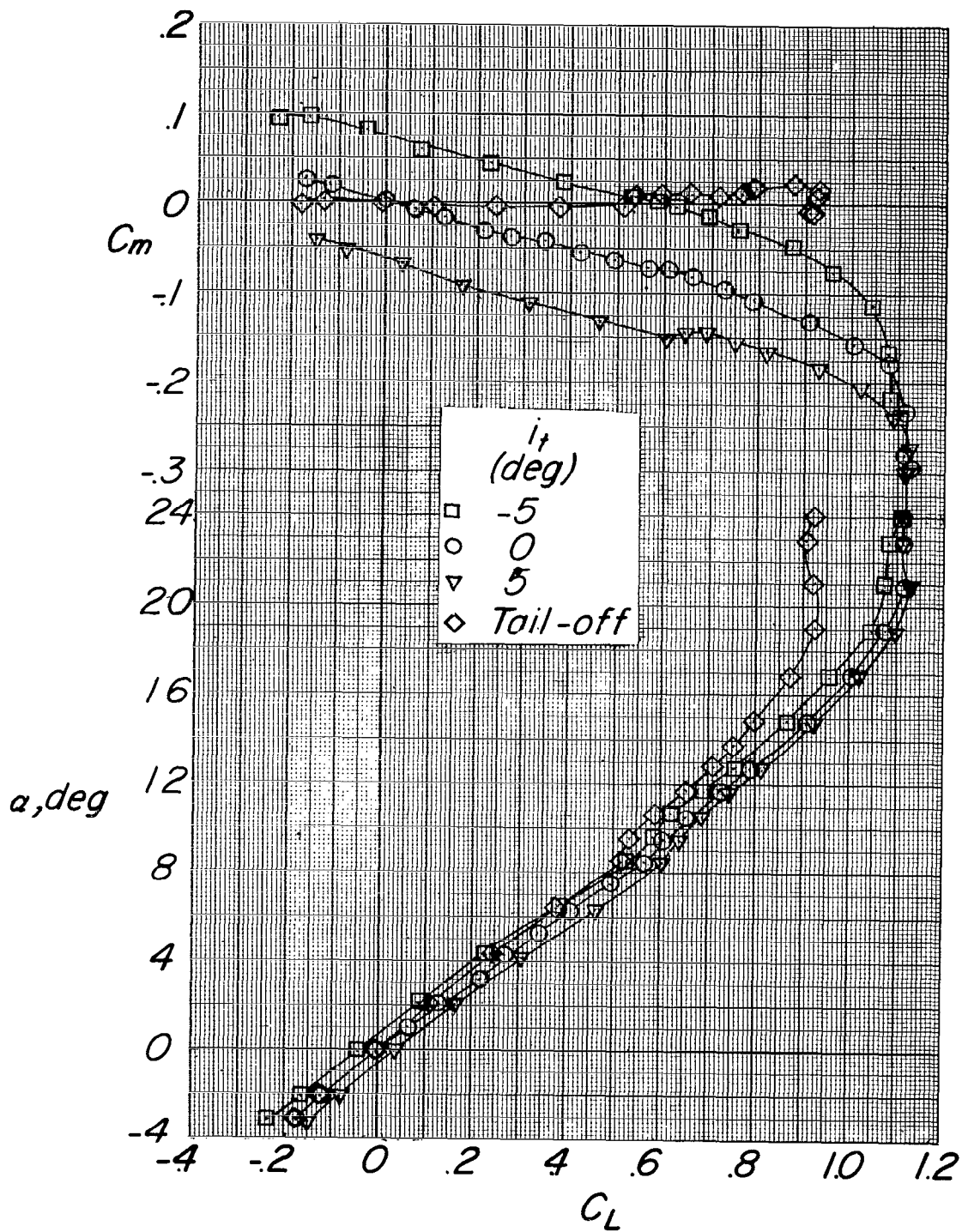
(b) $M = 0.70$.

Figure 12.- Continued.



(b) Concluded.

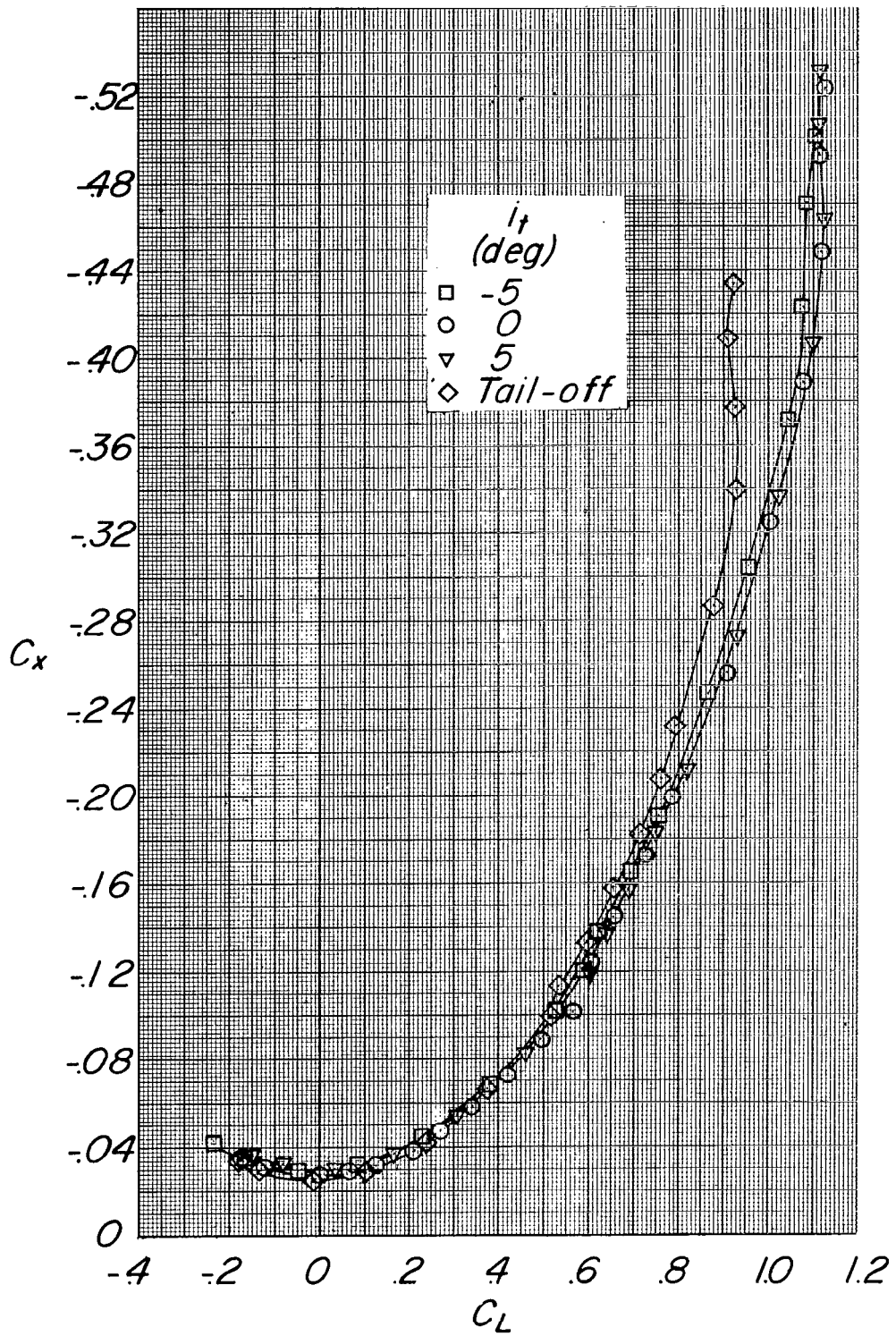
Figure 12.- Continued.



(c) $M = 0.80$.

Figure 12.- Continued.

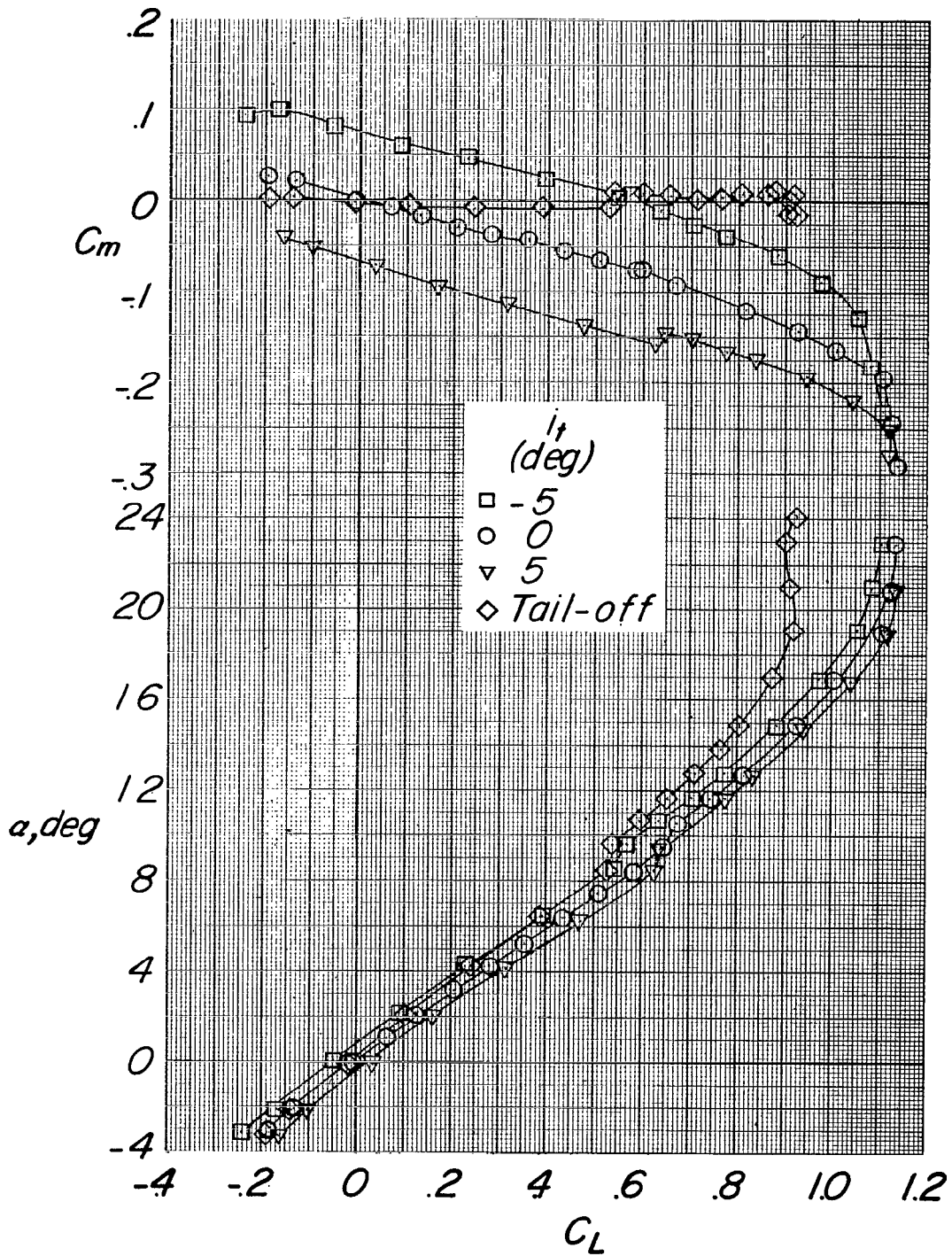
~~SECRET~~



(c) Concluded.

Figure 12.- Continued.

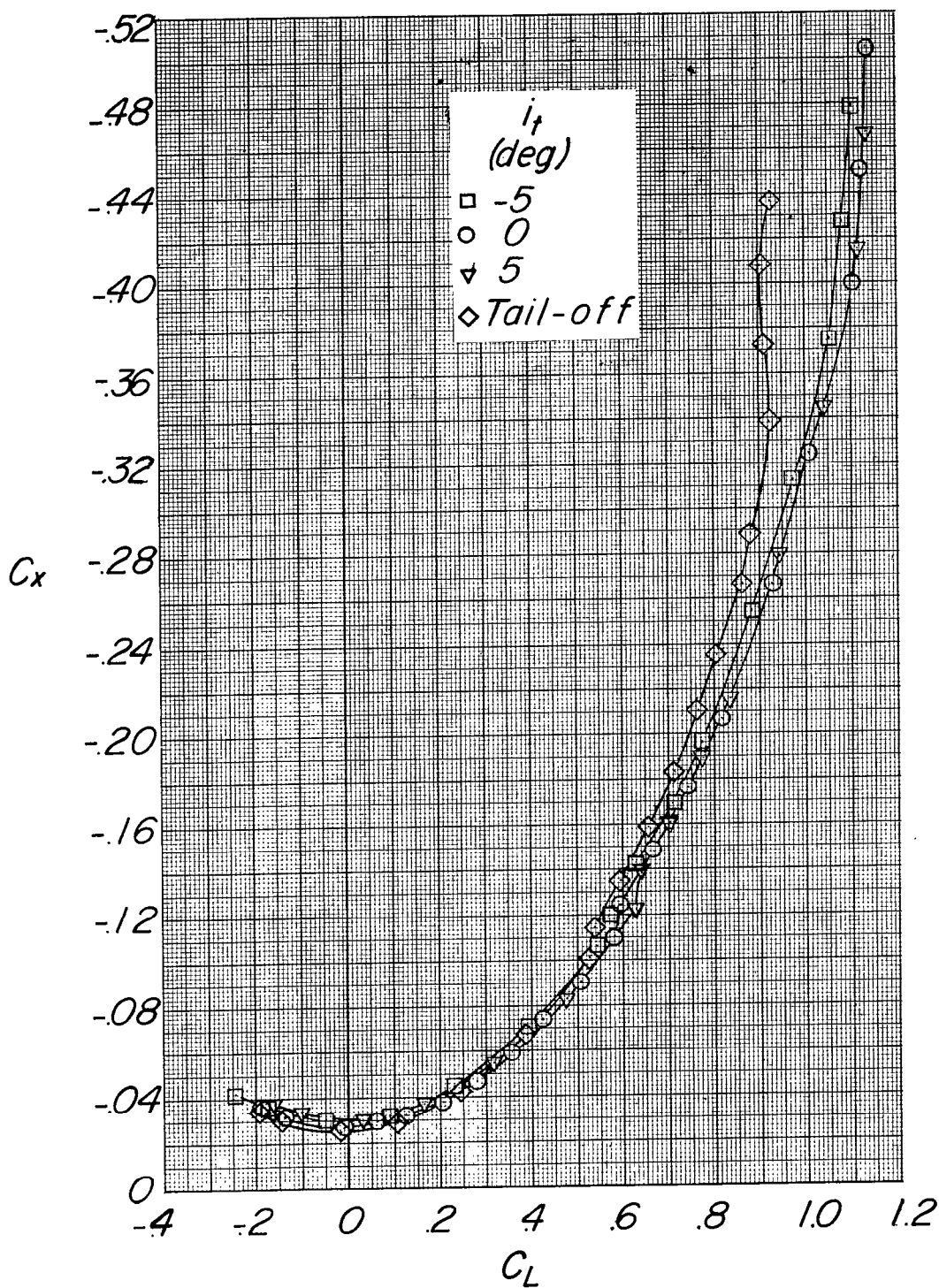
~~SECRET~~



(a) $M = 0.84$.

Figure 12.- Continued.

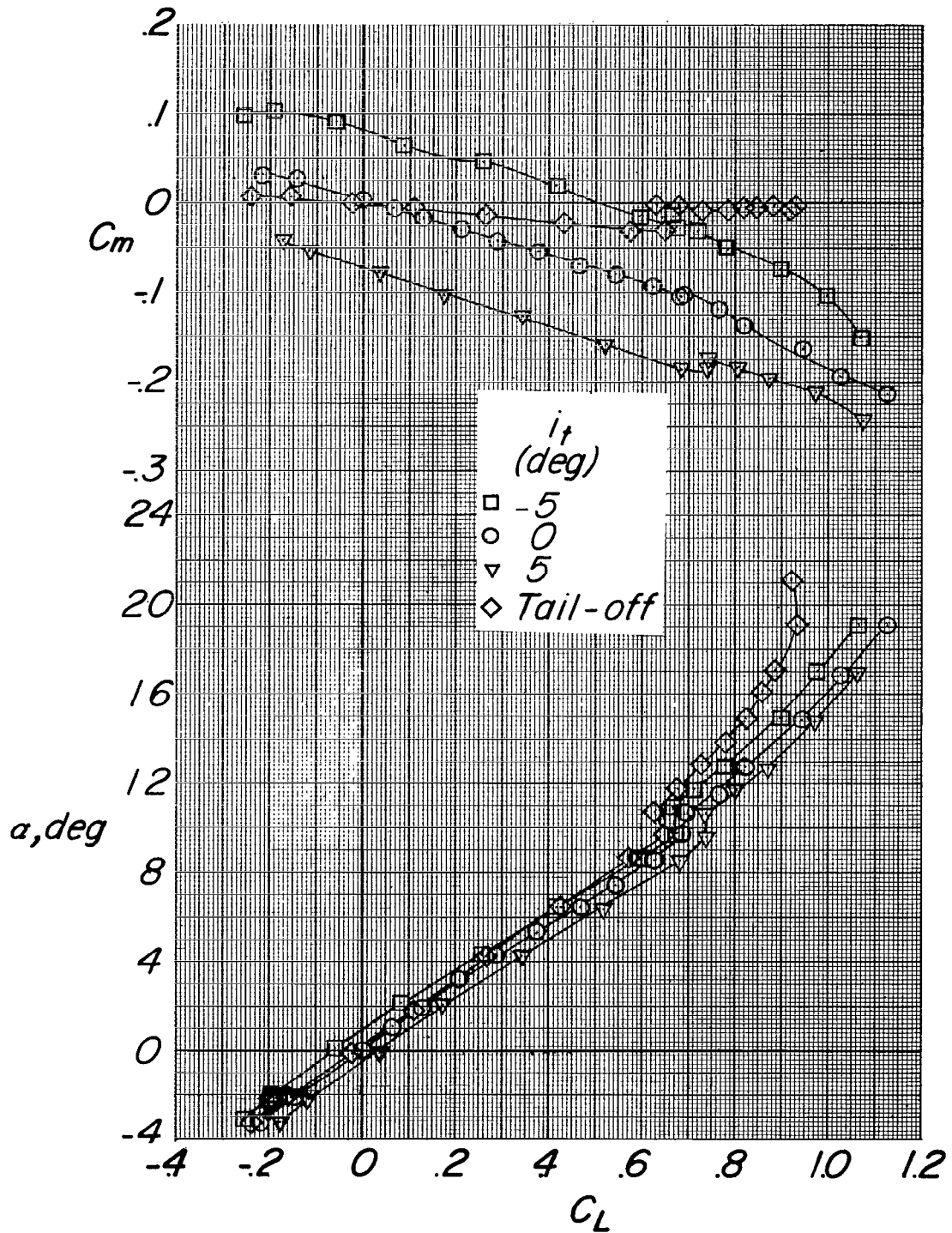
~~CONFIDENTIAL~~



(d) Concluded.

Figure 12.- Continued.

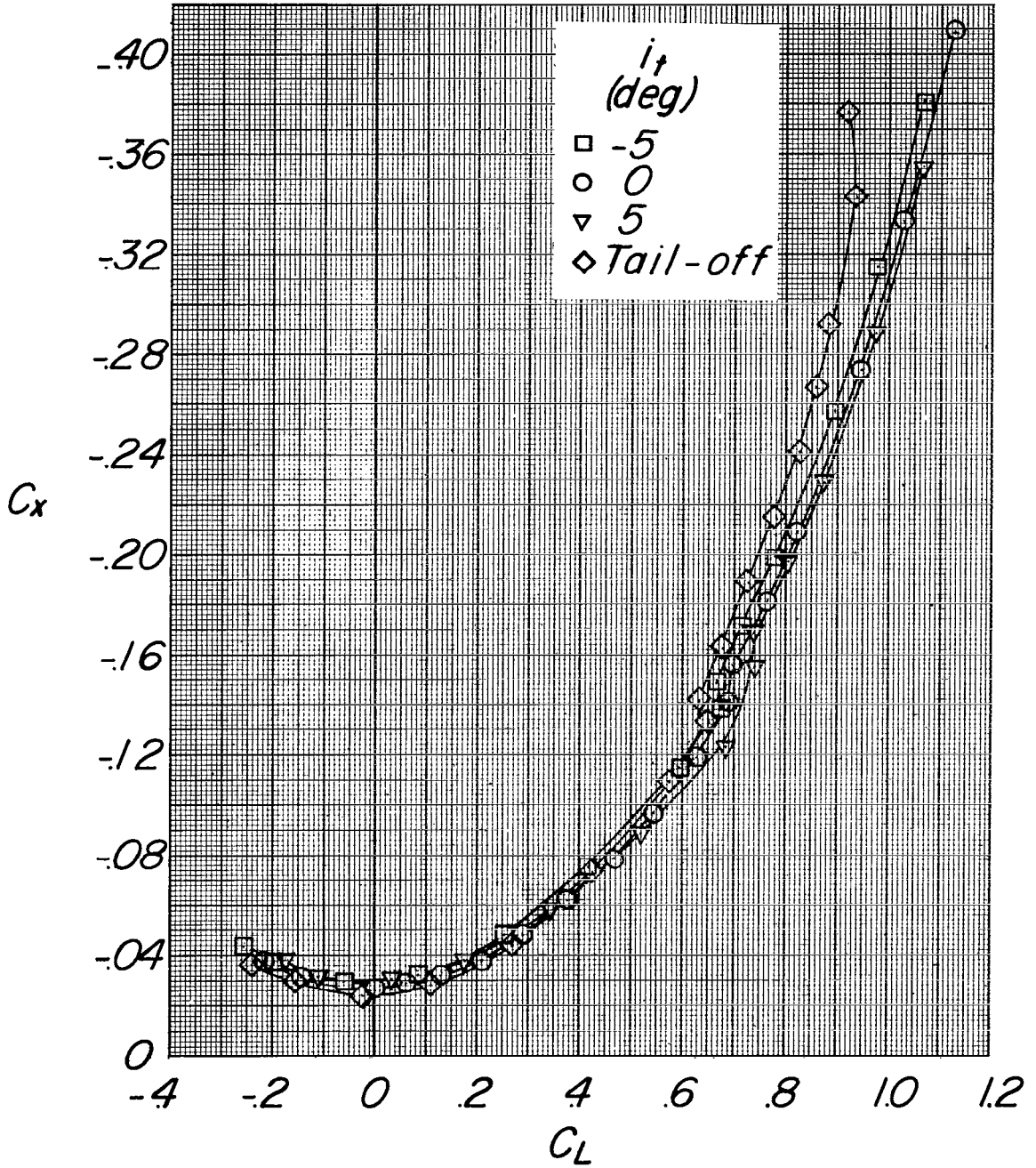
~~CONFIDENTIAL~~



(e) $M = 0.90$.

Figure 12.- Continued.

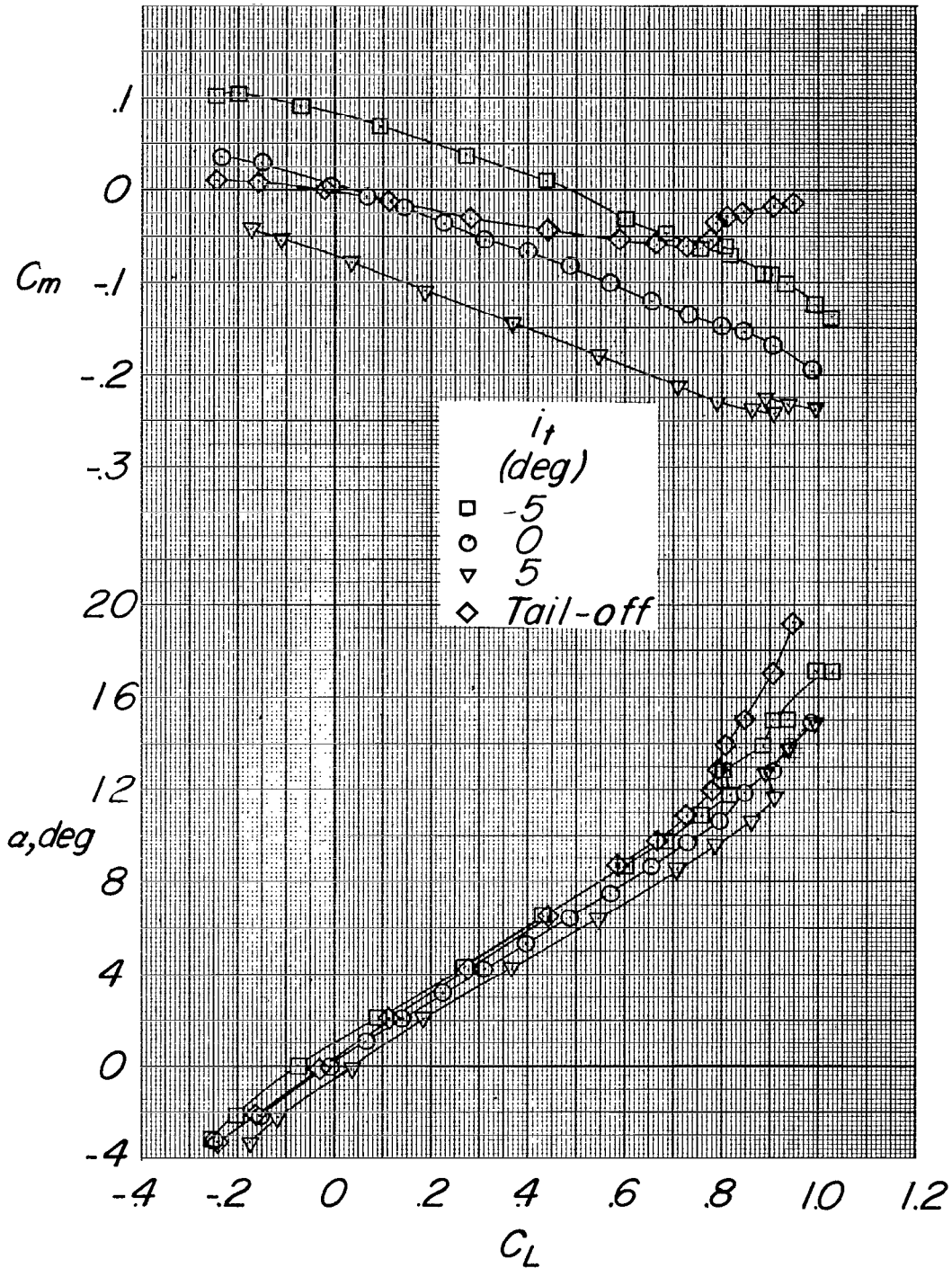
~~SECRET~~



(e) Concluded.

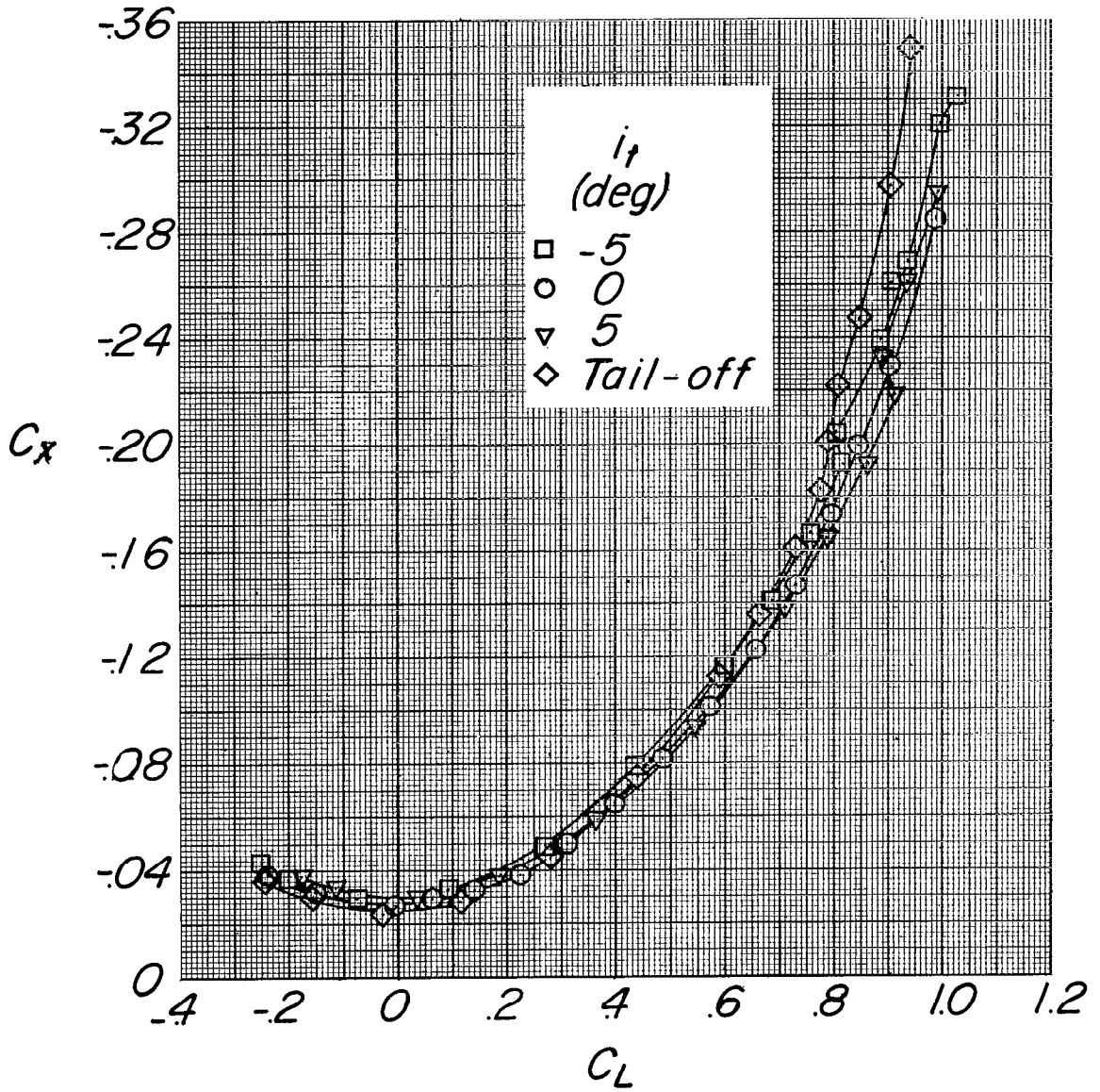
Figure 12.- Continued.

~~SECRET~~



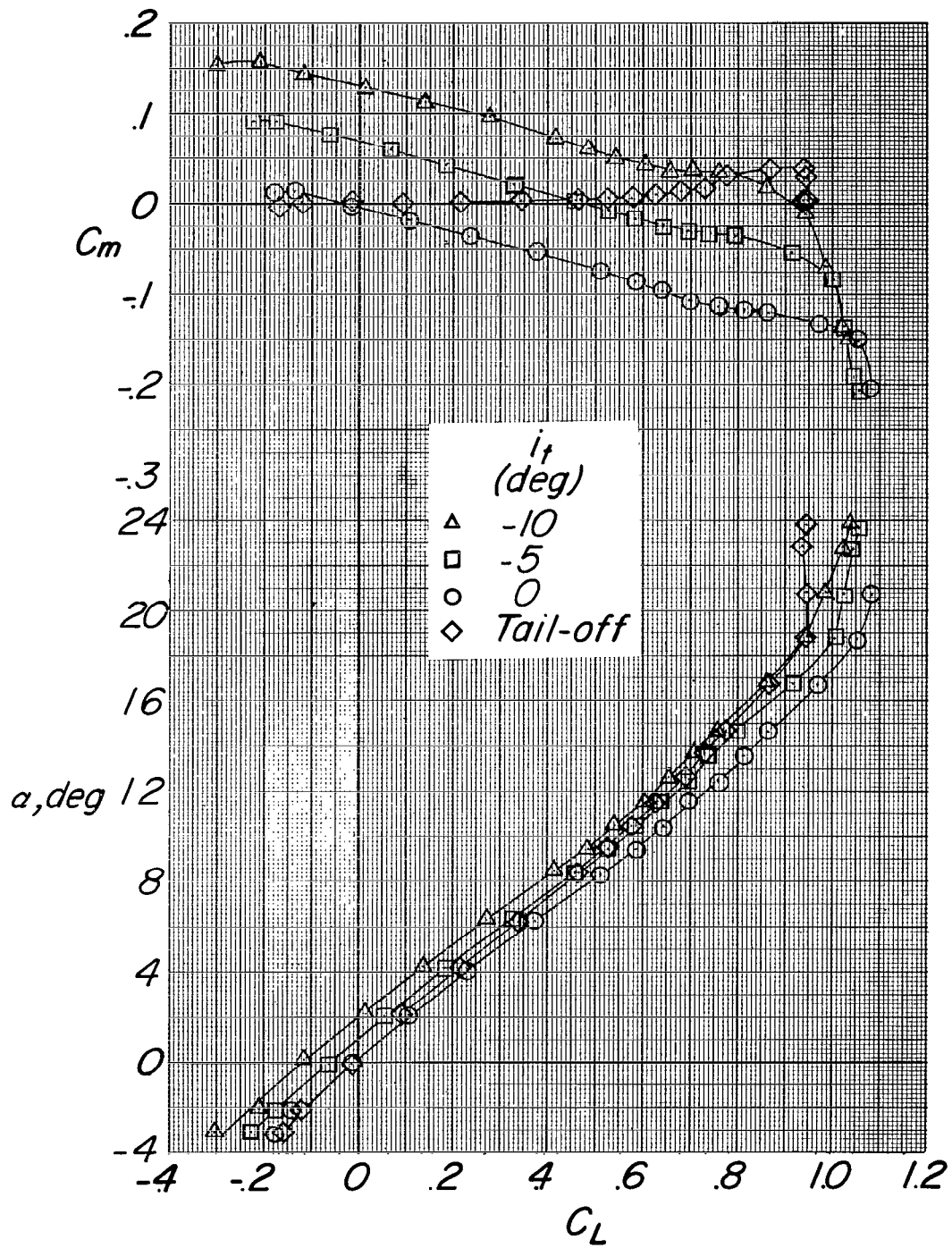
(f) $M = 0.95$.

Figure 12.- Continued.



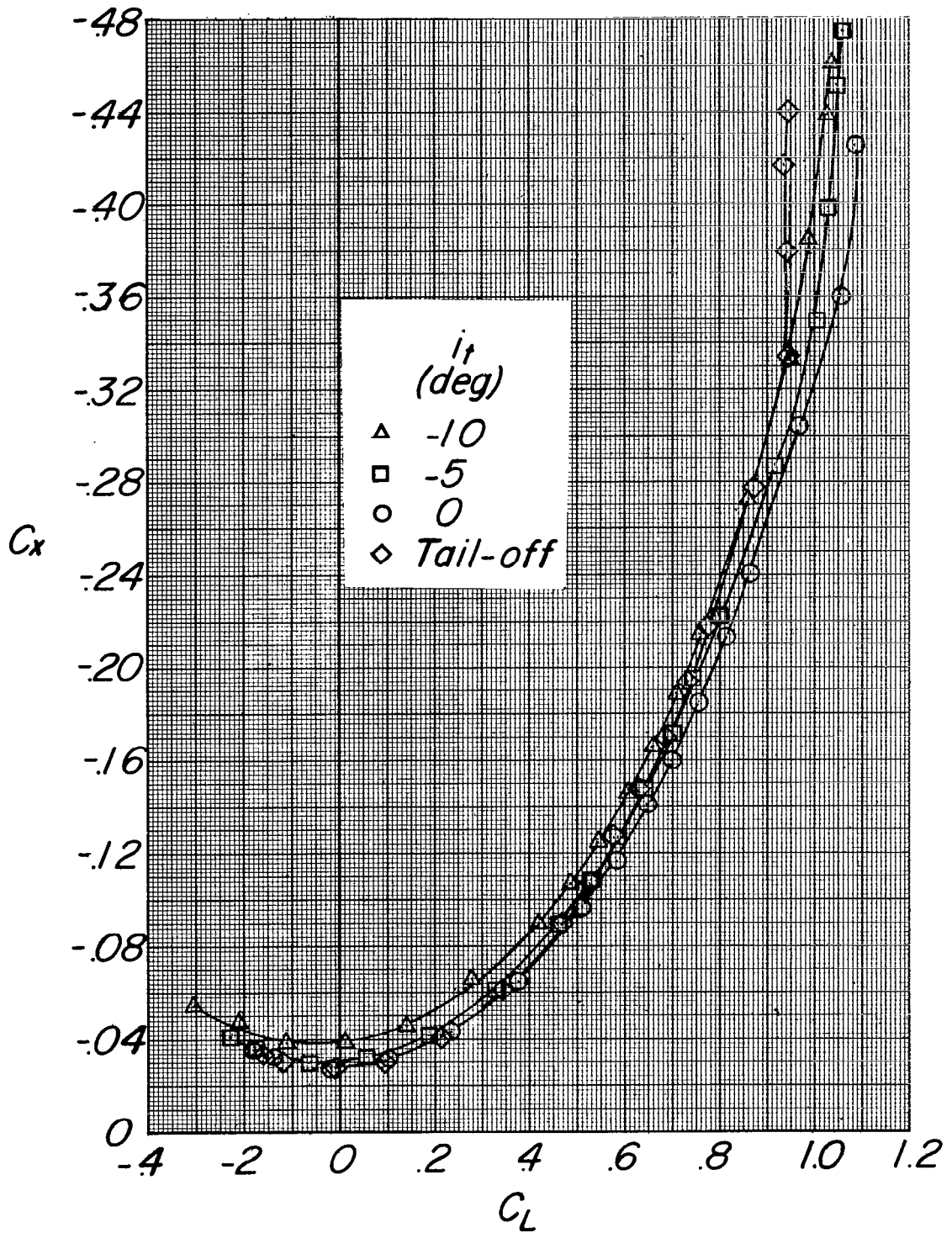
(f) Concluded.

Figure 12.- Concluded.



(a) $M = 0.70$.

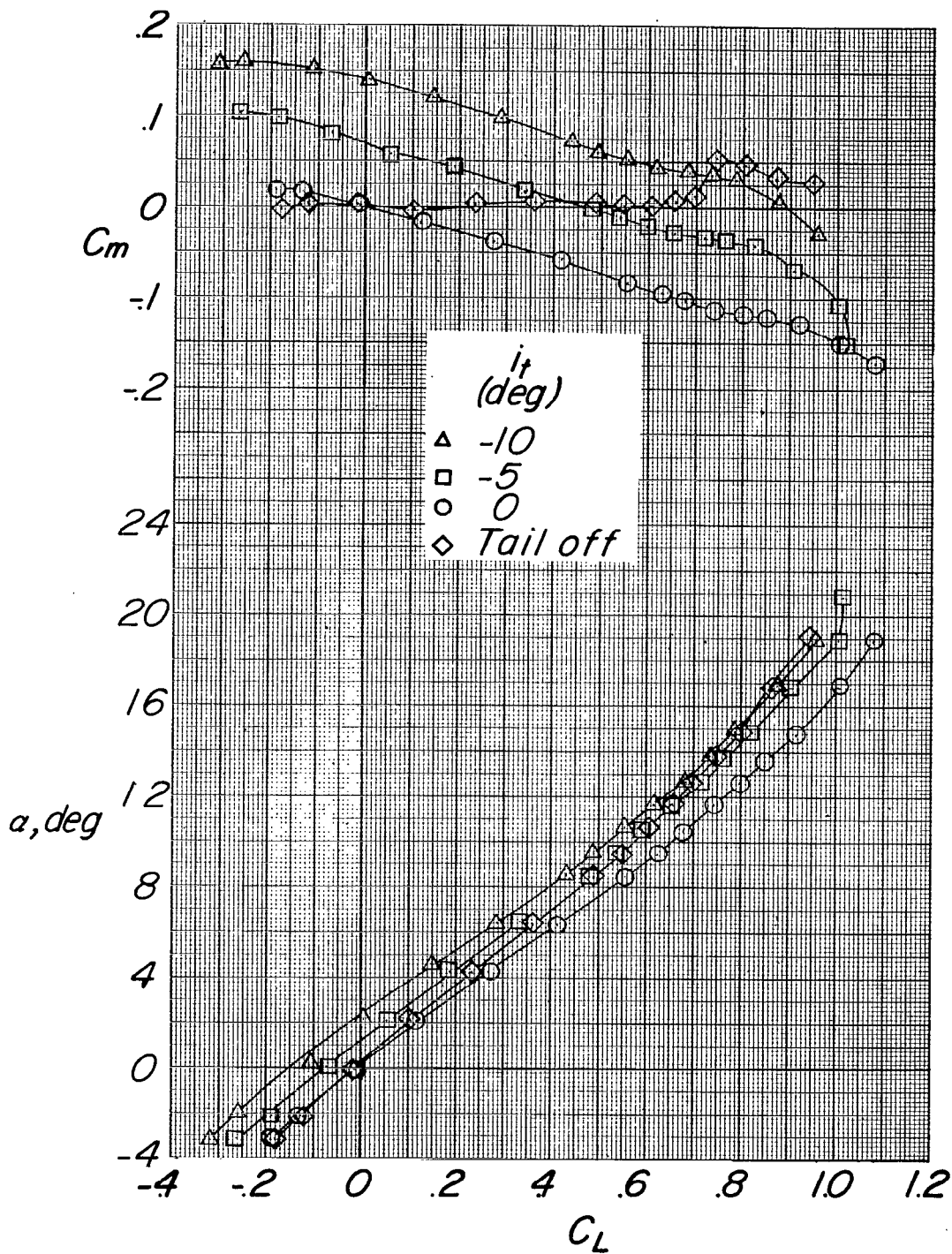
Figure 13.- The effect of stabilizer incidence on the aerodynamic characteristics in pitch. Fence A.



(a) Concluded.

Figure 13.- Continued.

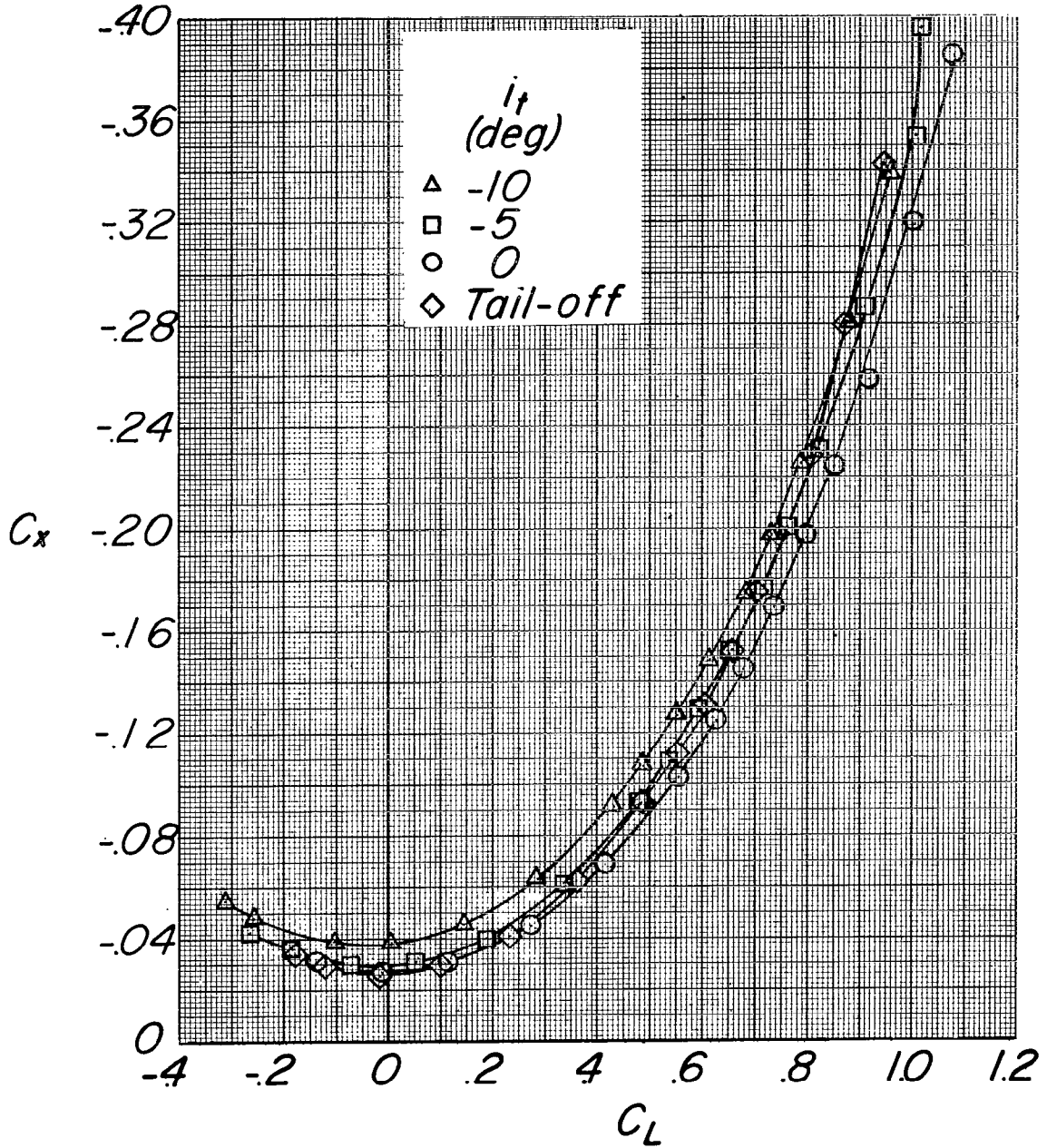
~~SECRET~~



(b) $M = 0.80$.

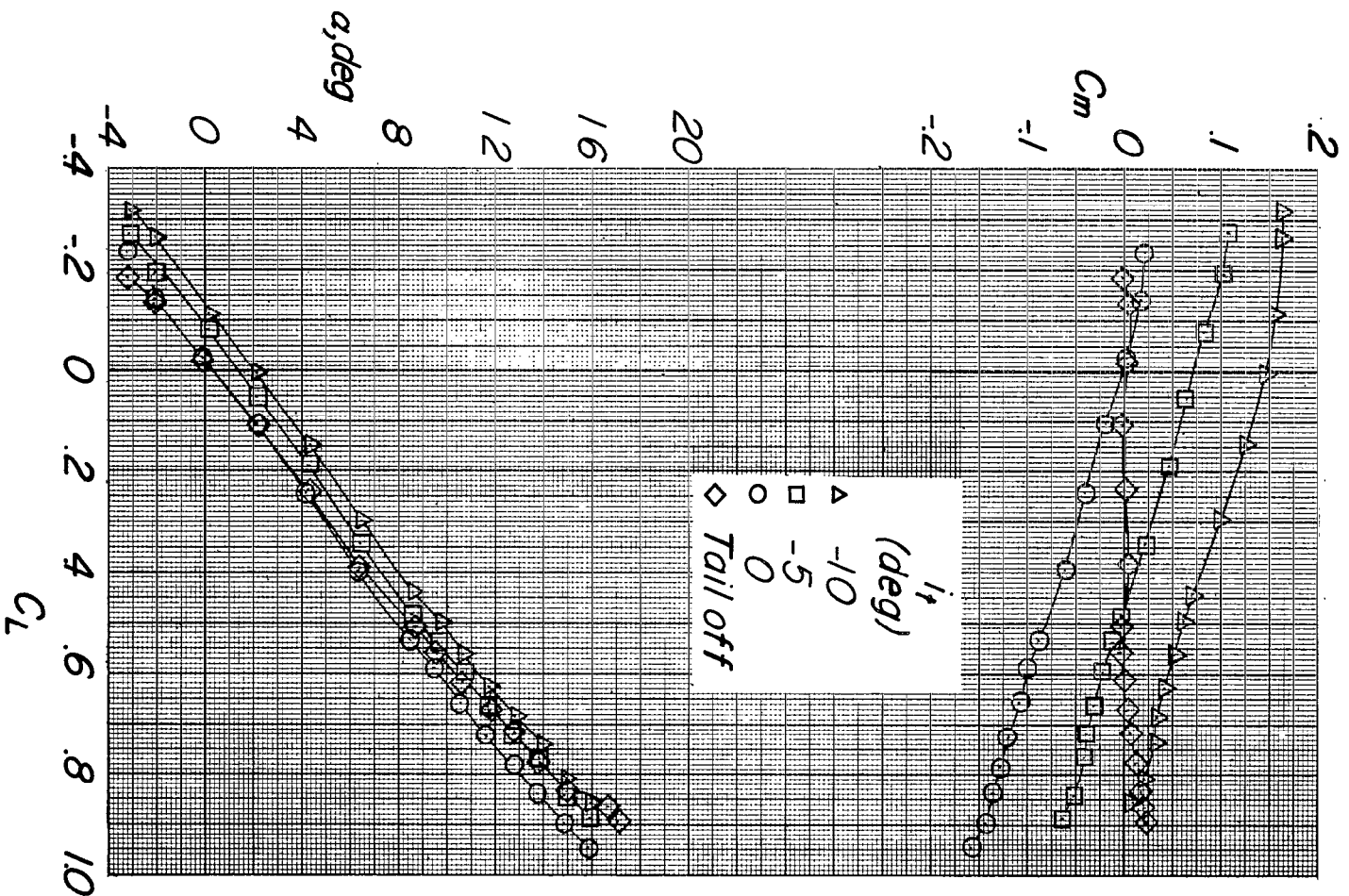
Figure 13.- Continued.

~~SECRET~~



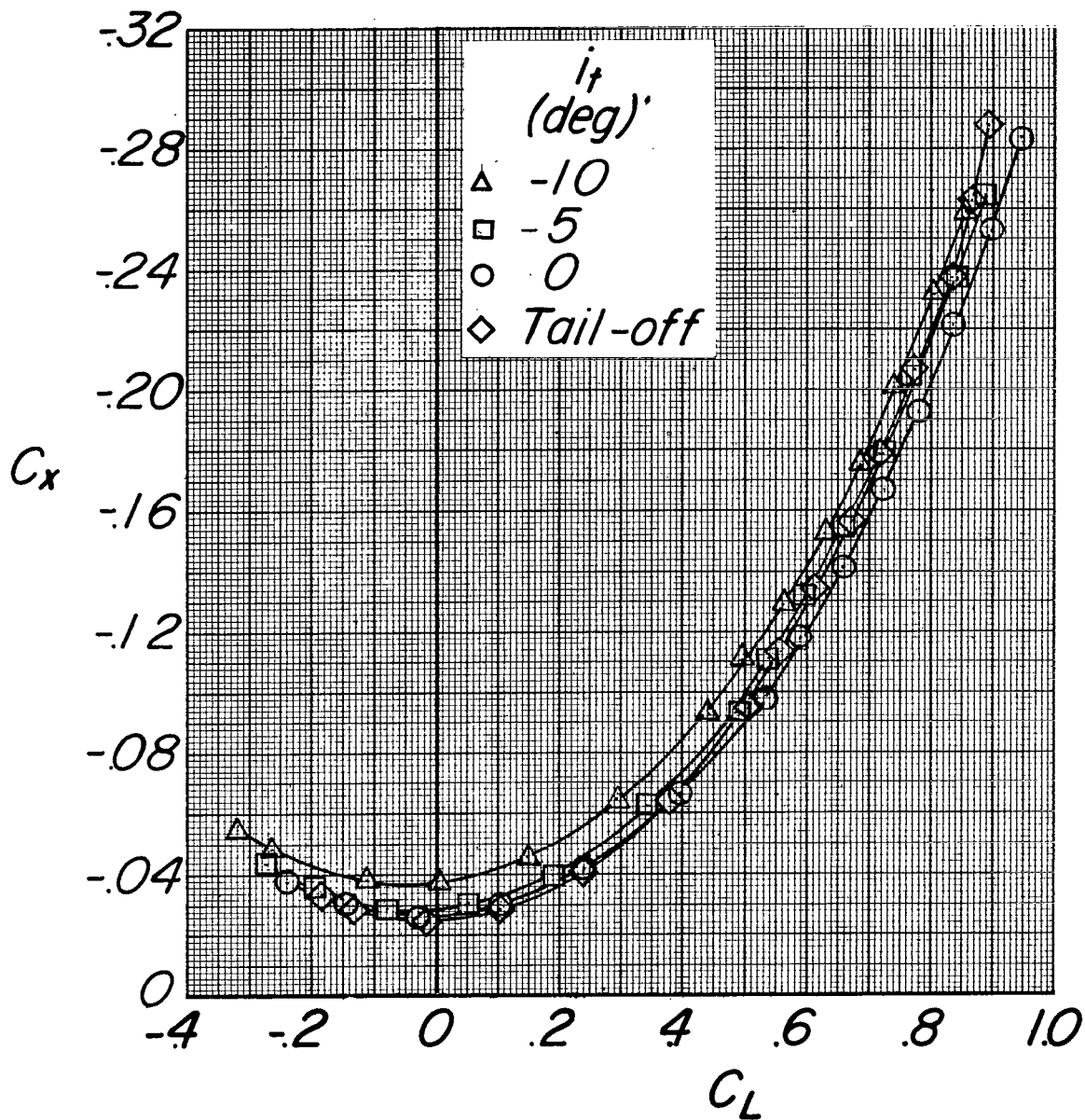
(b) Concluded.

Figure 13.- Continued.



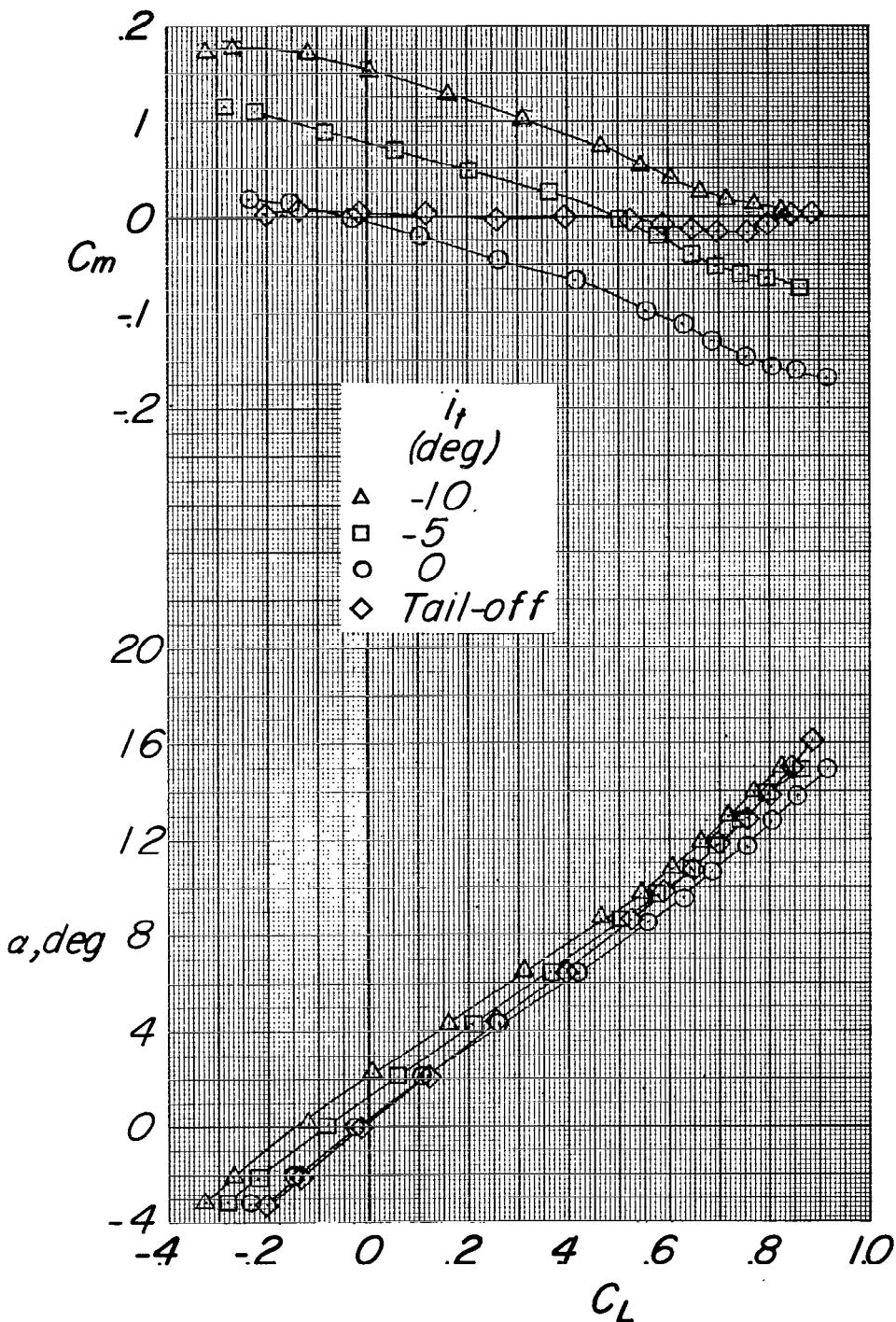
(c) $M = 0.84$.

Figure 13.- Continued.



(c) Concluded.

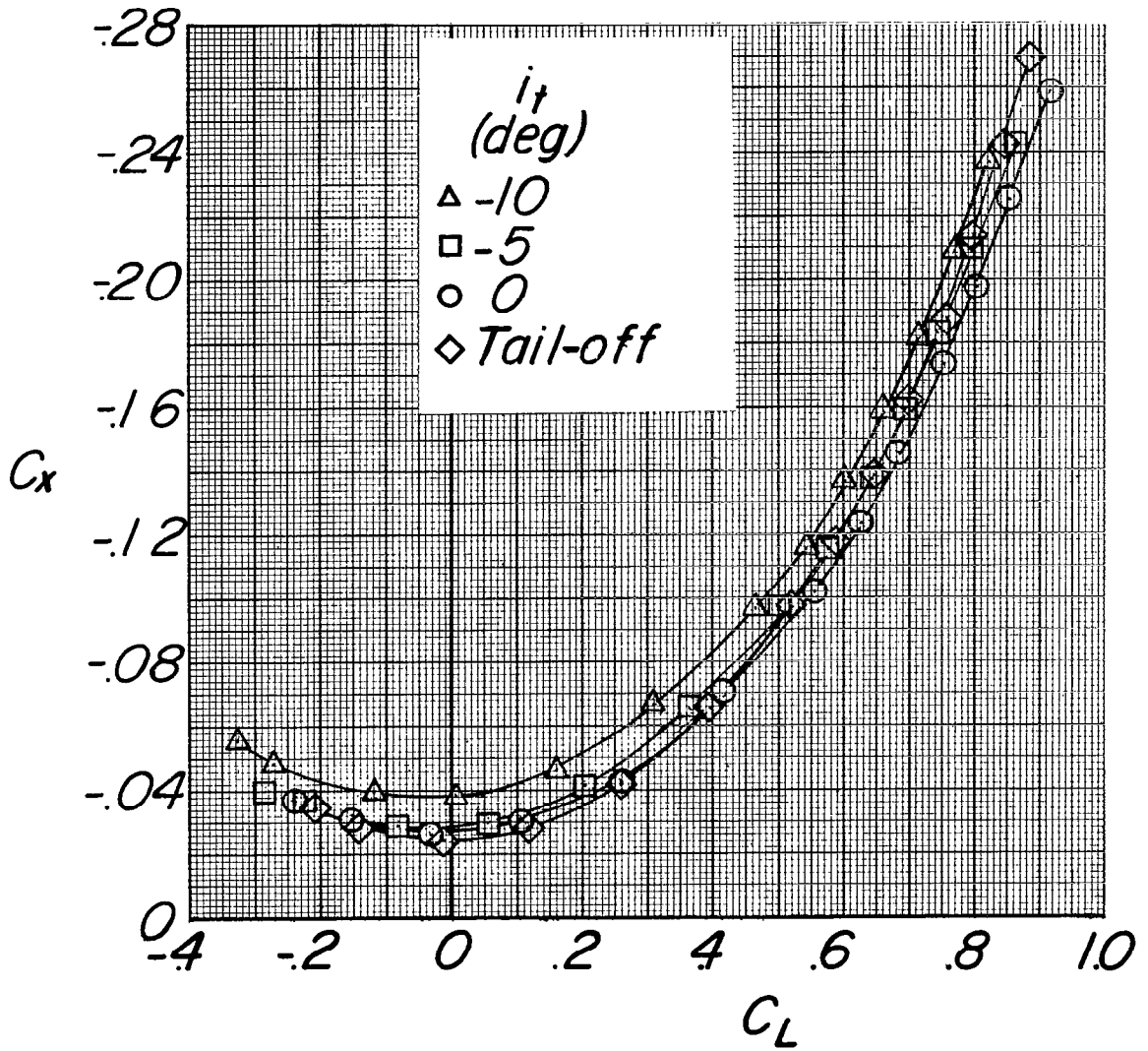
Figure 13.- Continued.



(d) $M = 0.90$.

Figure 13.- Continued.

~~SECRET~~

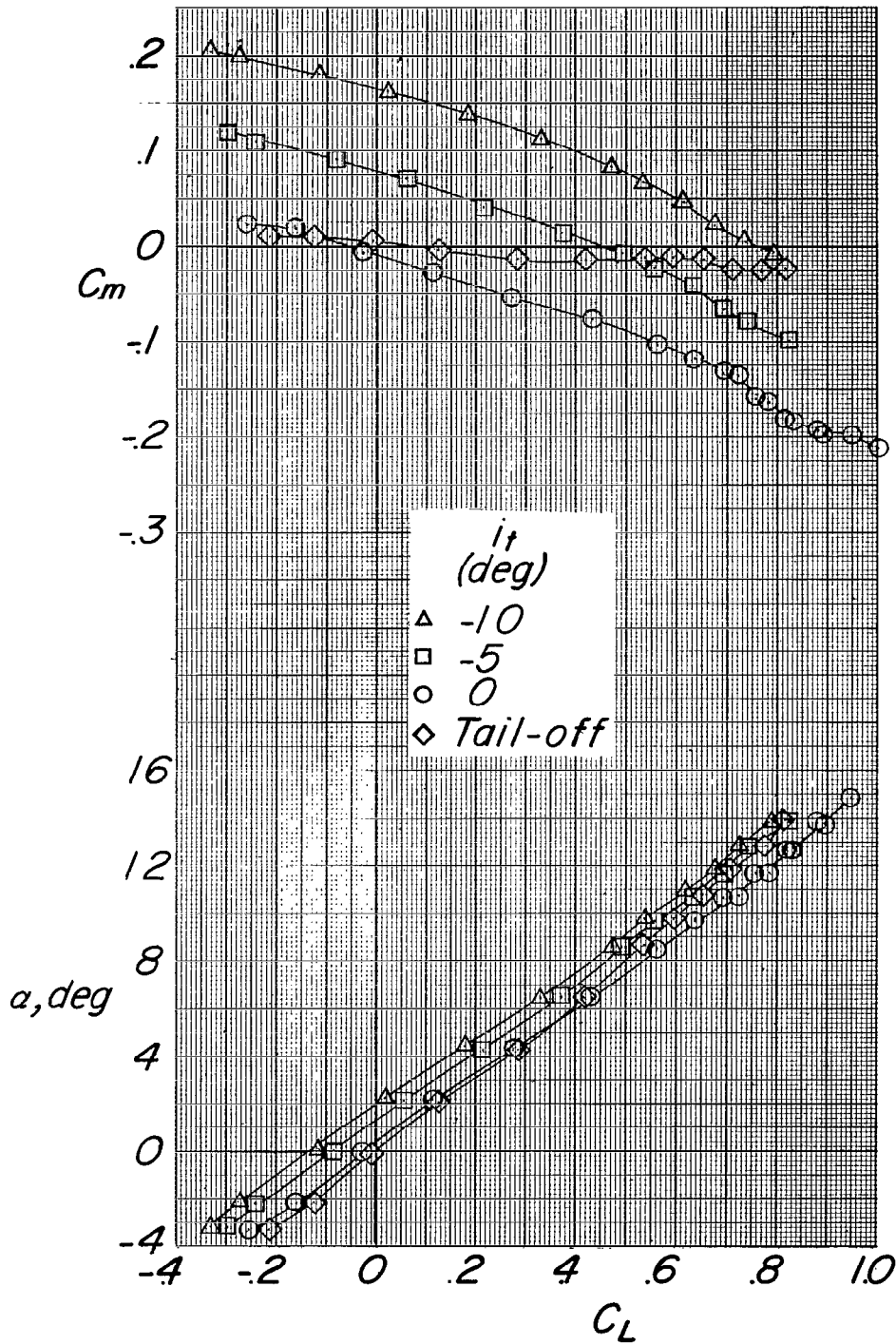


(d) Concluded.

Figure 13.- Continued.

~~SECRET~~

~~SECRET~~

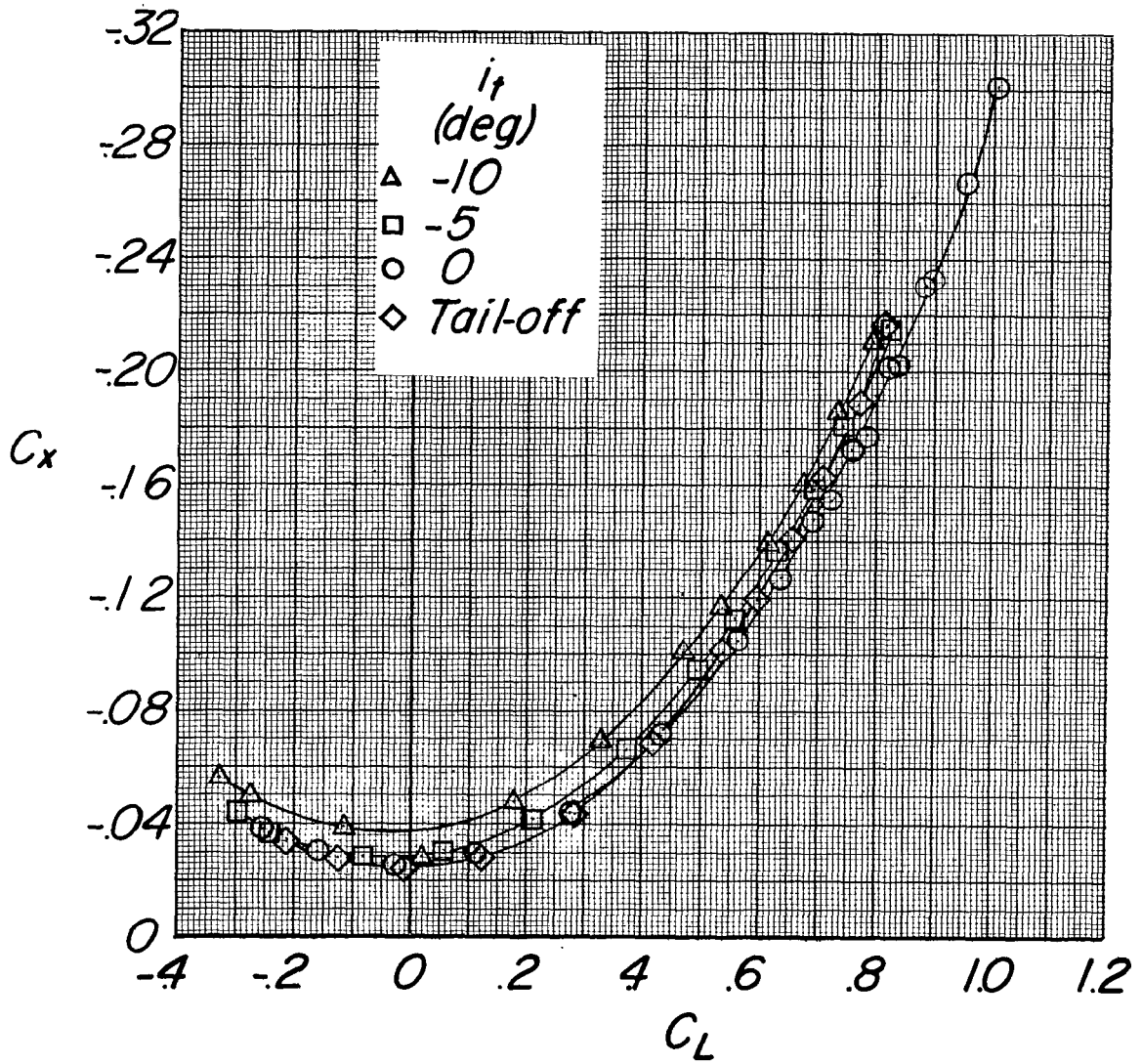


(e) $M = 0.95$.

Figure 13.- Continued.

~~SECRET~~

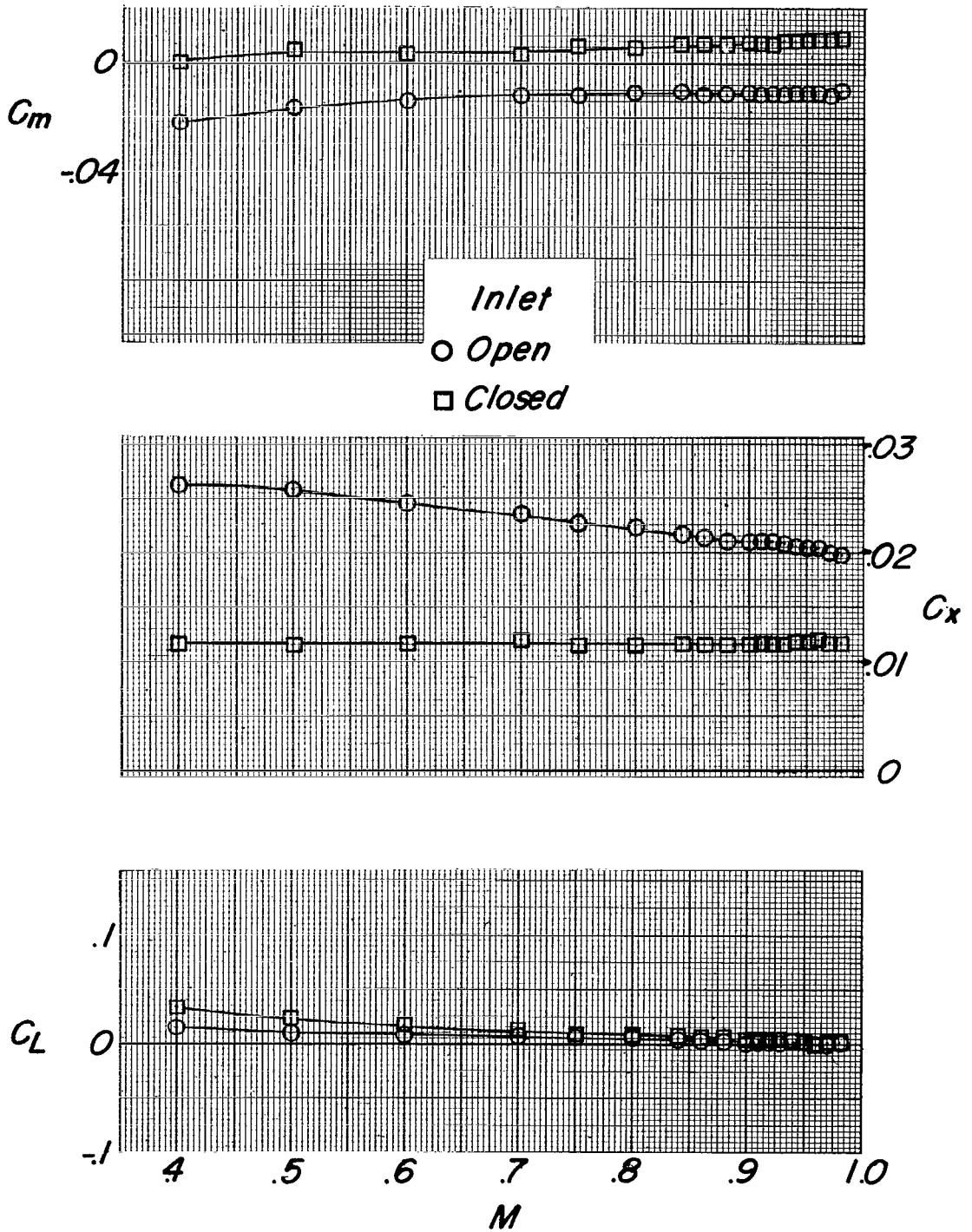
~~CONFIDENTIAL~~



(e) Concluded.

Figure 13.- Concluded.

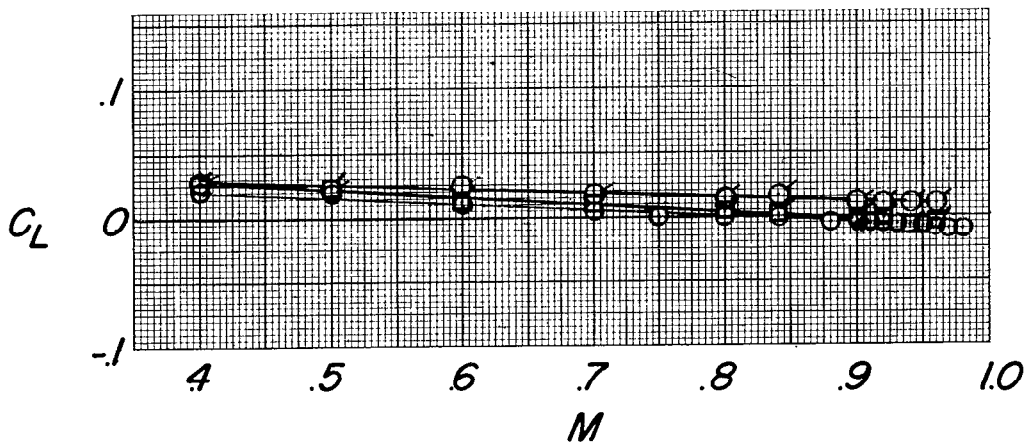
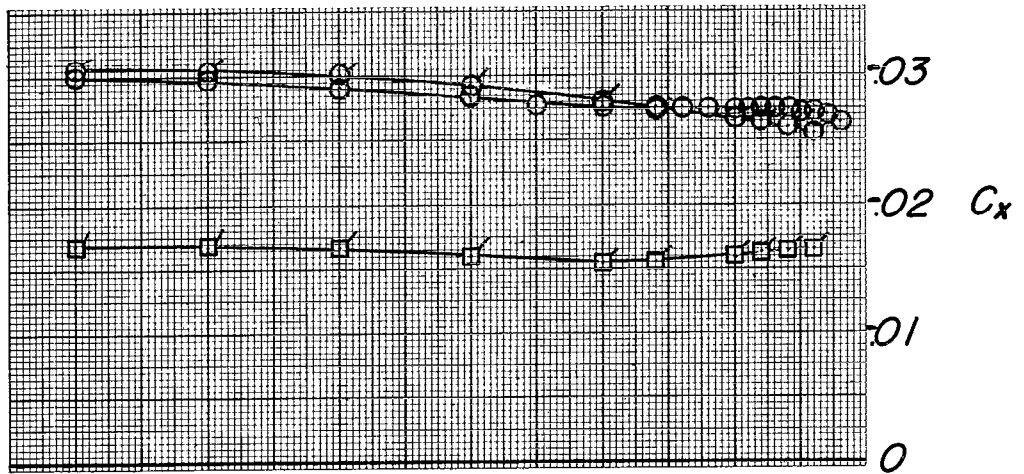
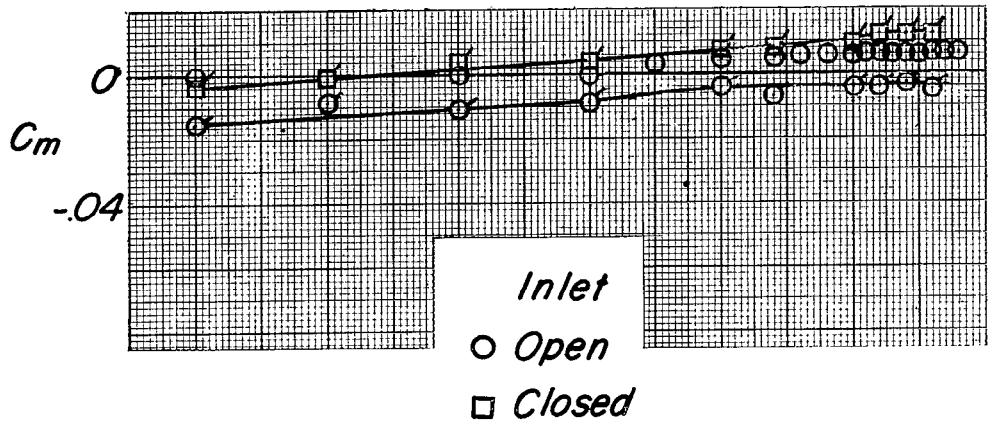
~~CONFIDENTIAL~~



(a) Fuselage alone.

Figure 14.- The effect of closing the inlet on the variation of the aerodynamic characteristics with Mach number. $\alpha = 0^\circ$.

~~CONFIDENTIAL~~

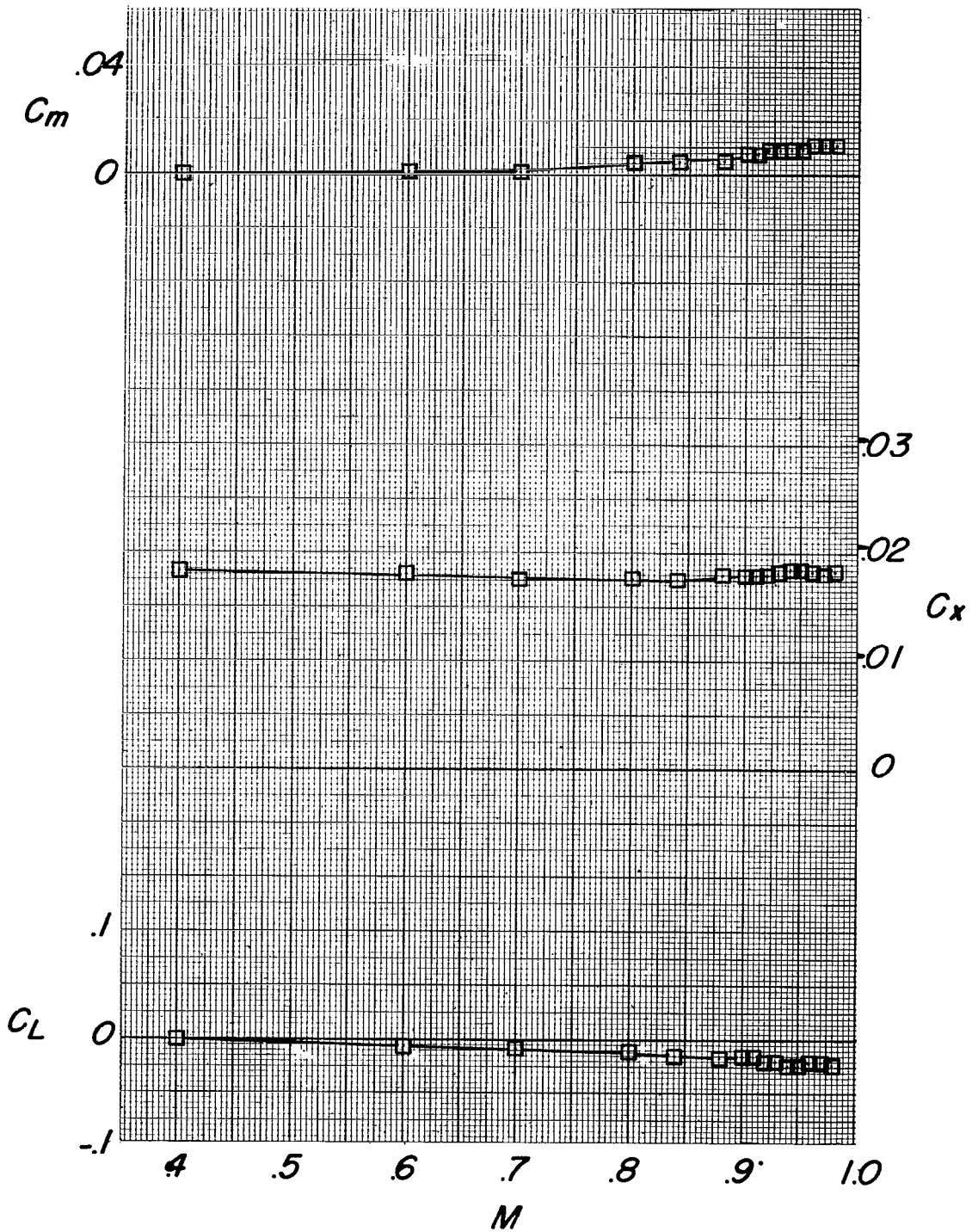


(b) Complete model; no fence; $i_t = 0^\circ$.

Figure 14.- Continued.

~~CONFIDENTIAL~~

~~SECRET~~



(c) Complete model; fence A; $i_t = 0^\circ$.

Figure 14.- Concluded.

~~SECRET~~

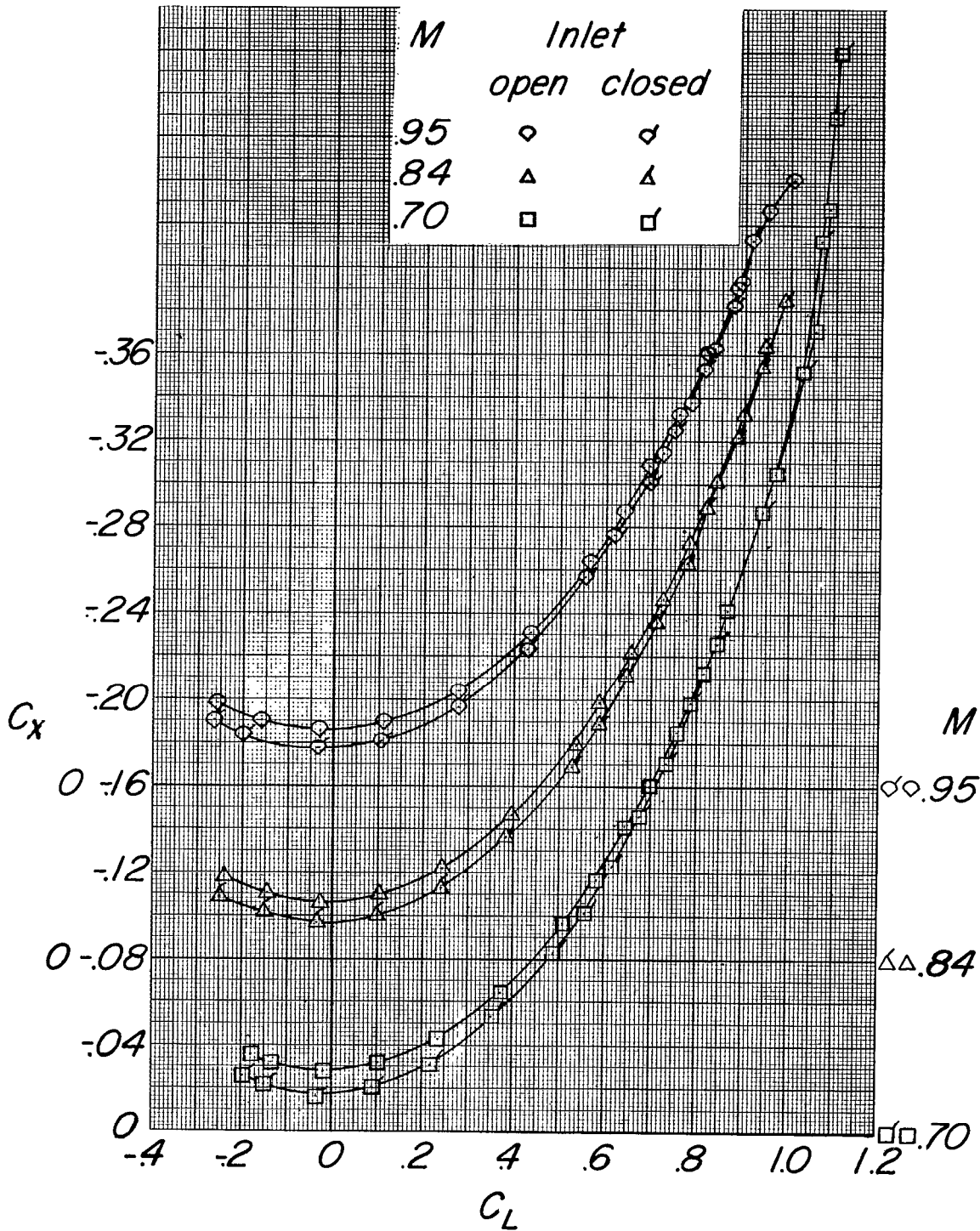


Figure 15.- Concluded.

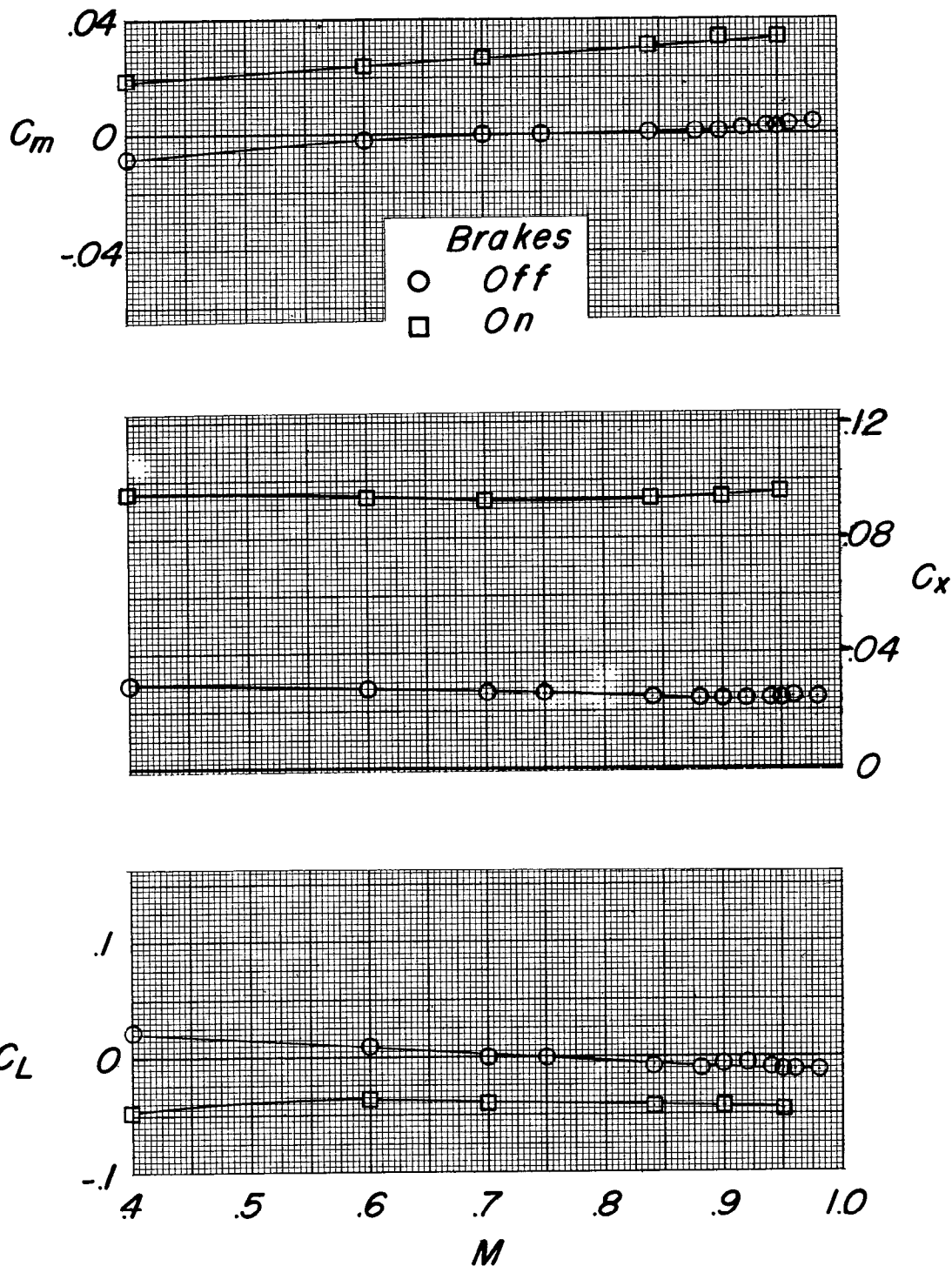
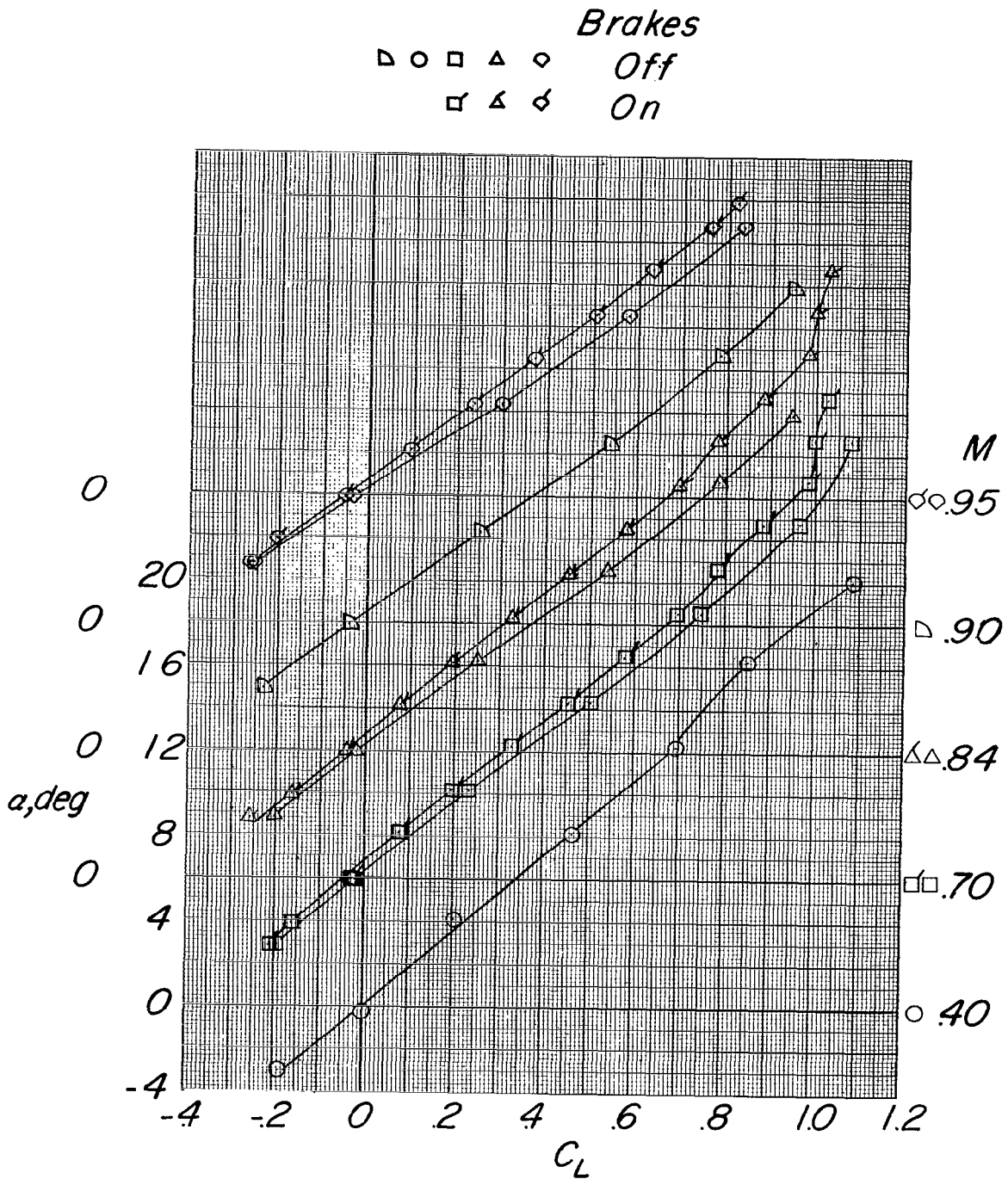


Figure 16.- The effect of speed brakes on the variation of the aerodynamic characteristics with Mach number. Fence A; $i_t = 0^\circ$; $\alpha = 0^\circ$. (Survey rake in place.)

~~SECRET~~



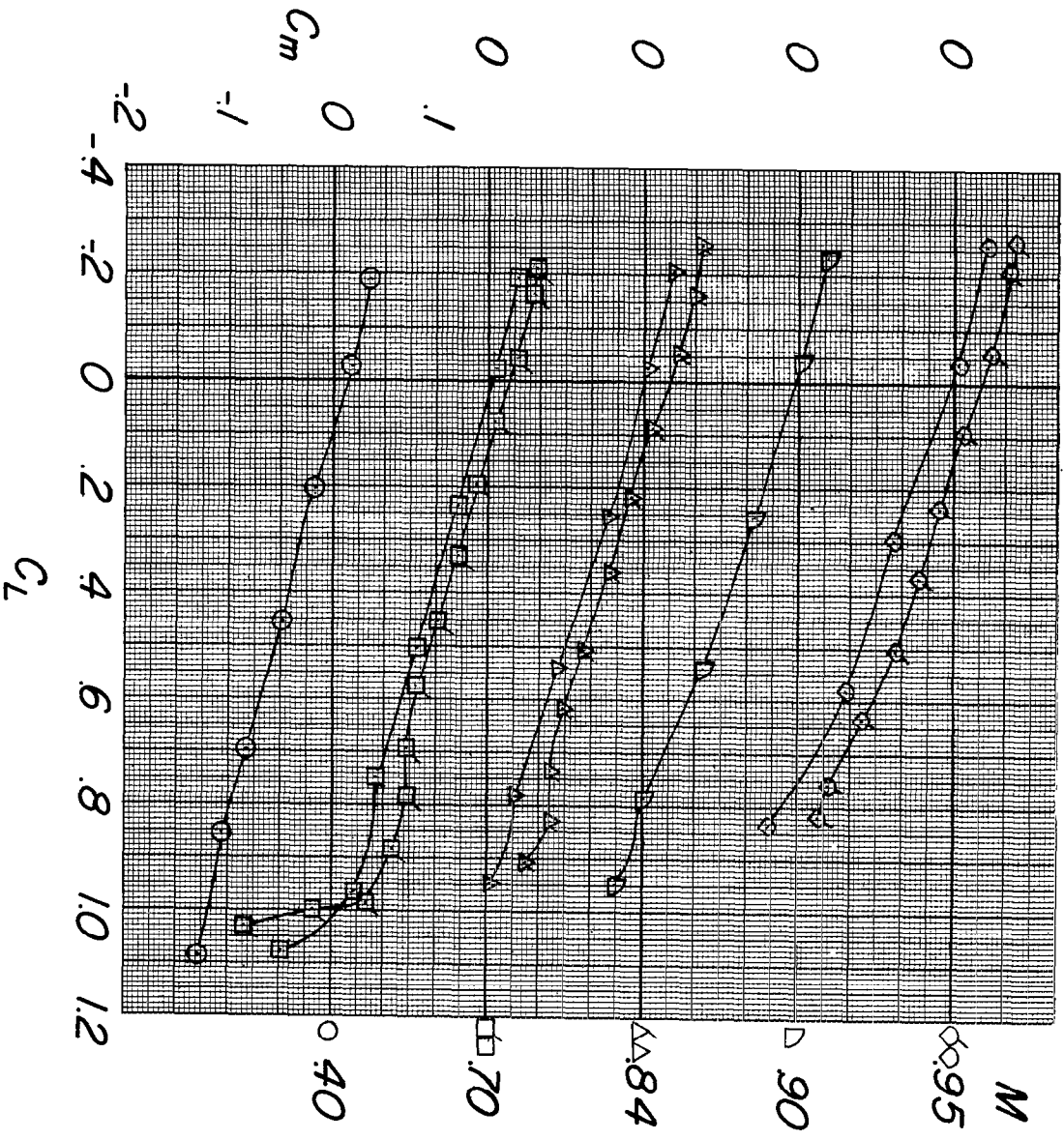
(a) α against C_L .

Figure 17.- The effect of speed brakes on the aerodynamic characteristics in pitch. Fence A; $i_t = 0^\circ$. (Survey rake in place.)

~~SECRET~~



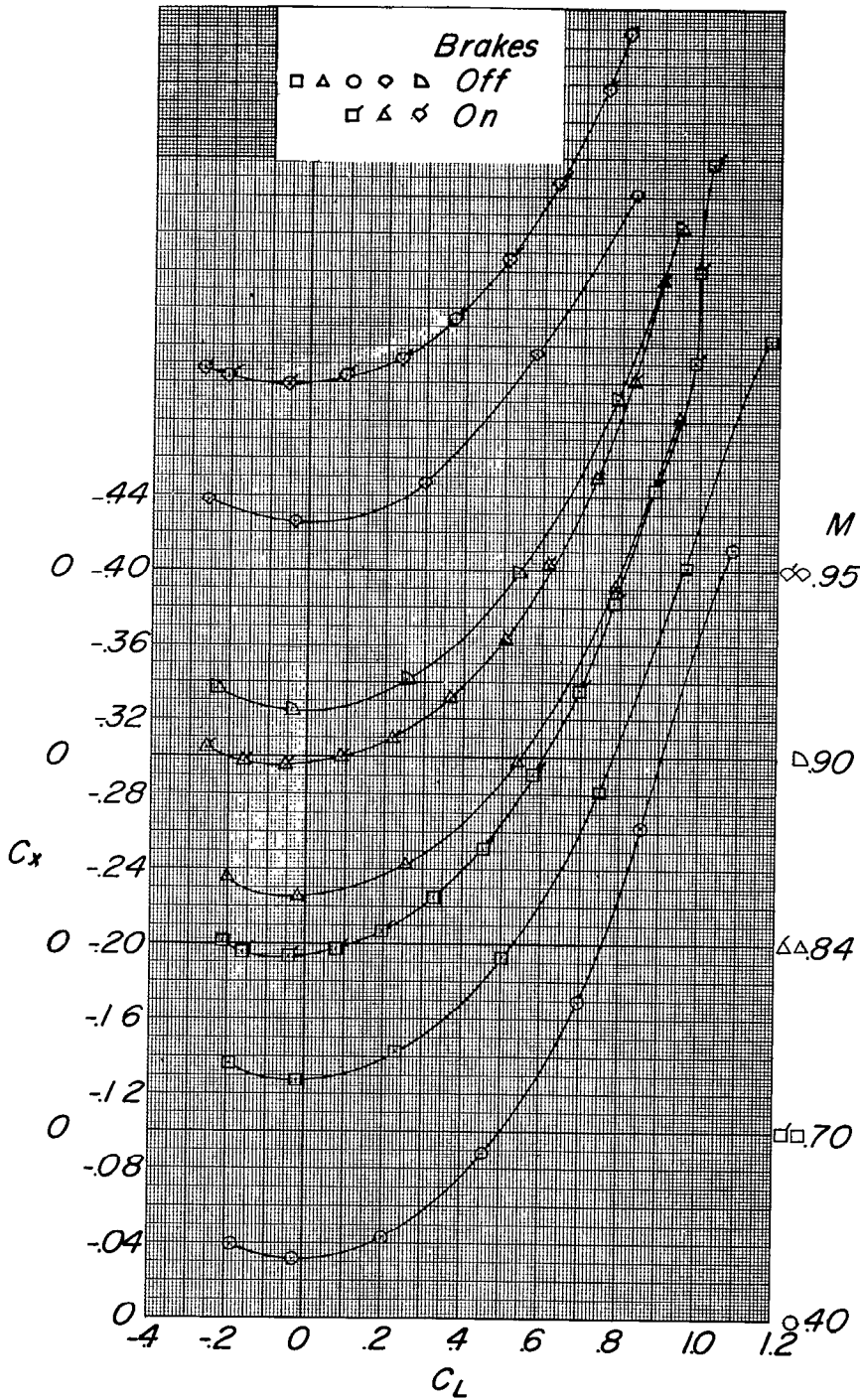
Brakes
 ▽ □ ▢ △ ○ Off
 ▽ □ ▢ △ ○ On



(b) C_m against C_L .

Figure 17.- Continued.





(c) C_x against C_L .

Figure 17.- Concluded.

~~SECRET~~

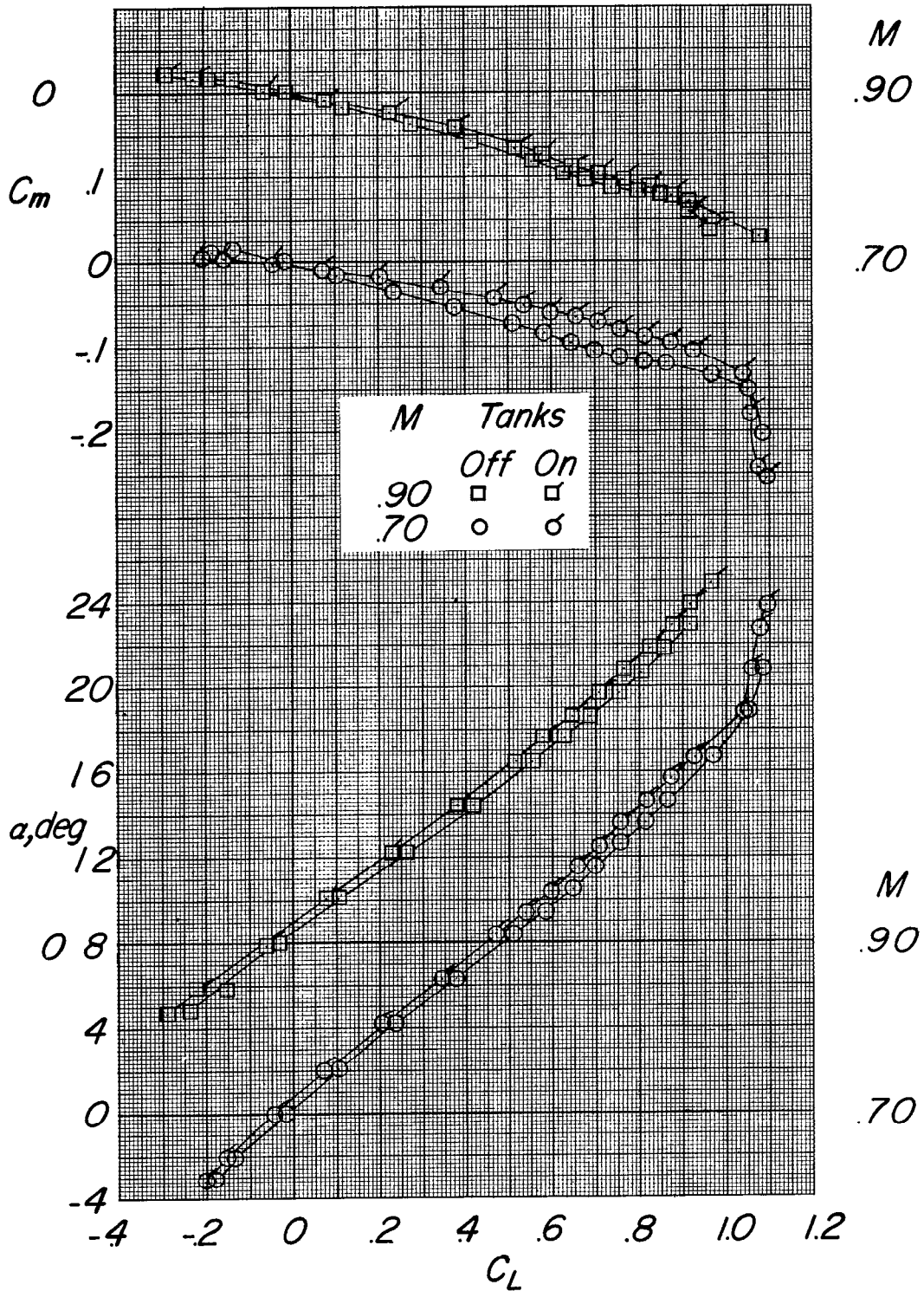


Figure 18.- The effect of the tanks on the aerodynamic characteristics in pitch. Fence A; $i_t = 0^\circ$.

~~SECRET~~

~~SECRET~~

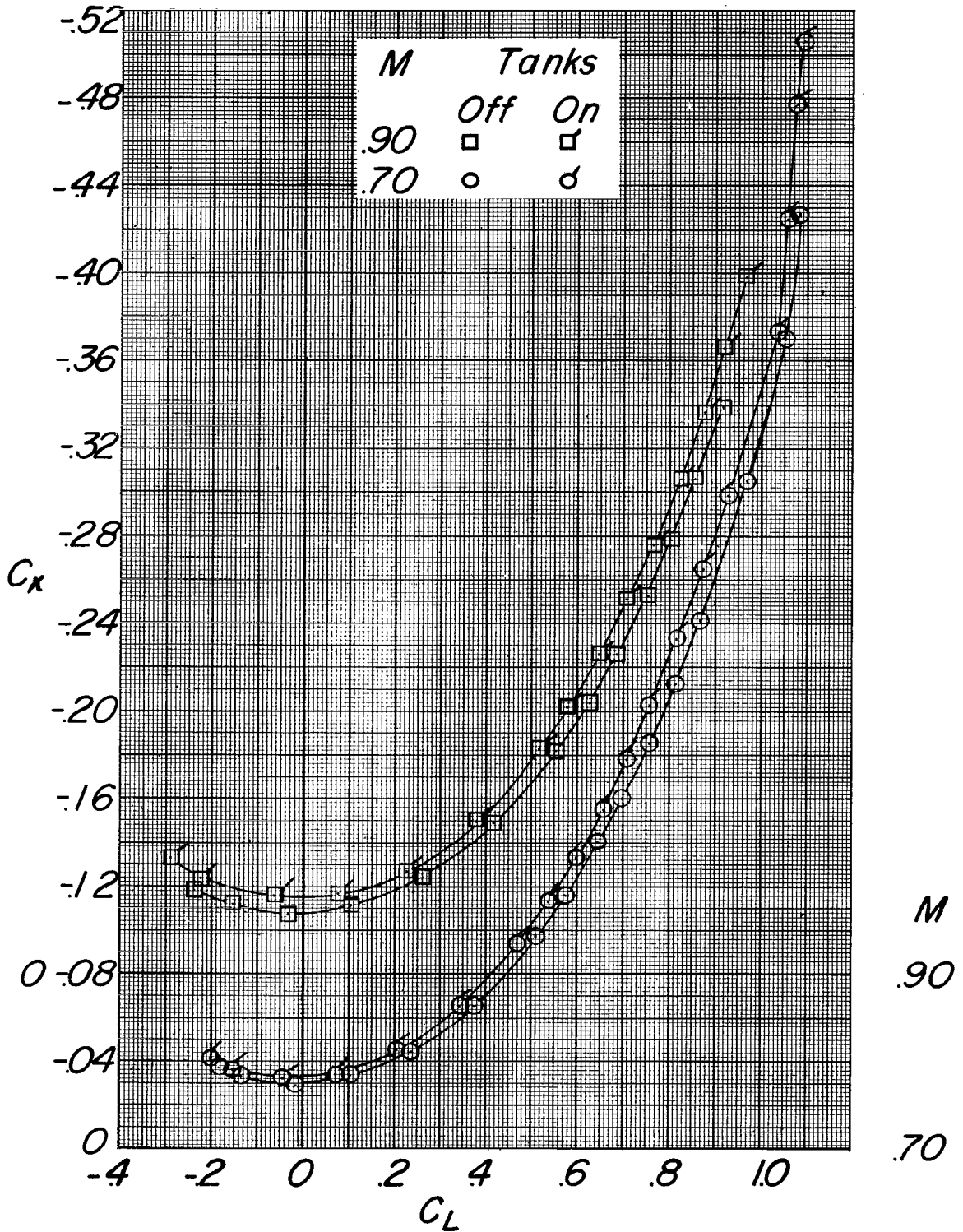
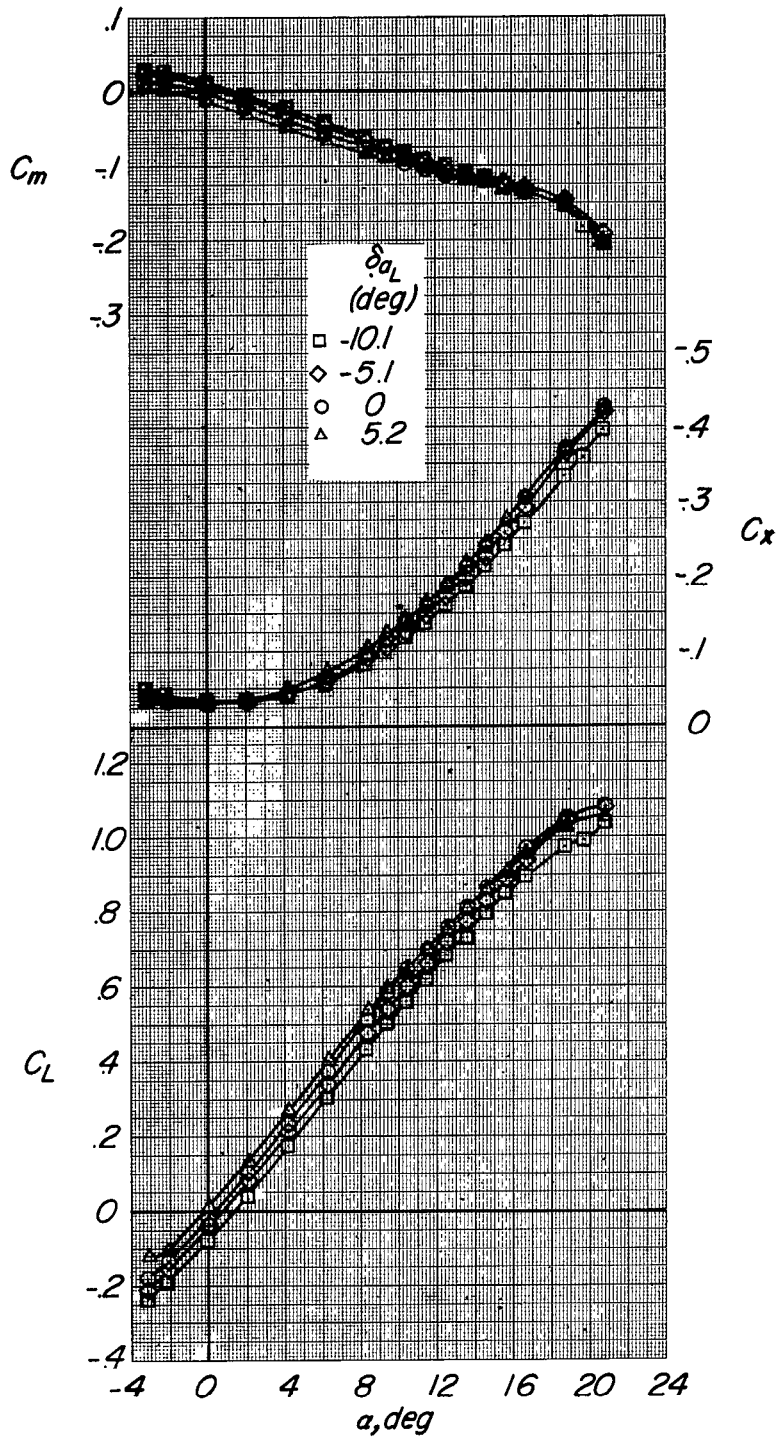


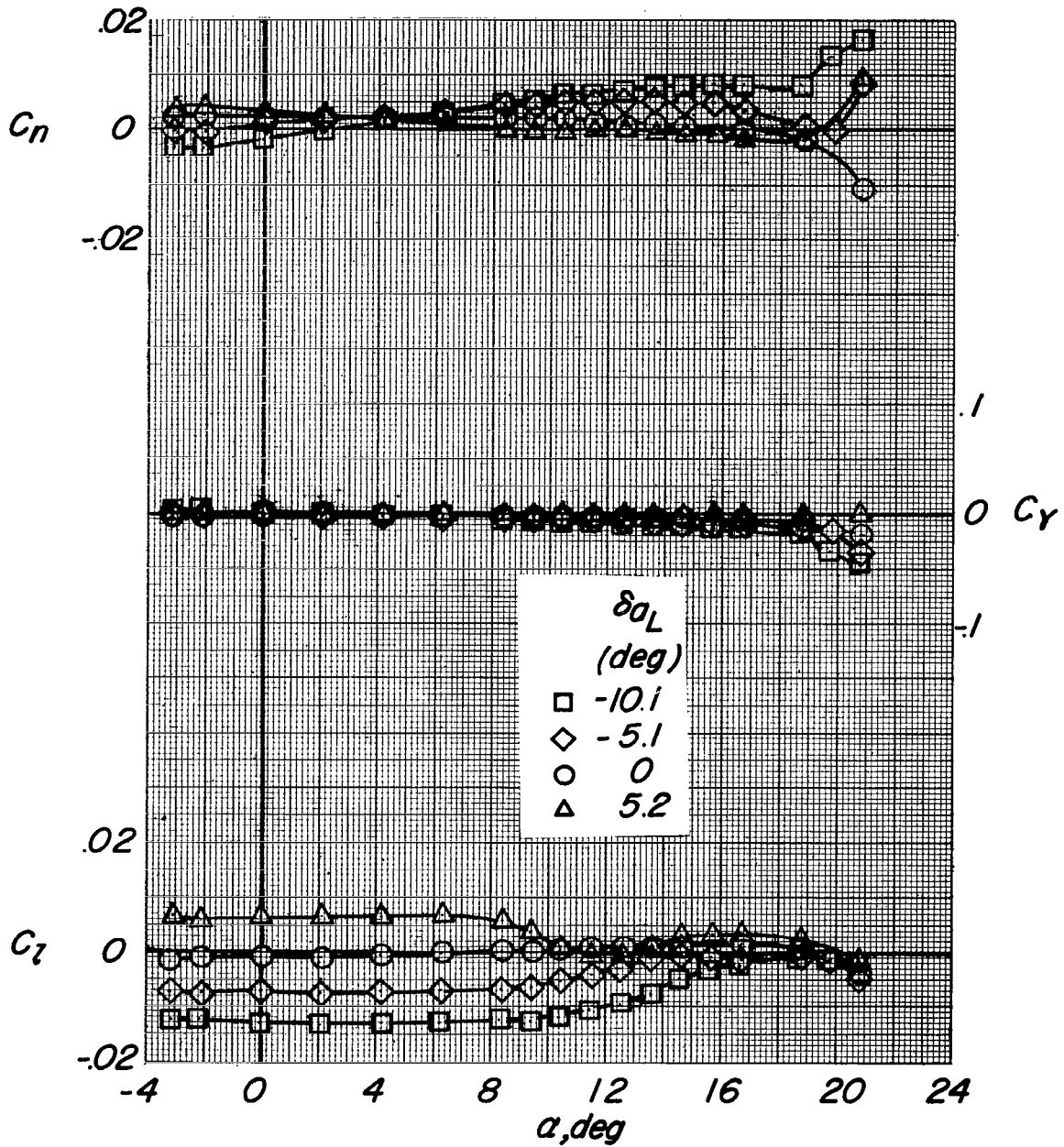
Figure 18.- Concluded.

~~SECRET~~



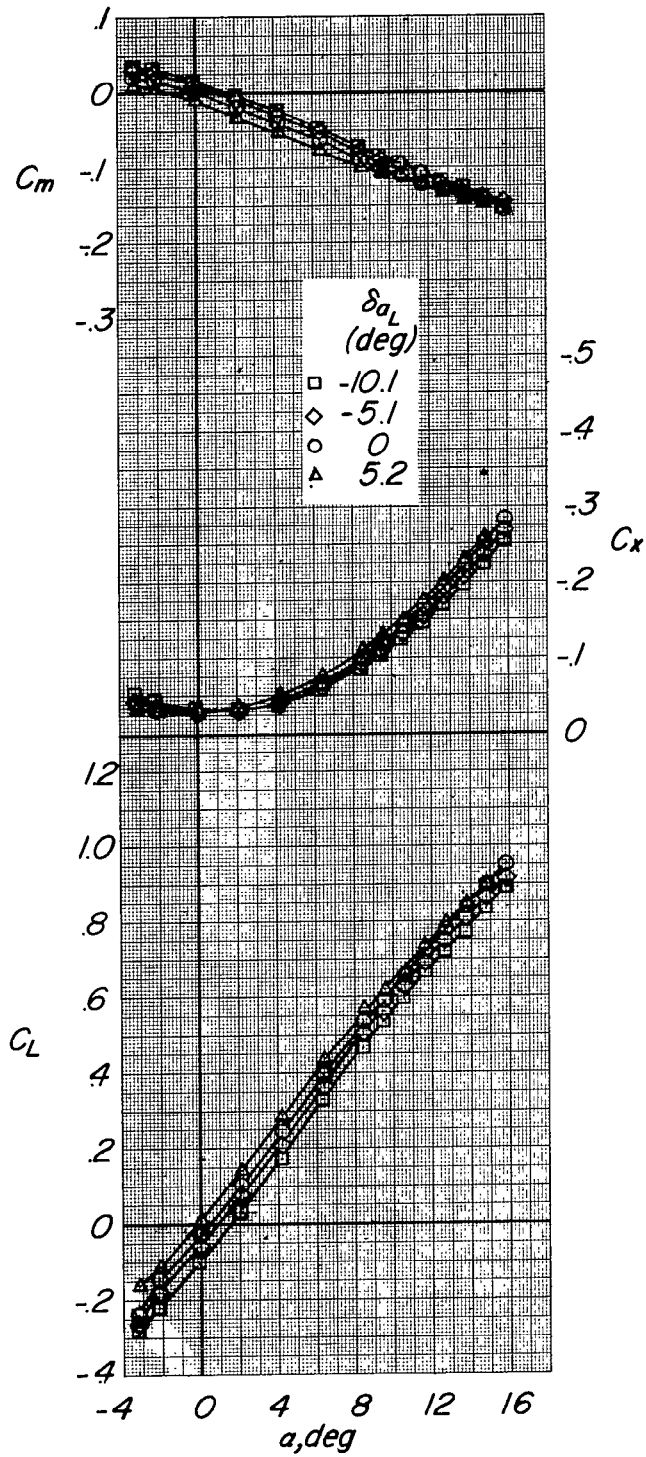
(a) $M = 0.70$.

Figure 19.- The effect of left aileron deflection on the aerodynamic characteristics in pitch. Fence A; $i_t = 0^\circ$.



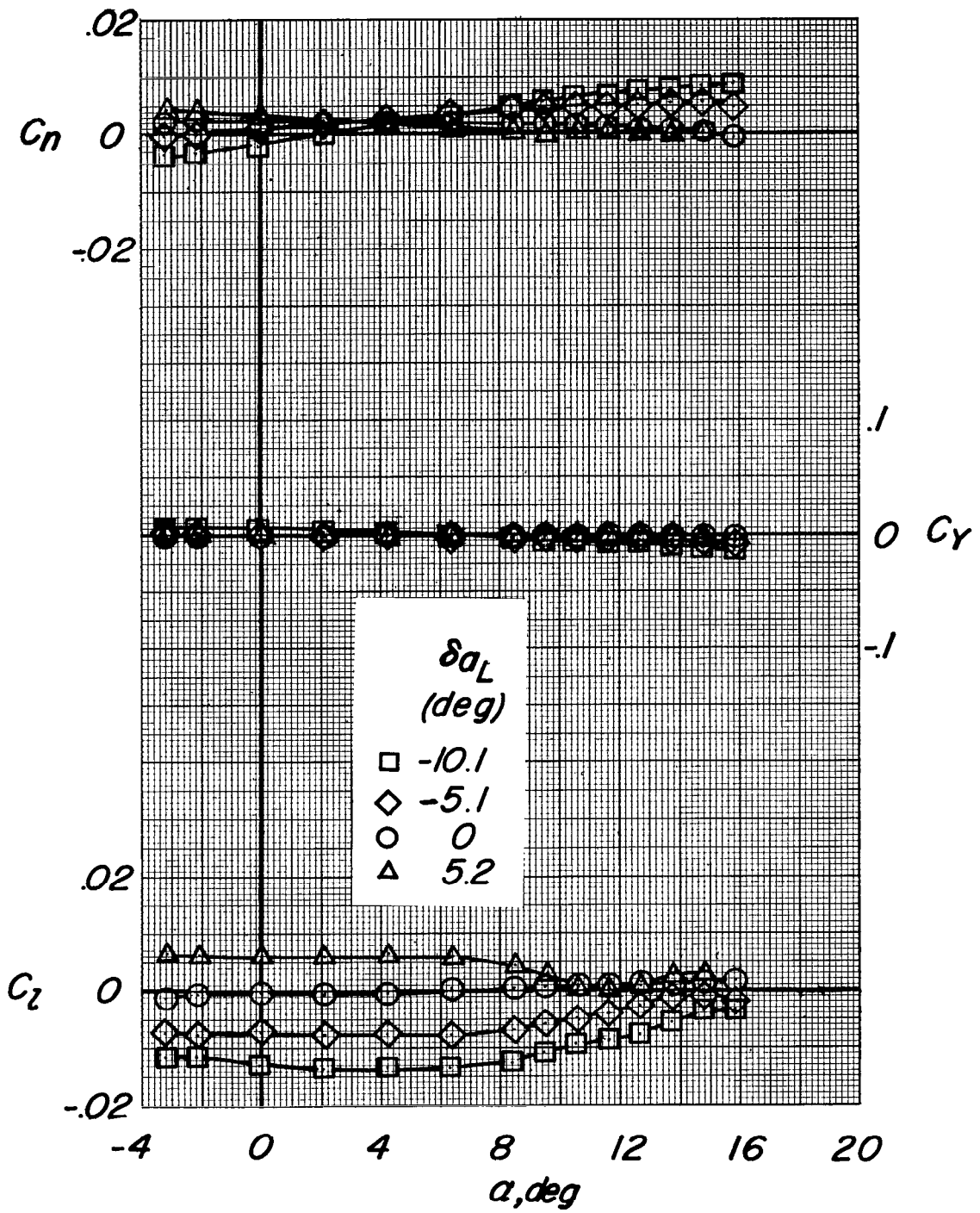
(a) Concluded.

Figure 19.- Continued.



(b) $M = 0.84$.

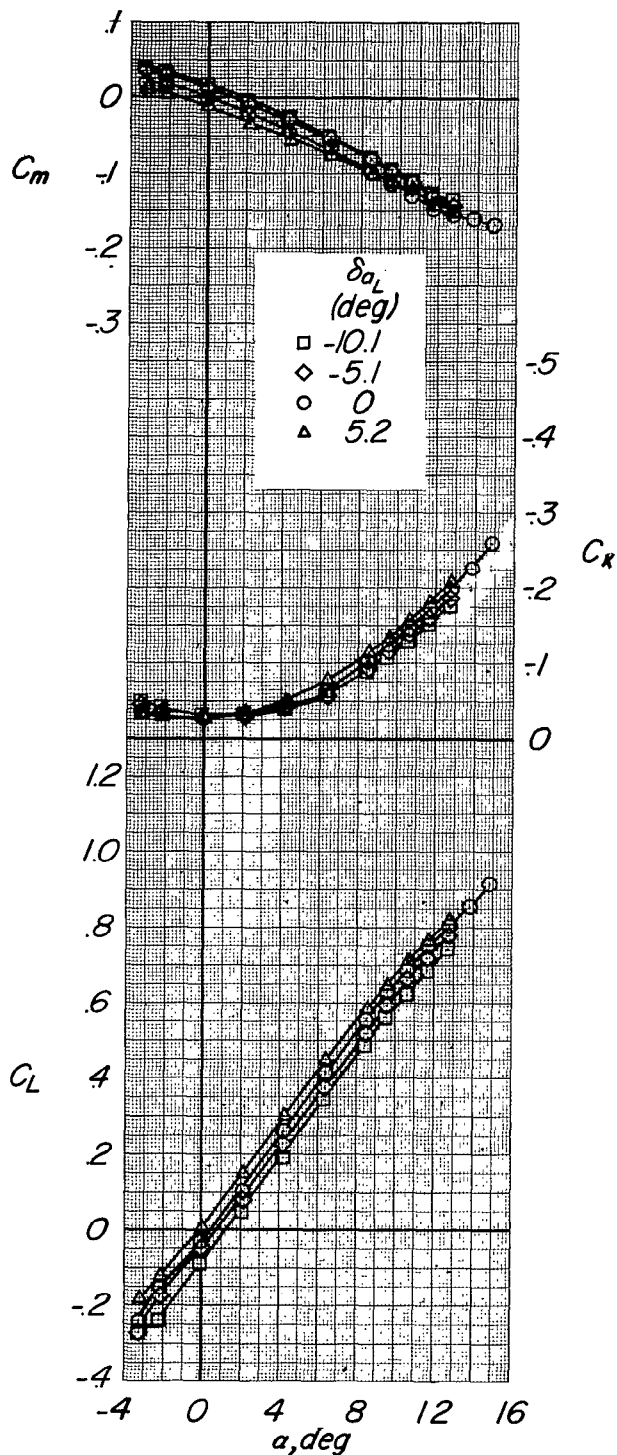
Figure 19.- Continued.



(b) Concluded.

Figure 19.- Continued.

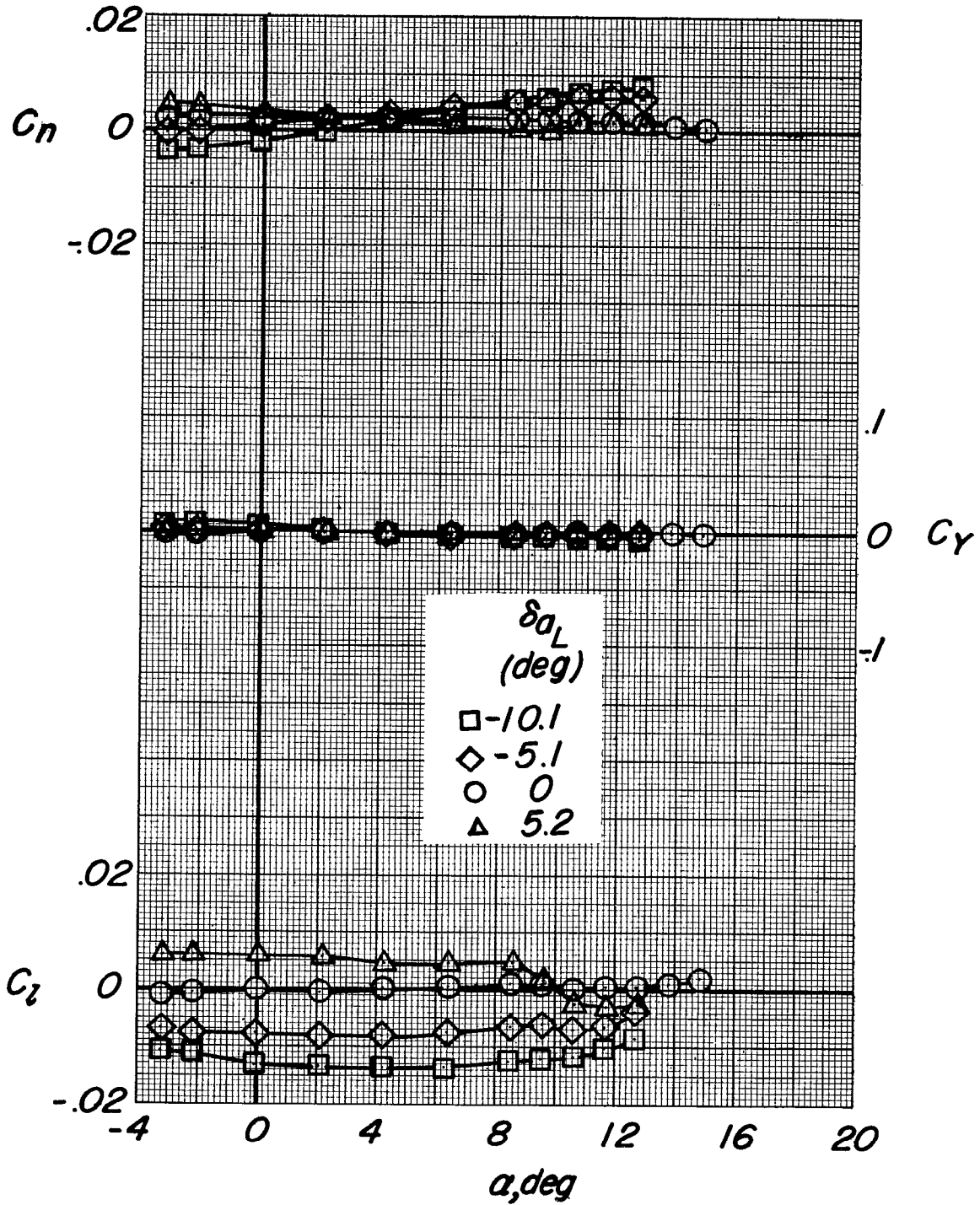
~~SECRET~~



(c) $M = 0.90$.

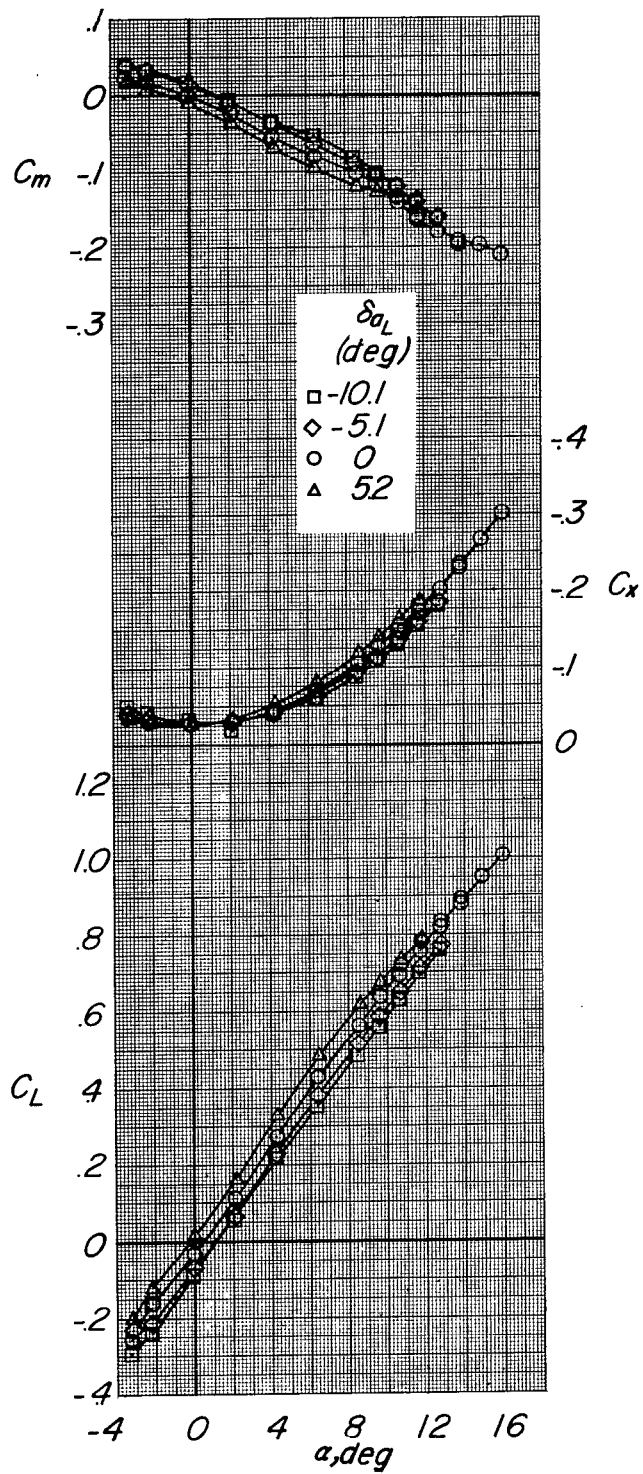
Figure 19.- Continued.

~~SECRET~~



(c) Concluded.

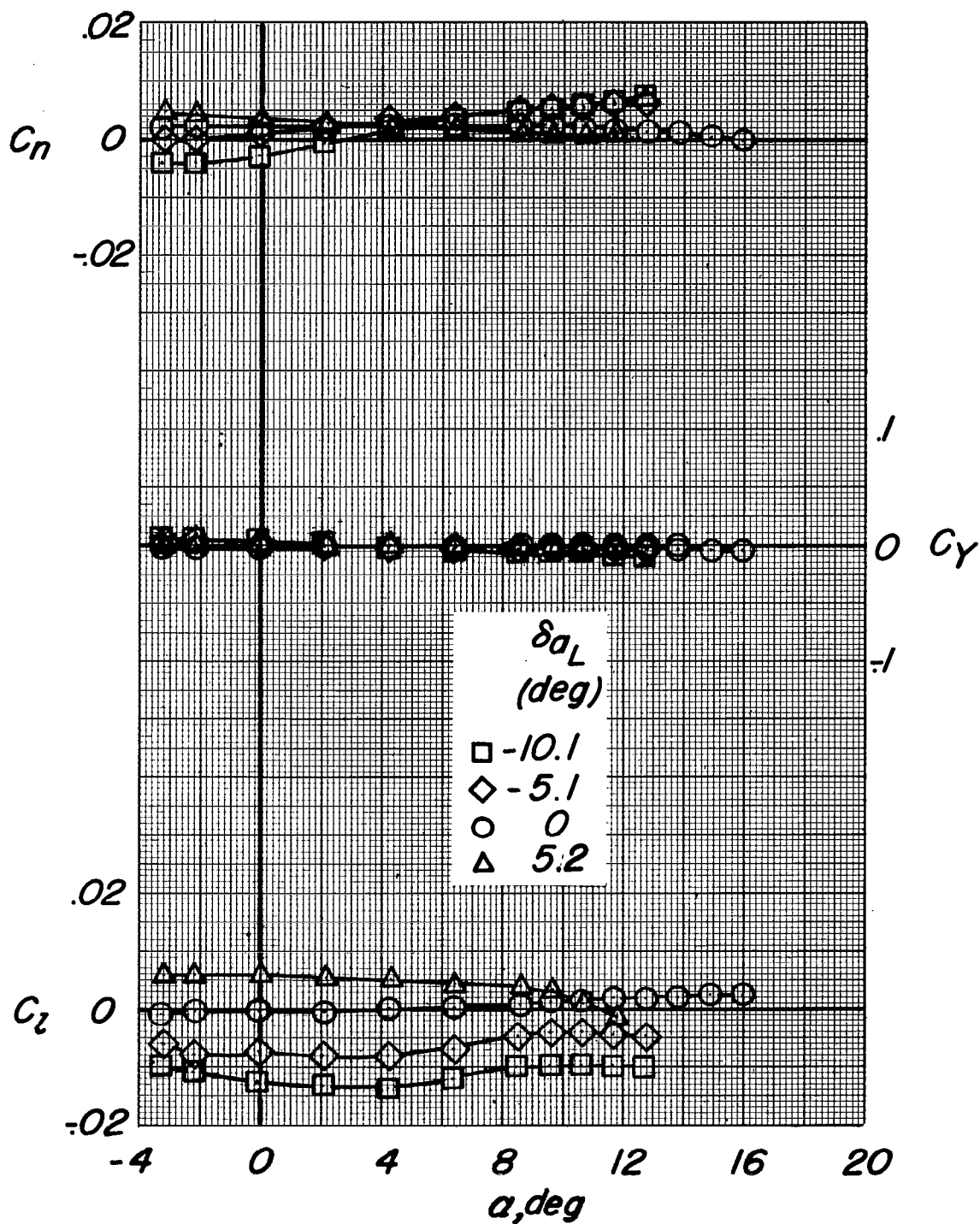
Figure 19.- Continued.



(d) $M = 0.95$.

Figure 19.- Continued.

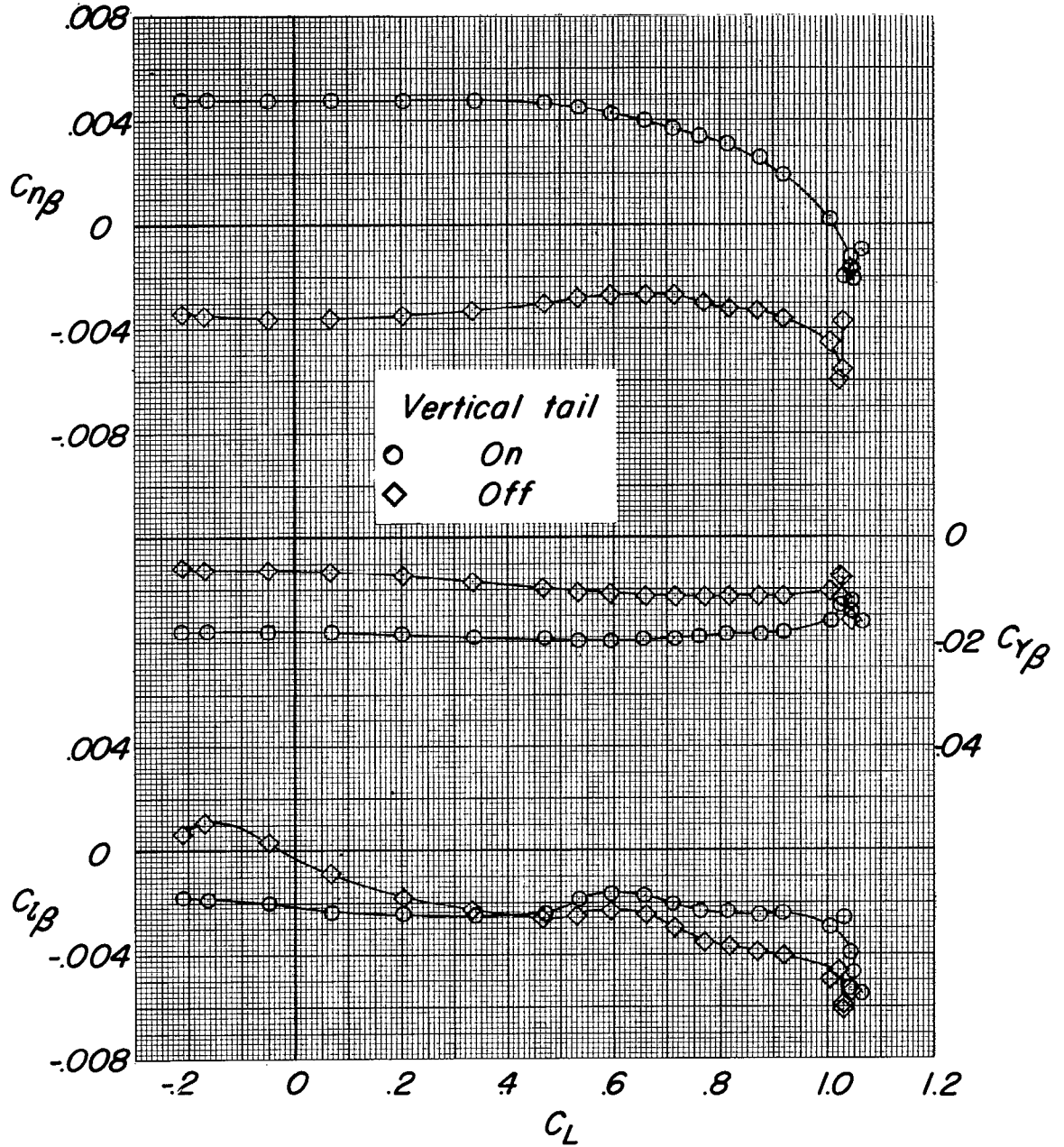
~~SECRET~~



(d) Concluded.

Figure 19.- Concluded.

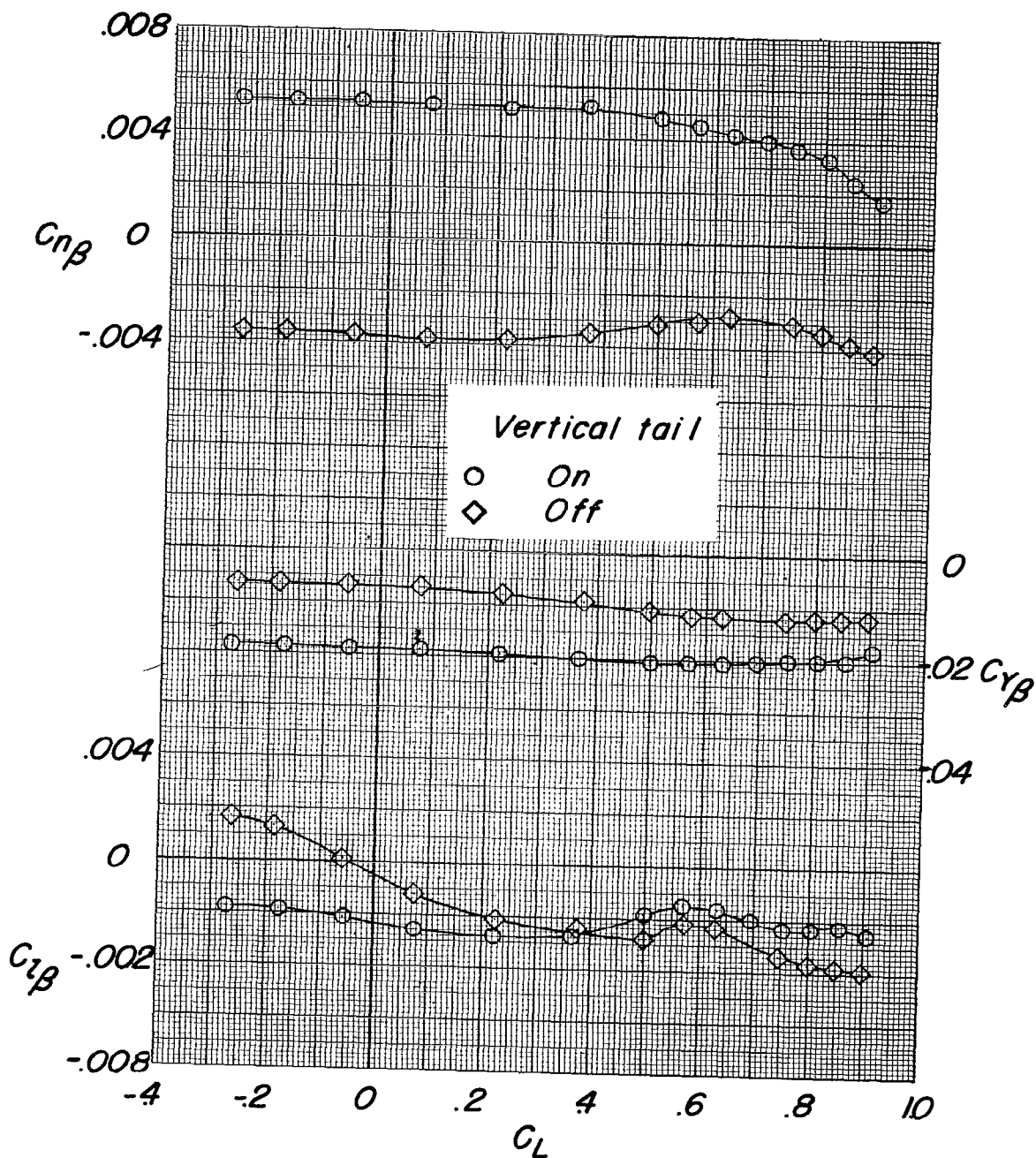
~~SECRET~~



(a) $M = 0.70$.

Figure 20.- The effect of the vertical fin on the variation of the lateral stability parameters with lift coefficient. Fence A; $i_t = -5^\circ$.

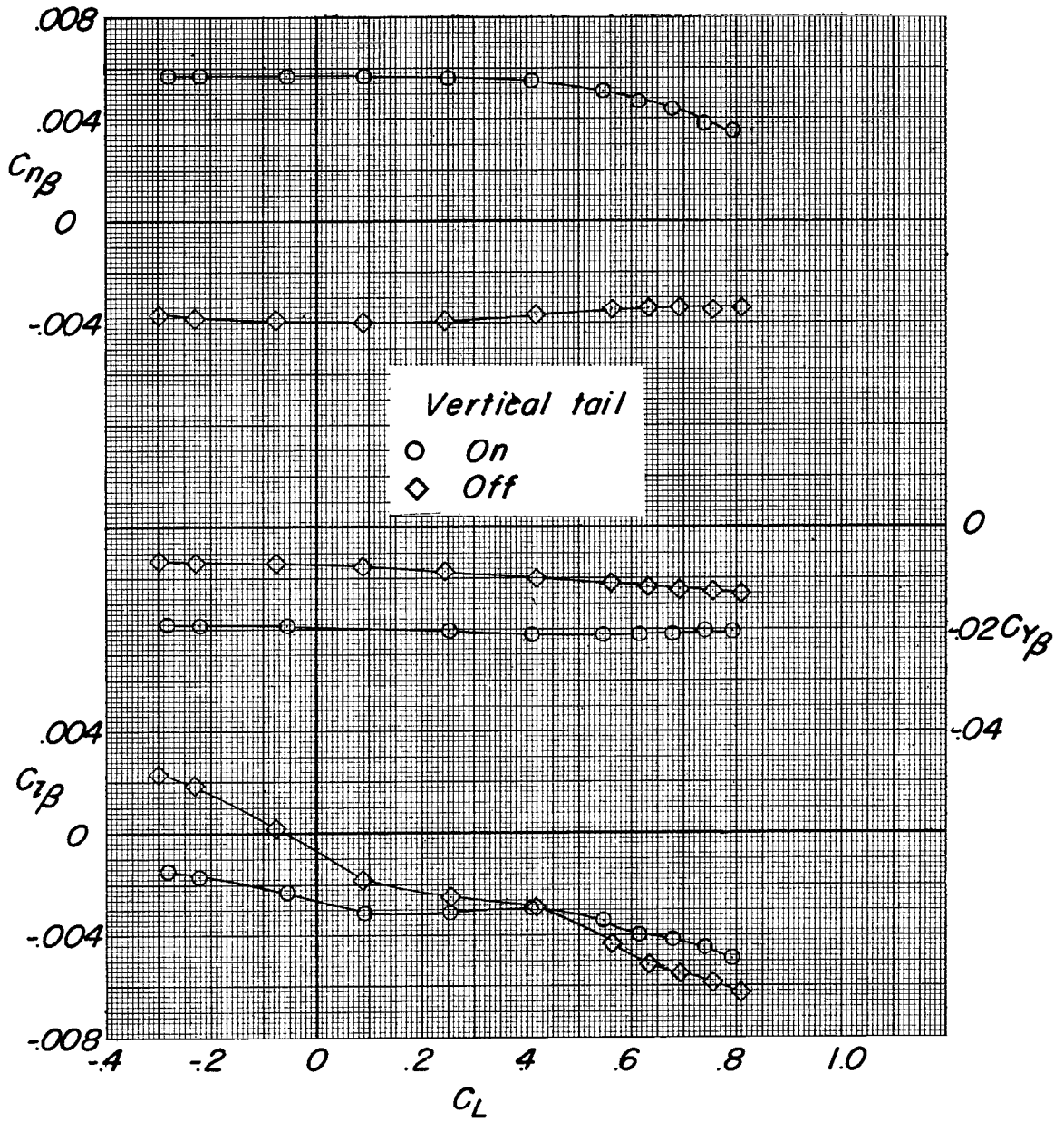
~~SECRET~~



(b) $M = 0.84$.

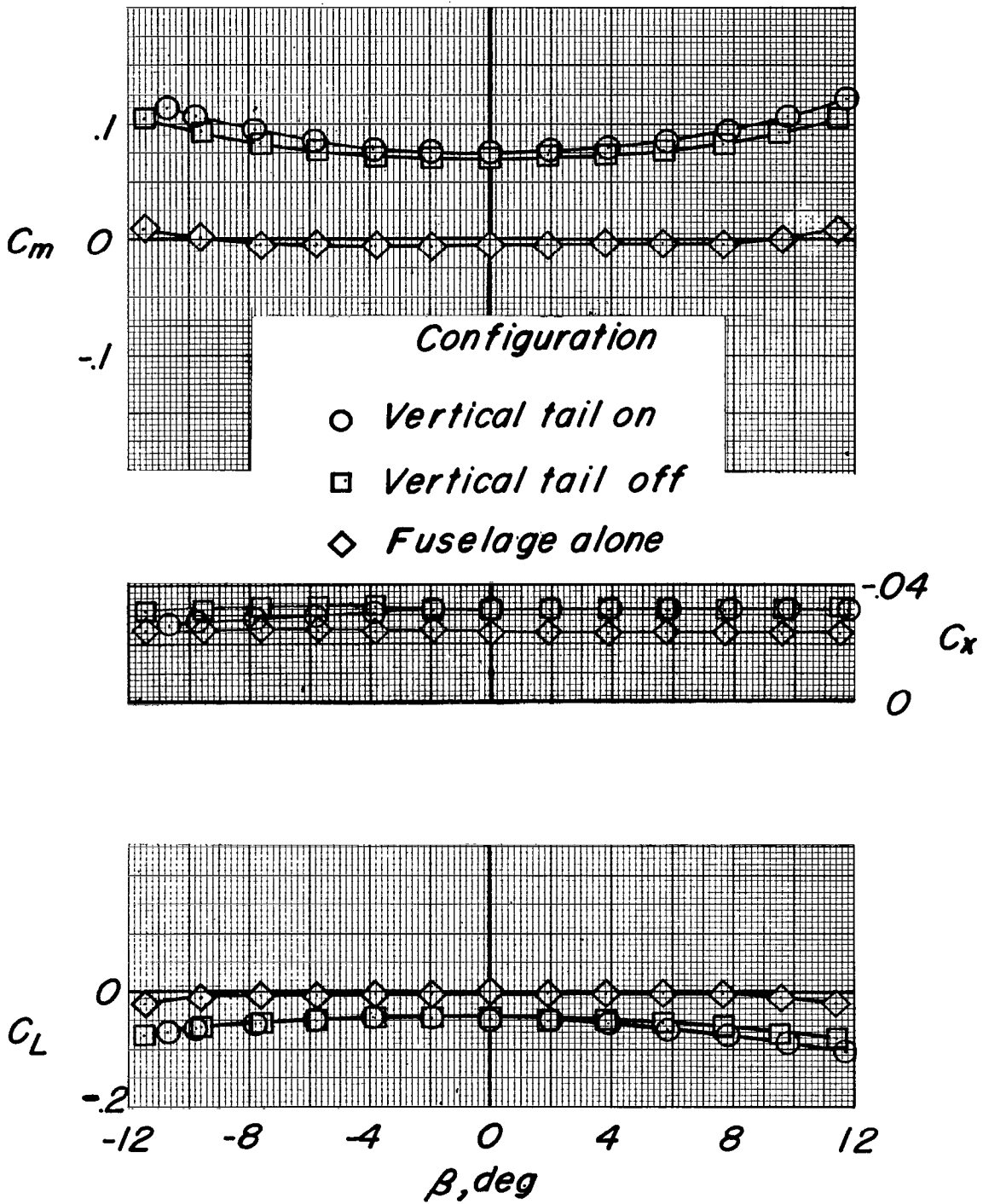
Figure 20.- Continued.

~~SECRET~~



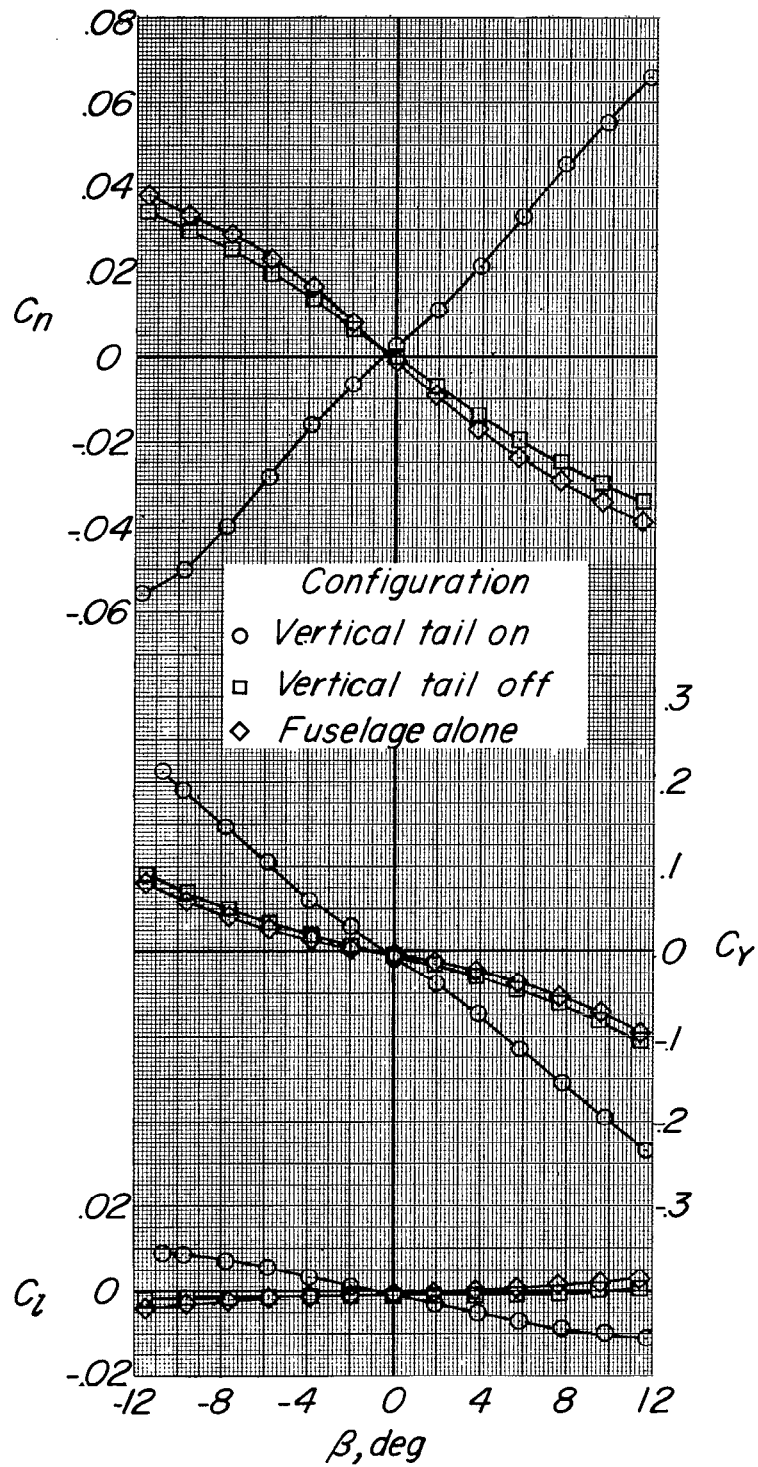
(c) $M = 0.95$.

Figure 20.- Concluded.



(a) $M = 0.70$.

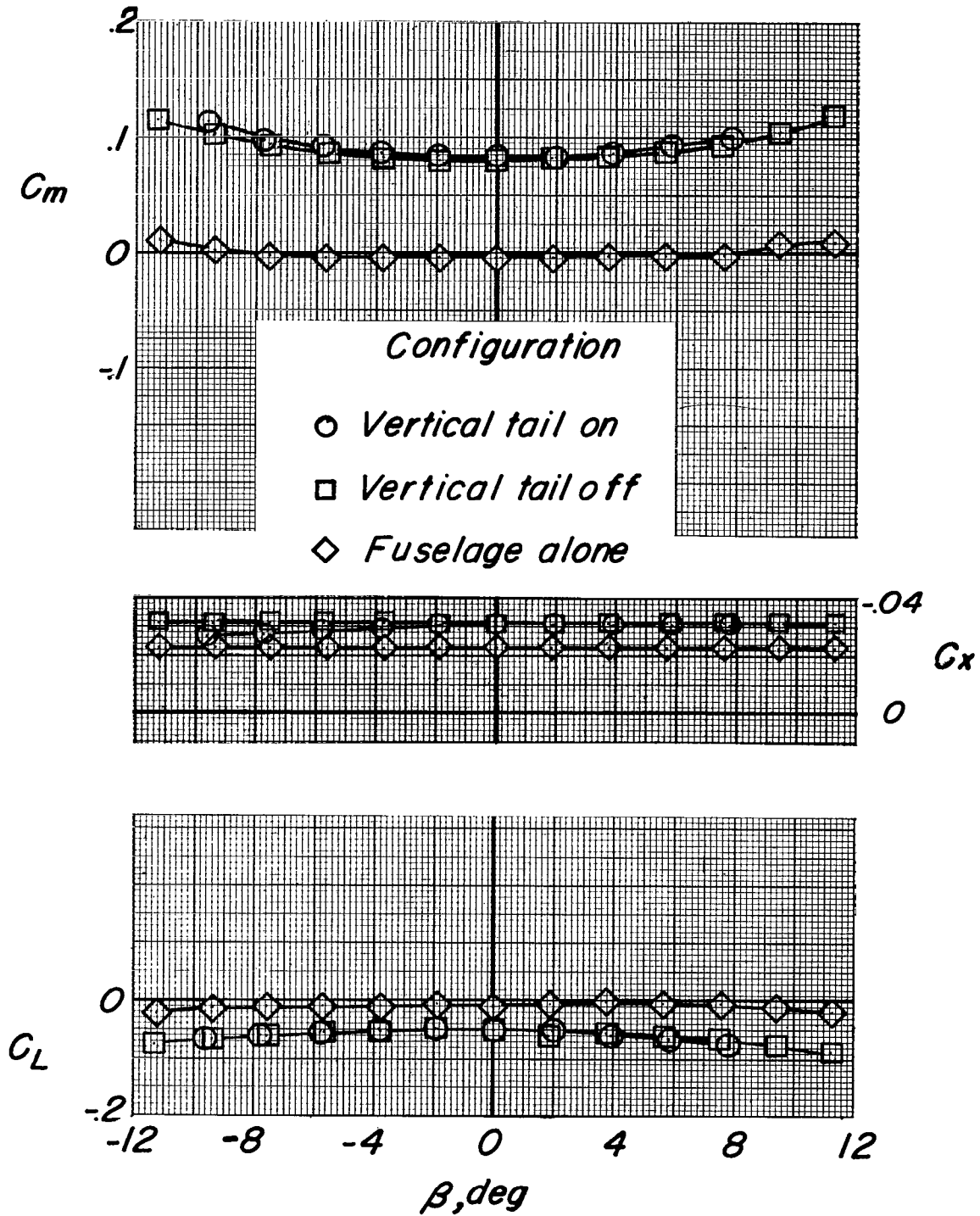
Figure 21.- The effect of model configuration on the aerodynamic characteristics in sideslip. Fence A; $i_t = -5$; $\alpha = 0^\circ$.



(a) Concluded.

Figure 21.- Continued.

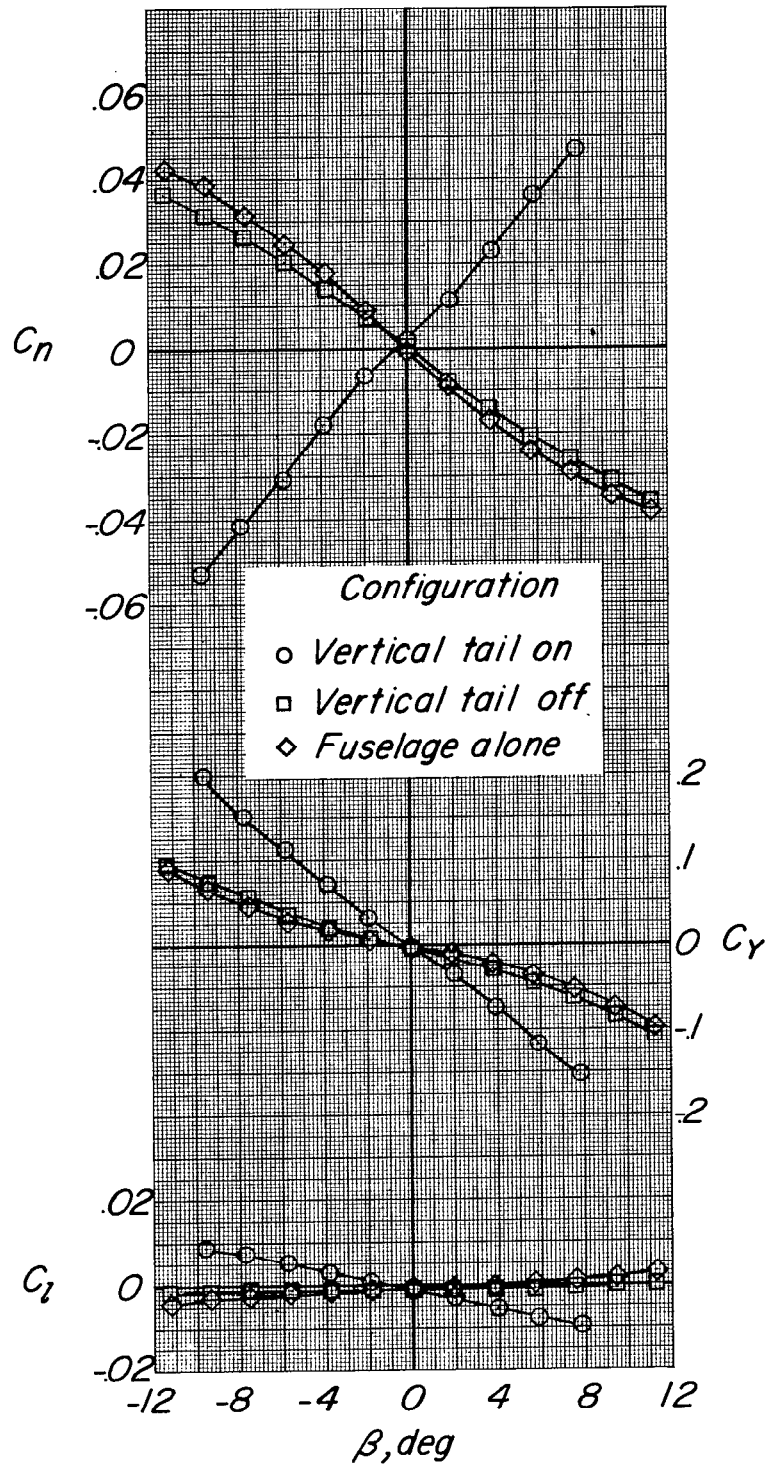
~~SECRET~~



(b) $M = 0.84$.

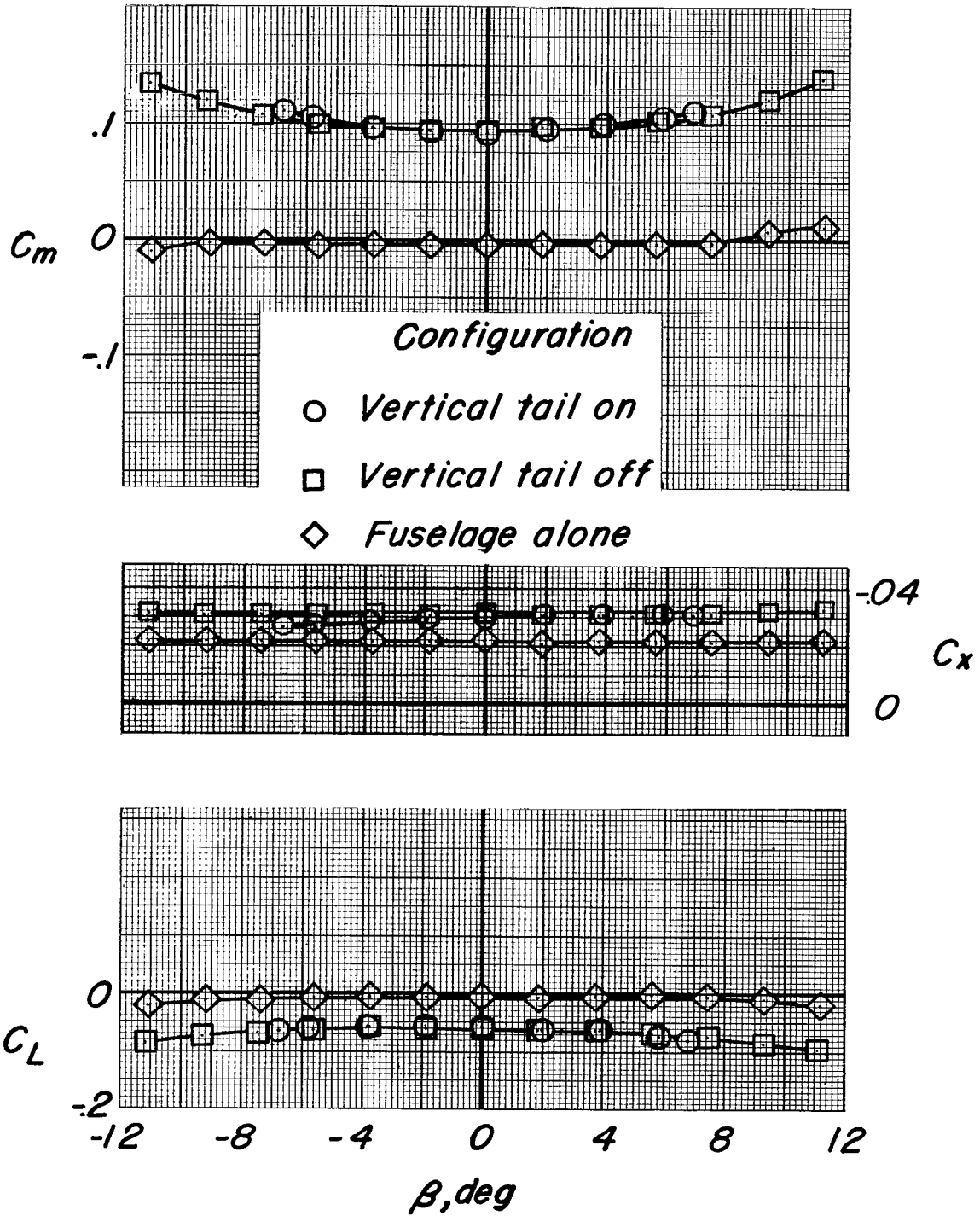
Figure 21.- Continued.

~~SECRET~~



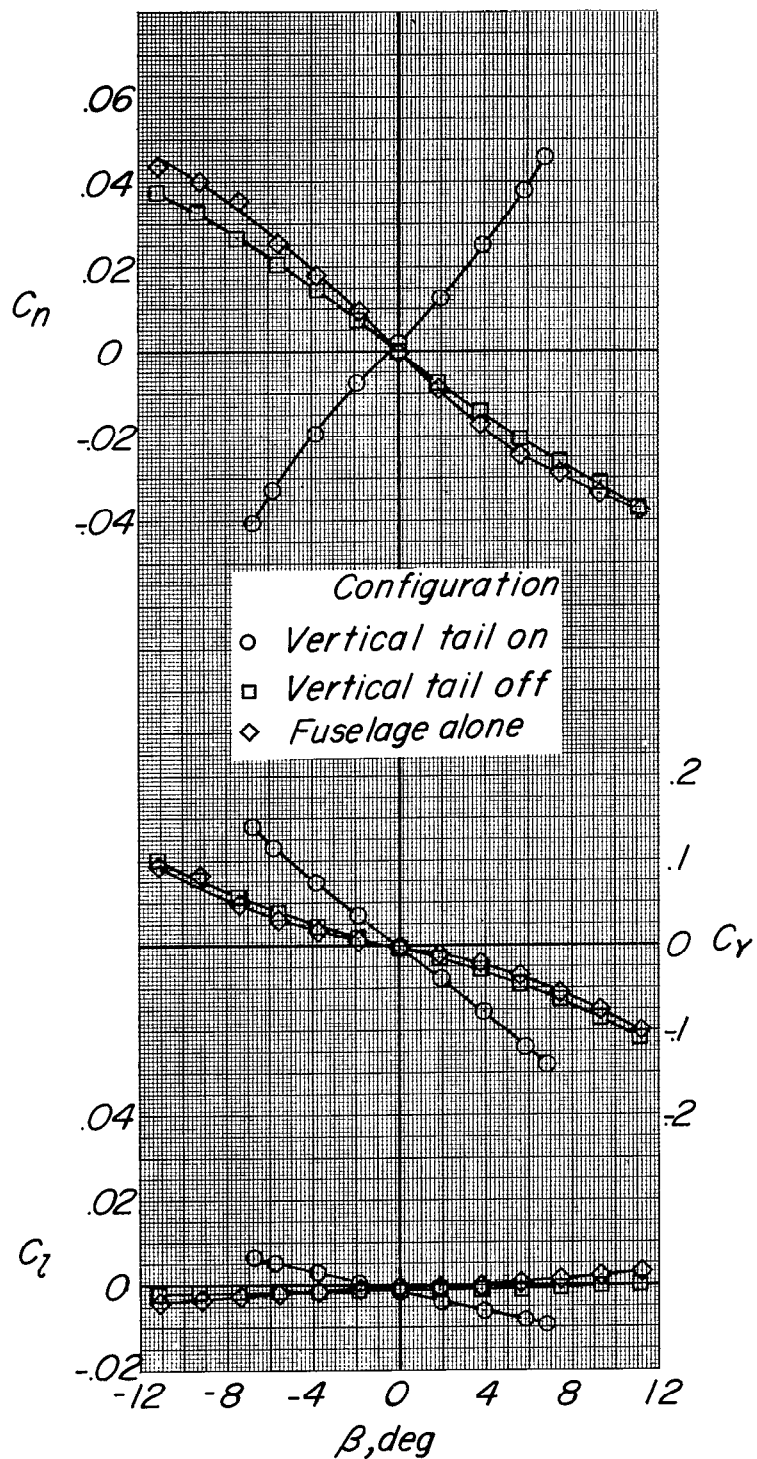
(b) Concluded.

Figure 21.- Continued.



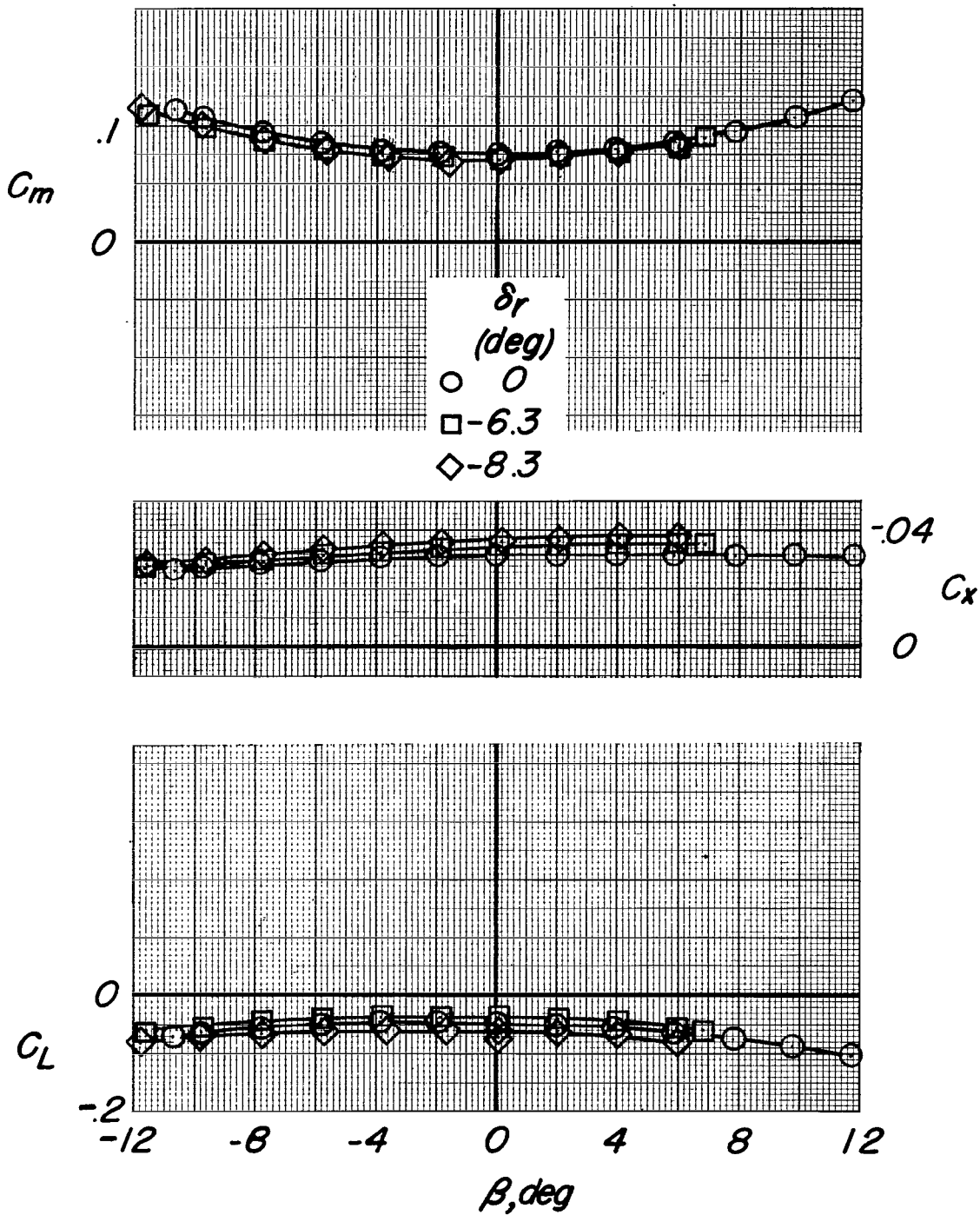
(c) $M = 0.95$.

Figure 21.- Continued.



(c) Concluded.

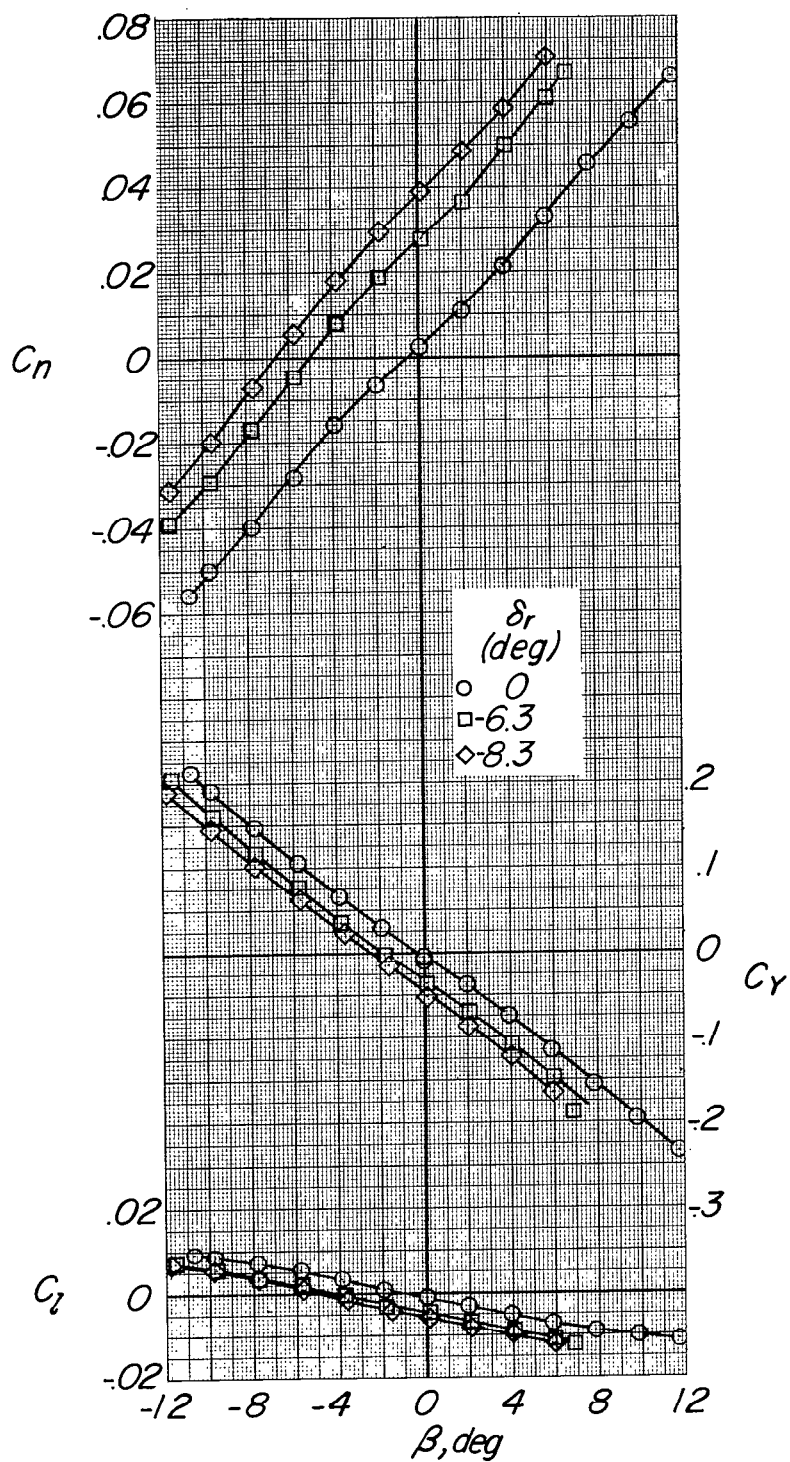
Figure 21.- Concluded.



(a) $M = 0.70$.

Figure 22.- The effect of rudder deflection on the aerodynamic characteristics in sideslip. Fence A; $i_t = 5^\circ$; $\alpha = 0^\circ$.

~~SECRET~~

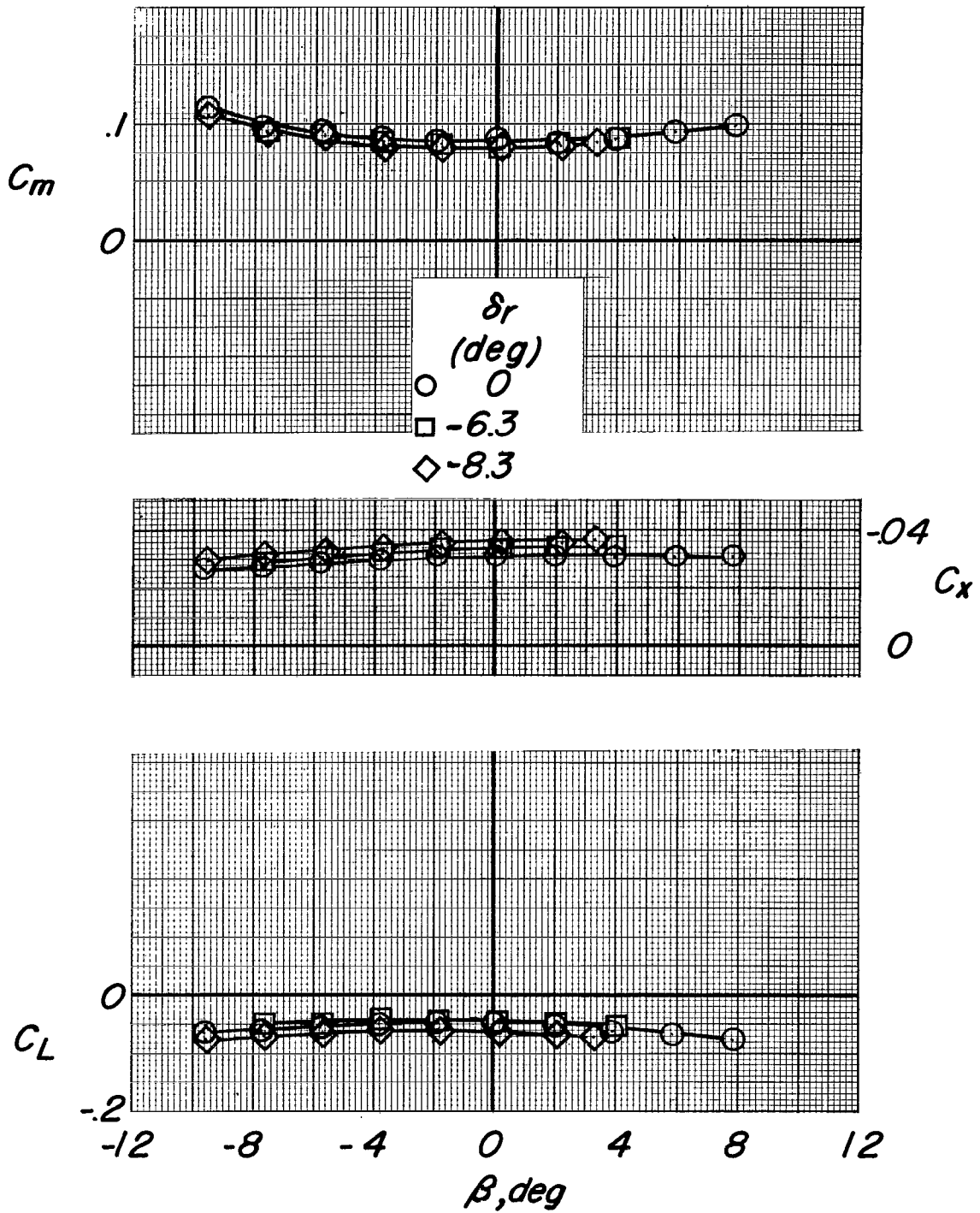


(a) Concluded.

Figure 22.- Continued.

~~SECRET~~

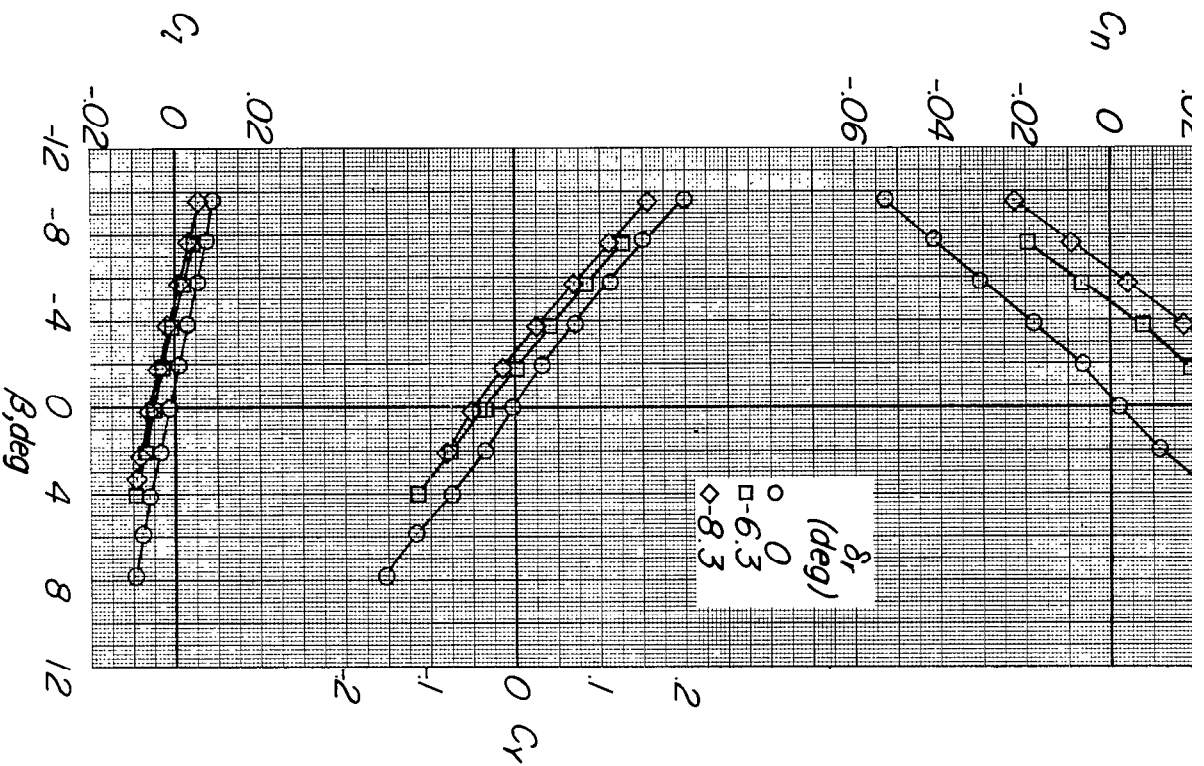
~~SECRET~~



(b) $M = 0.84$.

Figure 22.- Continued.

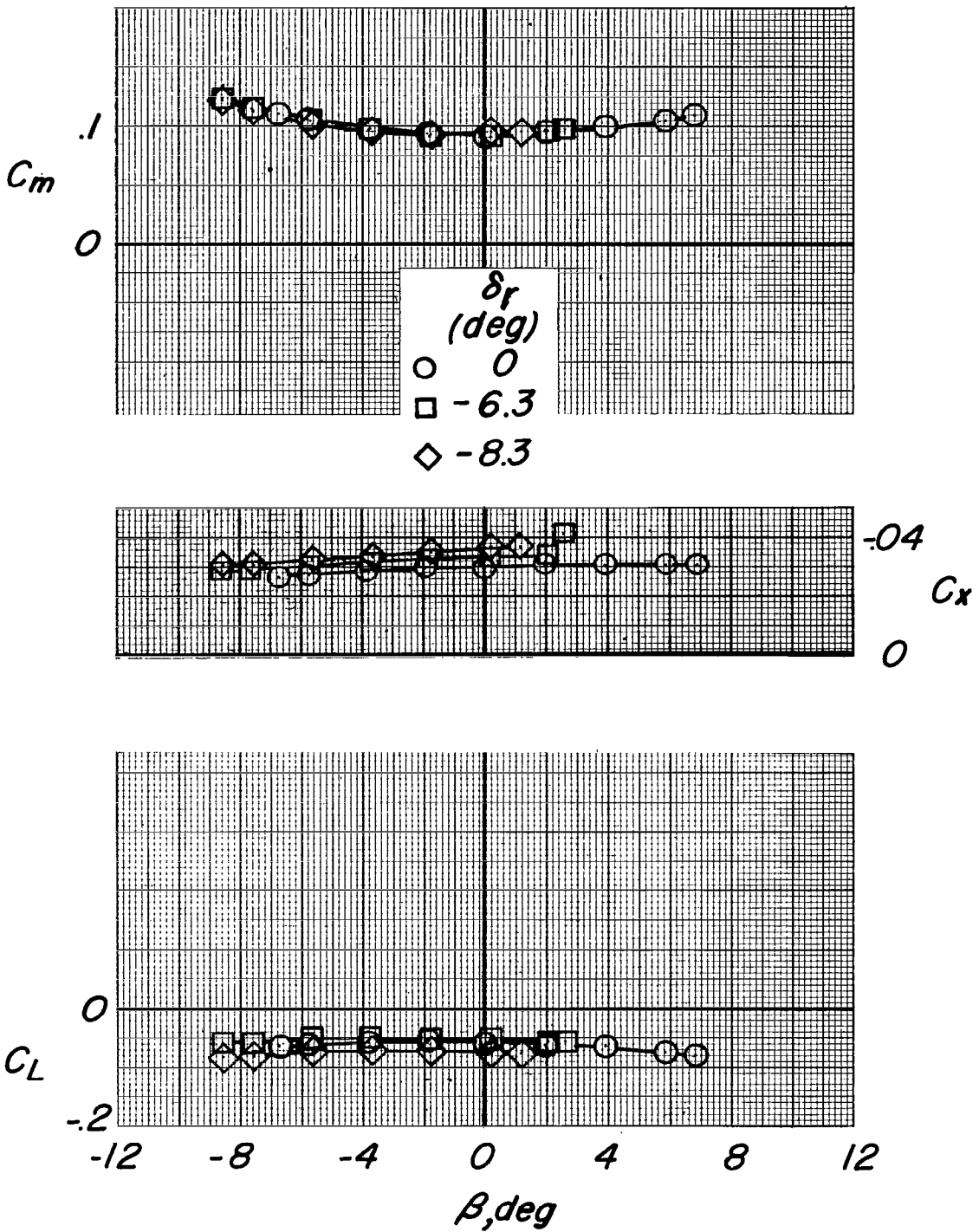
~~SECRET~~



(b) Concluded.

Figure 22.- Continued.

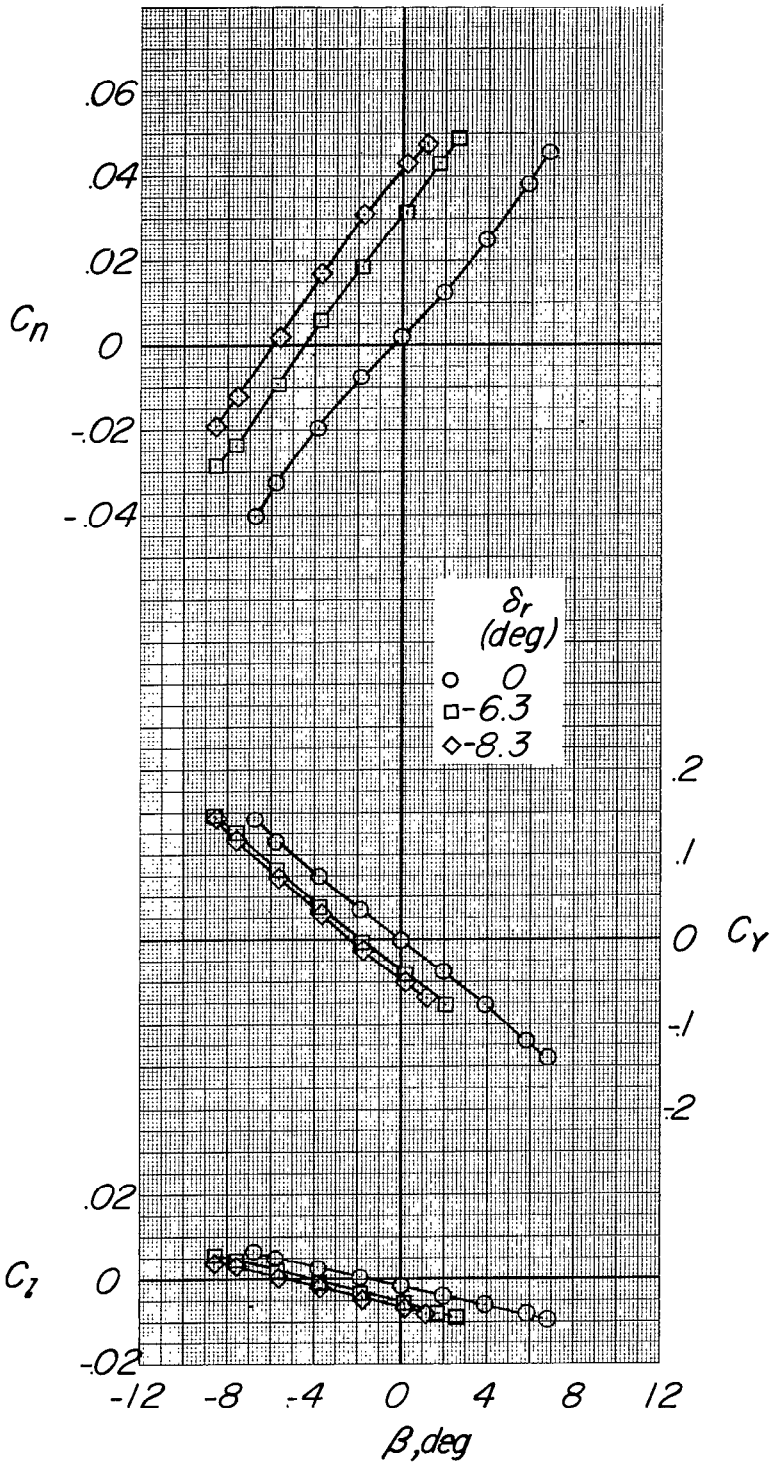
~~SECRET~~



(c) $M = 0.95$.

Figure 22.- Continued.

~~SECRET~~



(c) Concluded.

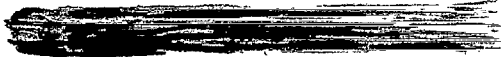
Figure 22.- Concluded.

SECURITY INFORMATION



3 1176 01438 6693

UNCL



SECRET